



Fakultät für Medizin

Comprehensive Cancer Center München^{TUM}

Schwerpunkt: Translationale Onkologie

The gp130/SHP2 Signaling Axis in Pancreatic Cancer

Katrin Jana Ciecieski

Vollständiger Abdruck der von der Fakultät für Medizin der Technischen Universität München zur Erlangung des akademischen Grades eines

Doctor of Philosophy (Ph.D.)

genehmigten Dissertation.

Vorsitzende: Prof. Dr. Angela Krackhardt

Betreuer: Prof. Dr. Hana Algül

Prüfer der Dissertation:

1. Prof. Dr. Maximilian Reichert

2. Prof. Dr. Philipp Jost

Die Dissertation wurde am 14.12.2020 bei der Fakultät für Medizin der Technischen Universität München eingereicht und durch die Fakultät für Medizin am 22.02.2021 angenommen.

1. ABSTRACT

Pancreatic ductal adenocarcinoma (PDAC) is one of the deadliest malignancies worldwide and despite considerable research efforts over the past decades, no significant headway was made to increase the 5-year survival rate. Unspecific symptoms which lead to late diagnosis, early onset of metastasis, a complex mutational landscape and a lack of effective therapeutics are the main reasons for the dismal prognosis associated with this disease. While it must be a goal to drastically improve the diagnostic possibilities and thus detect PDAC in earlier stages of development, the discovery and development of new and effective therapies is an equally important milestone on the path to improved patient outcome. Therefore, a better understanding of the pathways involved in pancreatic carcinogenesis and tumor maintenance is of utmost importance.

Pancreas-specific deletion of the *IL6st* gene encoding the glycoprotein 130 (gp130) a cytokine receptor subunit utilized by interleukin 6 (IL-6) family cytokines, in murine models of *Kras*^{G12D} (*Kras*) and *Kras*^{G12D};*Trp53*^{-/-} (*Kras*;*Trp53*^{-/-})-driven carcinogenesis showed significantly inhibited PDAC development. The importance of gp130 in *KRAS* mutant pancreatic cancer was further corroborated through *IL6st* deletion in *Kras*;*Socs3*^{-/-}-mice (*Kras*;*Socs3*^{-/-};*IL6st*^{-/-}) and a gp130-overactivity model. More specifically, additional deletion of the *IL6st* gene in *Socs3*-deficient mice led to significantly delayed tumor formation and prolonged survival compared to *IL6st*-proficient mice. Drastically accelerated tumor formation and significantly shortened lifespans in mice expressing a constitutively active leucine-zipper linked form of gp130 (Lg130) in a gp130-overactivity model of *Kras*-driven pancreatic cancer, further corroborated the relevance of gp130 in PDAC. While the impact of pharmacological gp130 inhibition in *Kras*;*Trp53*^{-/-} cells varied within the three tested cell lines, our results were promising enough to continue analyzing the effect of pharmacological gp130 inhibition in combination with standard chemotherapy drugs or targeted inhibitors, in further *in vitro* and *in vivo* models.

Since the role of gp130-effector molecules STAT3 and SOCS3 in pancreatic cancer had already been investigated, we decided to focus our further studies on Src homology domain 2 containing tyrosine phosphatase (SHP2), another interaction partner of gp130. Pancreas-specific deletion of the SHP2 encoding gene *Ptpn11* in *Kras* mice led to profound inhibition of pancreatic intraepithelial neoplasia (PanIN) development and desmoplasia. PDAC formation was almost completely blocked, and survival was drastically prolonged. A focused drug screen in multiple murine and human PDAC cell lines revealed a unique synergism between MEK and SHP2 as well as ERK and SHP2 inhibition which resulted in significant growth inhibition *in vitro*. This synergism and the superior efficacy of the combination treatment compared to monotherapy was also confirmed in several *in vivo* models.

In conclusion, we were able to show, that the gp130/SHP2-signaling axis is involved in both development and maintenance of *KRAS*-driven PDAC and that both the gp130-receptor subunit itself, as well as its downstream effector SHP2 are promising targets for novel therapeutic strategies. Especially the combination of ERK and SHP2 as well as MEK and SHP2 inhibition are strategies that should be tested in clinical studies of *KRAS*-driven cancer in PDAC, lung and colon cancer patients.

2. ZUSAMMENFASSUNG

Das duktales Pankreas-Adenokarzinom (PDAC) ist eine der tödlichsten Krebserkrankungen weltweit und trotz erheblicher Forschungsanstrengungen wurden in den letzten Jahrzehnten keine signifikanten Fortschritte zur Verbesserung der 5-Jahres-Überlebensrate erzielt. Unspezifische Symptome und eine damit verbundene späte Diagnose, das frühe Einsetzen der Metastasierung, eine komplexe Mutationslandschaft sowie das Fehlen wirksamer Therapeutika, sind die Hauptgründe für die mit dieser Krankheit verbundene schlechte Prognose. Neben den Bemühungen die diagnostischen Möglichkeiten signifikant zu verbessern und somit PDAC in früheren Entwicklungsstadien zu erkennen, ist die Erforschung und Entwicklung neuer, wirksamerer, Therapien ein essenzieller Meilenstein zur Verbesserung der Überlebensrate. Ein besseres Verständnis der an der Pankreaskarzinogenese und der Aufrechterhaltung des Tumors beteiligten Signalwege ist daher von größter Bedeutung.

Pankreas-spezifische Deletion des *IL6st*-Gens und somit der Zytokinrezeptoruntereinheit gp130, in Mausmodellen der *Kras*^{G12D} (*Kras*) und *Kras*^{G12D};*Trp53*^{-/-} (*Kras*;*Trp53*^{-/-})-getriebenen Karzinogenese zeigte eine signifikant gehemmte PDAC-Karzinogenese. Die Bedeutung von gp130 im *KRAS*-mutierten Pankreaskarzinom wurde durch *IL6st*-Deletion in *Kras*;*Socs3*^{-/-} Mäusen (*Kras*;*Socs3*^{-/-};*IL6st*^{-/-}) und einem gp130-Überaktivierungsmodell bestätigt. Die zusätzliche Deletion des *IL6st*-Gens bei Mäusen mit *Socs3*-Mangel führte zu einer signifikant verzögerten Tumorbildung und einem verlängerten Überleben im Vergleich zu Mäusen ohne gp130-Verlust. Eine drastisch beschleunigte Tumorbildung und eine signifikant verkürzte Lebensdauer bei Mäusen, welche eine konstitutiv aktive Leucin-Zipper-verknüpfte Form von gp130 (Lg130) in einem gp130-Überaktivitätsmodell des *Kras*-getriebenen Pankreaskarzinoms exprimieren, bestätigten die Relevanz von gp130 in Pankreastumoren weiter. Obwohl die Effektivität der pharmakologischen gp130-Hemmung in *Kras*;*Trp53*^{-/-}-Zellen innerhalb der drei getesteten Zelllinien variierte, erscheint es dennoch sinnvoll, weiterhin gp130-Inhibitoren wie Bazedoxifen in Kombination mit Chemotherapeutika oder anderen spezifischeren Inhibitoren wie zum Beispiel dem MEK-Inhibitor Trametinib, in weiteren *In-vitro*- und *In-vivo*-Modellen zu testen.

Da die Rolle von STAT3 und SOCS3 im Bauchspeicheldrüsenkrebs bereits in unserer Gruppe untersucht wurde, konzentrieren wir uns hier auf einen weiteren Interaktionspartner von gp130, die Tyrosinphosphatase (SHP2). Die pankreas-spezifische Deletion des SHP2-kodierenden Gens *Ptpn11* in *Kras*-Mäusen führte zu einer drastischen Hemmung bei der Entwicklung der Pankreas-intraepithelialen Neoplasie (PanIN) sowie des desmoplastischen Stromas. Die PDAC-Bildung wurde fast vollständig verhindert und das Überleben drastisch verlängert. Ein fokussiertes Inhibitor-Screening in mehreren murinen und humanen PDAC-Zelllinien ergab

einen einzigartigen Synergismus zwischen MEK- oder ERK-Inhibitoren in Kombination mit SHP2-Inhibition, der *in vitro* zu einer signifikanten Wachstumshemmung führte. Dieser Synergismus und die bessere Wirksamkeit der Kombinationsbehandlung im Vergleich zur Monotherapie wurden auch in mehreren *In-vivo*-Modellen bestätigt.

Zusammenfassend konnten wir zeigen, dass der gp130/SHP2-Signalweg sowohl an der Entwicklung als auch an der Aufrechterhaltung des *KRAS*-gesteuerten duktales Pankreaskarzinoms beteiligt ist und dass, sowohl die gp130-Rezeptor-Untereinheit selbst als auch die nachgeschaltete Tyrosinphosphatase SHP2, vielversprechende Angriffspunkte für neuartige Therapiestrategien sind. Insbesondere die Kombination von ERK- und SHP2- sowie MEK- und SHP2-Inhibitoren sind Strategien, die in klinischen Studien mit PDAC-Patienten und Patienten anderer Krebsleiden, welche eine *KRAS* Mutation aufweisen getestet werden sollten.

3. TABLE OF CONTENT

1. ABSTRACT	1
2. ZUSAMMENFASSUNG	3
3. TABLE OF CONTENT	5
4. INTRODUCTION	8
4.1 Localization, structure, and physiological function of the pancreas	8
4.2 Pancreatic cancer	9
4.3 Murine models of pancreatic cancer	10
4.4 Glycoprotein 130 (gp130).....	11
4.4.1 gp130 ligands and downstream signaling	11
4.4.2 gp130 signaling in pancreatic cancer	13
4.5 Research Focus	15
5 MATERIALS AND METHODS	16
5.1 Mouse strains	16
5.2 Genotyping	17
5.2.1 DNA extraction and polymerase chain reaction (PCR)	17
5.2.2 Agarose gel electrophoresis	18
5.3 Histology	19
5.3.1 Tissue sections	19
5.3.2 Hematoxylin and eosin (H&E) staining	19
5.3.3 Immunohistochemistry	19
5.4. Quantification of Relative Pancreatic Weight, Tumor Incidence	20
5.5. Human PDAC Samples.....	20
5.6 <i>In vitro</i> experiments and protein biochemistry.....	21
5.6.1 Isolation and culture of primary tumor cells and cell lines.....	21
5.6.2 Protein Extraction and Quantification	21
5.6.3 SDS-PAGE	22
5.6.4 Western Blot	24
5.6.5 Plasmids, cloning and transfection.....	25
5.6.6 <i>In vitro</i> drug screening and colony formation assays.....	25
5.6.7 Quantitative analysis of drug synergy	26
5.7. <i>In vivo</i> experiments	26
5.7.1. Anesthesia.....	26
5.7.3 Human PDAC specimens and patient-derived tissue xenografts	27

5.7.5 Drugs and inhibitors.....	28
5.7.6 <i>In vivo</i> drug combination dose finding escalation.....	28
5.7.7 <i>In vivo</i> therapy dosing.....	29
5.8 Statistics	29
6. RESULTS.....	30
6.1 <i>IL6st</i> deletion impedes pancreatic carcinogenesis in mice with <i>Kras</i> and <i>Kras;Trp53^{-/-}</i> background	30
6.2 Expression of a constitutively active, transgenic, gp130 receptor accelerates pancreatic carcinogenesis and decreases the life span of mice in a <i>Kras^{G12D}</i> -driven model of murine pancreatic cancer.....	34
6.3 Pancreas-specific gp130 deletion rescues the phenotype of accelerated carcinogenesis and shortened survival seen in <i>Kras;Socs3^{-/-}</i> mice.	36
6.4 gp130 as therapeutic target in PDAC	37
6.4.1 <i>Kras;Trp53^{-/-}</i> cells are sensitive to gp130 inhibition	37
6.4.2 gp130 inhibition in combination with classic chemotherapy	38
6.4.3 gp130 inhibition in combination with MEK targeted therapy.....	39
6.5 Pancreas-specific deletion of the gp130-downstream effector SHP2 abrogates pancreatic tumor formation in <i>Kras</i> and <i>Kras;Trp53^{-/-}</i> mice	40
6.6 SHP2 is expressed and phosphorylated to different extents in human pancreatic cancer tissues and human PDAC cell lines	42
6.7 <i>Ptpn11</i> knockout sensitizes human PDAC cells to MEK inhibition	42
6.8 SHP2 inhibition shows remarkable synergy with MEK inhibition in <i>KRAS</i> mutant murine and human PDAC cell lines.....	44
6.9 MEK and SHP2 inhibitor combination therapy shows superior <i>in vivo</i> efficacy in endogenous <i>Kras;Trp53^{-/-}</i> tumors compared to MEK or SHP2 monotherapy	46
6.10 Combined ERK and SHP2 inhibition shows synergism in <i>in vitro</i> growth inhibition assay and leads to a stronger and more sustained ERK activity inhibition compared to ERKi monotherapy.....	48
6.11 Continuous (daily) treatment with combined LY3214996 + RMC-4550 treatment is well tolerated in wild-type and NSG mice up to a dose of 100 mg/kg LY3214996 + 10 mg/kg RMC-4550	51
6.12 Combined ERK plus SHP2 inhibition shows superior <i>in vivo</i> efficacy compared to either inhibitor alone.....	53
6.13. All LY3214996 + RMC-4550 treatment schedules show significant tumor growth inhibition in endogenous and orthotopic PDAC models, however continuous treatment is the only schedule able to significantly reduce the number of proliferating cells.....	54
6.14 LY3214996 + RMC-4550 combination therapy significantly inhibits tumor growth, and induces tumor volume reduction as well as sustained disease control in models of patient-derived <i>KRAS</i> -mutant PDAC xenografts	56

7. DISCUSSION.....	59
7.1 gp130-signaling is an important driver in pancreatic carcinogenesis	59
7.2 The gp130-receptor is a potential therapeutic target in PDAC.....	60
7.3 The tyrosine phosphatase SHP2 is critically important for <i>KRAS</i>-driven pancreatic carcinogenesis.....	62
7.4 Synergism between SHP2 and RAS-effector Kinases MEK and ERK provides rationale for a “two-pronged” therapy approach for <i>KRAS</i>-mutant cancer	64
8. CONCLUSION AND OUTLOOK.....	66
9. REFERENCES	67
10. ABBREVIATIONS	77
11. ACKNOWLEDGEMENTS	79

4. INTRODUCTION

4.1 Localization, structure, and physiological function of the pancreas

The human pancreas is a well-defined solitary organ located deep within the abdominal cavity. It can be macroscopically divided into three major regions called head, body, and tail of the pancreas. Named because of their shape rather than their anatomical orientation, the head of the pancreas is the downward facing C-shaped, and slightly bulbous part attached to the duodenum, and the pancreas tail is the upward facing part attached to the spleen. The body of the pancreas is the flat, narrow, part located underneath the stomach extending almost horizontally across the abdominal cavity. The distal end of the common bile duct passes through the head of the pancreas and joins the pancreatic duct as it enters the intestine. This anatomical proximity means that diseases of the pancreas head such as cancer, or swelling or scarring from pancreatitis can lead to biliary obstruction resulting in jaundice (Dolenšek, Rupnik and Stožer, 2015; Pandol, 2015).

The pancreas plays a central role in the control of energy consumption and metabolism and is composed of two morphologically and functionally distinct compartments: the exocrine and the endocrine pancreas. The exocrine pancreas mainly consists of acini and ductal cells. An acinus is a cluster of roughly pyramid-shaped acinar cells which form a dome-like structure that funnels secretions from the acinar cells into ducts. The two types of cellular units are combined to direct digestive enzymes like lipases, proteinases, and amylases produced by the acinar cells into the duodenum where digestion of fats, proteins, and carbohydrates is initiated (Dolenšek, Rupnik and Stožer, 2015; Pandol, 2015; Zhou and Melton, 2018).

The endocrine compartment makes up only about 5% of the total pancreatic volume and is comprised of so-called islets of Langerhans. The islets of Langerhans can basically be considered as hormone-producing micro-organs within the pancreas, and are microscopically distinct, mostly circular to oval shaped, cell clusters composed of a few to several thousand endocrine cells. There are five major types of islet cells, each of which synthesizes and secretes a principal hormone. These hormones are insulin produced by β -cells, glucagon produced by α -cells, somatostatin produced by δ -cells, pancreatic polypeptide made by PP cells, and ghrelin produced by ϵ -cells. All of which are needed for digestive homeostasis. In addition to islets, single endocrine cells can be found scattered throughout the acinar and ductal tissue (Dolenšek, Rupnik and Stožer, 2015; Zhou and Melton, 2018).

4.2 Pancreatic cancer

The pancreas is a vital organ, and pancreatic diseases including inflammatory diseases like acute and chronic pancreatitis, diabetes mellitus, and pancreatic cancer (PC), occur in more than 10% of the population worldwide (Guo *et al.*, 2019). Acute and chronic pancreatitis, as well as diabetes are of significant clinical relevance, they affect millions of people and cause severe suffering in patients and thus merit extensive research. However, the focus of this thesis will be on pancreatic cancer. More specifically on pancreatic ductal adenocarcinoma (PDAC).

PDAC is the third leading cause of cancer-related death in the western countries, the seventh worldwide, and is predicted to become the second most common cause of cancer mortality in the US in the next decades (Carioli *et al.*, 2020; Mizrahi *et al.*, 2020; Siegel, Miller and Jemal, 2020). The main risk factors associated with PDAC are misuse of alcohol, smoking, obesity, western diet, diabetes mellitus, chronic pancreatitis, and hereditary genetic alterations. Men are at higher risk than women and it is generally considered to be a disease associated with elderly people (Rawla, Sunkara and Gaduputi, 2019; Zeng *et al.*, 2019). The dismal prognosis, i.e., a 5-year overall survival (OS) of less than 10% has two major causes: 1. the high variability in clinical symptoms leading to late diagnosis and 2. the high potential to metastasize. Only 10–20% of all PDAC patients are diagnosed with PDAC at resectable stages (Sheahan *et al.*, 2018; Siegel, Miller and Jemal, 2020) and even in those few resectable cases, PDAC is prone to relapse and develop resistance to supportive chemotherapy, making treatment options challenging (Amrutkar and Gladhaug, 2017; Grasso, Jansen and Giovannetti, 2017; Morrison, Byrne and Vonderheide, 2018; Orth *et al.*, 2019).

Like all cancers, PDAC is a disease caused by genetic alterations. With over 90% by far the most common alteration in PDAC is a mutation in the *KRAS* gene, followed by 80% of cases with alterations in *p16/CDKN2A*, 70% with mutations in *TP53* and 50% with loss or loss-of-function mutations in the *TGFβ/SMAD4* pathway (Ruess *et al.*, 2017).

Despite concentrated research efforts, novel therapeutic options remain extremely limited, and apart from PARP inhibitors, which are used in *BRCA*-mutant PDAC (Golan *et al.*, 2019), no targeted therapies have proven successful in the clinic. Leaving the 90% of patients carrying *KRAS* mutations in dire need.

4.3 Murine models of pancreatic cancer

While a lot of pre-clinical research regarding the understanding of carcinogenic pathways and the development of targeted therapies is done in 2- and 3-D cell culture, the current gold standard is still the application of *in vivo* models. Apart from transplantation models of murine or human pancreatic cancer cells or tissue, genetically engineered mouse models (GEMMs) are used to study PDAC development and maintenance (Lee *et al.*, 2016). Two of the most used models are, the *Pdx-1-Cre* or the *p48-Cre* driven model developed by Hingorani *et al.*, (2003), which induces site directed, endogenous, expression of mutant $Kras^{G12D}$ proteins in progenitor cells of the murine pancreas. This model replicates the entire progression of pancreatic ductal adenocarcinoma from preinvasive neoplasia to invasive and metastatic disease (Hingorani *et al.*, 2003). The second widely used model was also developed by Hingorani *et al.*, (2005) and incorporates another common feature of human PDAC, a point-mutation in *TP53*. Co-expression of mutated p53 together with $Kras^{G12D}$ greatly hastens the development of locally invasive and widely metastatic pancreatic ductal adenocarcinoma that faithfully recapitulates all of the known features of pancreatic carcinoma (Hingorani *et al.*, 2005). Our group however uses a *Trp53^{fllox/fllox}* model (Marino *et al.*, 2000) which together with *Ptf1a-Cre* and $Kras^{G12D}$ expression leads to pancreas-specific loss of p53 and expression of mutant $Kras^{G12D}$ proteins which result in rapid carcinogenesis and severe morbidity in mice prior to the development of metastases.

4.4 Glycoprotein 130 (gp130)

4.4.1 gp130 ligands and downstream signaling

In 1978, Andersson et al., were the first to describe the glycoprotein 130 (gp130) in mice, as a membrane bound glycoprotein which is absent on resting lymphocytes but present on blasting T cells. Through extensive research in the past 40 years, it is now recognized that gp130 is almost ubiquitously expressed on hematopoietic and non-hematopoietic cells with varying expression levels depending on the state of cellular activation (Andersson *et al.*, 1978; Silver and Hunter, 2010). gp130 is a receptor subunit utilized by several cytokines of the IL-6 family, i.e., IL-6, IL-11, Leukemia Inhibitory Factor (LIF), Oncostatin M (OSM), Ciliary Neurotrophic Factor (CNTF), Cardiotrophin 1 (CT1), Neuropoietin (NP or CT-2) and Cardiotrophin like Cytokine (CLC), and two members of the IL-12-family (IL-27 and IL-35) (Silver and Hunter, 2010; Rose-John, Scheller and Schaper, 2015; Rose-John, 2018). IL-6 family cytokines are grouped together, because the receptor complex of each cytokine contains at least one, if not two (IL-6 and IL-11) molecules of the signaling receptor subunit gp130. Cytokines in the IL-6 family have overlapping but also distinct physiological roles. These include regulating the hepatic acute phase reaction, B-cell stimulation, regulating the balance between regulatory and effector T-cells, metabolic regulation, and several neural functions (Rose-John, 2018).

Complex-formation between gp130 and ligand-bound cytokine-specific receptor α chains, like the IL-6 receptor α (IL-6R α) triggers the activation of three downstream signaling cascades (**Figure 1**). The Janus kinases JAK1, JAK2, and tyrosine kinase 2 (TYK2) are constitutively associated with gp130 and get phosphorylated and activated through ligand-receptor-gp130 complex formation (Ohtani *et al.*, 2000; Silver and Hunter, 2010). Upon activation, these JAK kinases catalyze the phosphorylation of specific tyrosine motifs in the cytoplasmic domain of gp130. Tyrosine residues at position 759, 767, 814, 905, and 915, i.e., the five most membrane-distal tyrosine motifs, act as recruitment sites for signaling components containing Src homology 2 (SH2) domains, the most prominent among them being signal transducer and activator of transcription (STAT) 1, STAT3 and STAT5 (Silver and Hunter, 2010; Schaper and Rose-John, 2015). STAT binding to the gp130 phospho-tyrosine motifs induces STAT phosphorylation, homo- or heterodimerization of phosphorylated STATs and subsequent nuclear translocation. In the nucleus, STAT dimers bind to specific regions in the promoters of STAT-inducible genes and initiate gene transcription (Silver and Hunter, 2010; Schaper and Rose-John, 2015). One of the transcriptional targets of STAT3 signaling is the SOCS3 gene which encodes the JAK inhibitor suppressor of cytokine signaling 3 (SOCS3). SOCS3 acts in a negative feedback loop to limit gp130-mediated signaling by binding to a phospho-tyrosine residue at position 757 in mice and 759 in humans. Interaction with gp130 activates SOCS3's

kinase inhibitory region (KIR), which binds and inhibits the catalytic domain of the JAK kinase (Silver and Hunter, 2010; Schaper and Rose-John, 2015).

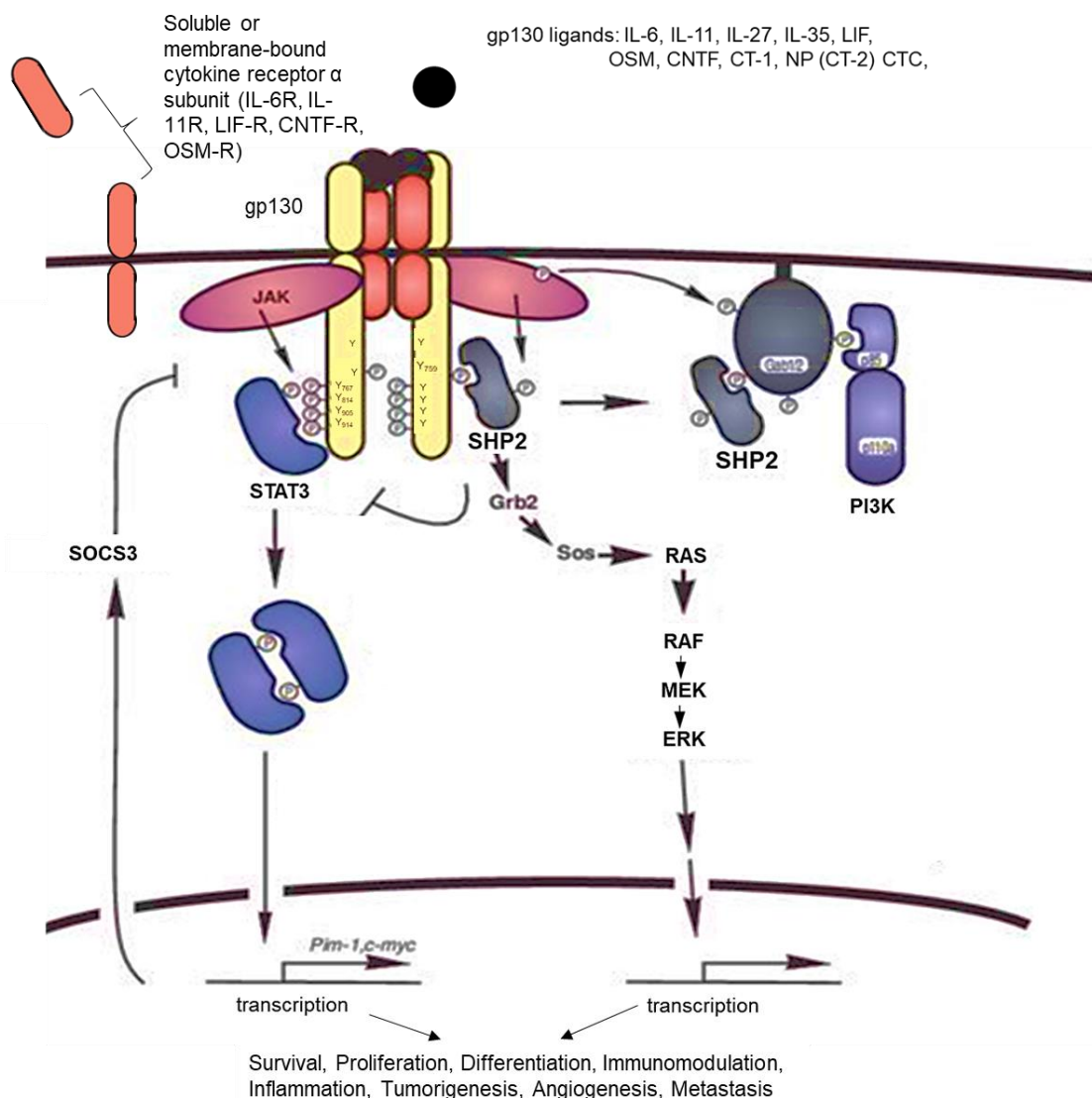


Figure 1: The gp130 signaling axis (adapted from (Ohtani *et al.*, 2000)). Ligand binding to the α -receptor followed by gp130 binding leads to the formation of a signaling complex which activates JAK1. JAK1 phosphorylates tyrosine residues within the cytoplasmic part of gp130. These phosphotyrosine motifs are recruitment sites for STAT transcription factors, the STAT inhibitor SOCS3, and for the adapter protein and tyrosine phosphatase SHP2. SHP2 links to the RAS-RAF-ERK cascade as well as to PI3K signaling (Schaper and Rose-John, 2015). Gp130-mediated signaling is involved in a variety of cellular processes, in the context of cancer these processes are amongst others: proliferation and survival, regulation of immune cell subtypes as well as pro-inflammatory processes and angiogenesis (Heo, Wahler and Suh, 2016).

STAT (and especially STAT3) activation is often considered to be the main signaling cascade, however IL-6 family cytokines also induce the RAS-MAPK cascade and the PI3K/AKT pathway, and regulation of a balanced pathway activation is crucial for controlled cell proliferation and cellular homeostasis within the organism (Silver and Hunter, 2010; Eulenfeld *et al.*, 2012; Schaper and Rose-John, 2015). Critically important for this balance is the phosphorylation of tyrosine 759, which attracts not only the JAK/STAT inhibitor SOCS3, but also the SH2 domain-containing phosphatase 2 (SHP2). Tyrosine 759-mediated activation of the protein tyrosine phosphatase SHP2 leads to dephosphorylation of JAK/STAT pathway components on the one (Schaper and Rose-John, 2015), and activation of the RAS/MAPK and PI3K/AKT pathways on the other hand (Silver and Hunter, 2010; Schaper and Rose-John, 2015).

Because gp130-mediated signaling is involved in a variety of physiological processes, its dysregulation is associated with a multitude of inflammatory and malignant diseases (Xu *et al.*, 2013). Inflammatory diseases associated with IL-6-type cytokines and gp130-mediated signaling are amongst others, allergic asthma, chronic obstructive pulmonary disease (COPD), pulmonary hypertension, multiple sclerosis (MS), and rheumatoid arthritis (RA) (Silver and Hunter, 2010). Additionally, almost all IL-6 family members are associated with at least one type of cancer. Some, like IL-6 are involved in development and maintenance of multiple cancer types and in certain cancer types, like breast cancer, several members of the IL-6 family play important roles (Xu *et al.*, 2013).

4.4.2 gp130 signaling in pancreatic cancer

Pancreatic inflammation is a known risk factor for the development of pancreatic cancer and the presence of a dense desmoplastic stroma is known to be a hallmark of PDAC (Algül *et al.*, 2007; Neesse *et al.*, 2015). The tumor microenvironment in PDAC includes various cell types like proliferating fibroblasts and pancreatic stellate cells producing extra cellular matrix (ECM) components like fibronectin and collagen, as well as immune cells releasing chemokines and cytokines (Lesina *et al.*, 2011). Some of these cytokines, like the proinflammatory cytokine IL-6, are detectable in the serum of PDAC patients and correlate with cachexia, advanced tumor stage and poor survival (Ebrahimi *et al.*, 2004; Holmer *et al.*, 2014). Congruently, the majority of pancreatic ductal adenocarcinomas show constitutive STAT3 activation while pSTAT3 is dispensable in the normal pancreas (Corcoran *et al.*, 2011). In 2011, our group showed that mutant *KRAS* is enough to initiate ADM and PanIN formation but STAT3 activation is necessary for the progression to high-grade PanIN lesions and PDAC (Lesina *et al.*, 2011). Histological analysis of the tumor microenvironment and pancreas-specific overexpression of

the soluble gp130-receptor (sgp130) showed that IL-6 in the pancreas is derived from the myeloid compartment, especially macrophages, and activates STAT3 signaling via soluble IL-6 receptor (sIL-6R)-mediated transsignaling (Lesina *et al.*, 2011). The importance of gp130-mediated signaling in pancreatic carcinogenesis was further shown through the deletion of IL-6 or STAT3, which abrogated the carcinogenic process, and the deletion of STAT3 inhibitor SOCS3, which accelerated tumor formation and shortened the survival of *KRAS*-mutant mice (Lesina *et al.*, 2011). Other groups corroborated these findings (Corcoran *et al.*, 2011) and further supported them by showing the importance of gp130/LIF (Shi *et al.*, 2019; Wang *et al.*, 2019), gp130/IL-35 (Huang *et al.*, 2017), and gp130/OSM (Smigiel, Parameswaran and Jackson, 2017) signaling in pancreatic carcinogenesis, metastasis, and therapy response. Our group also showed that loss and/or mutation of the tumor suppressor p53 leads to gp130-independent activation of STAT3. However, p53-deficient cells remained sensitive to IL-6 stimulation and might thus also be affected by gp130-pathway inhibition (Wörmann *et al.*, 2016).

4.5 Research Focus

The aim of this study was to further elucidate the role of gp130 and its downstream signaling axis in *Kras*-mutant driven murine pancreatic carcinogenesis and to investigate a possible clinical relevance and targetability of both gp130 and its downstream interaction partners using various *in vivo* and *in vitro* models.

The effects of pancreas-specific deletion of the gp130-encoding gene *IL6st* on murine pancreatic carcinogenesis was analyzed in both timepoint and survival mice with *Kras*^{G12D}- (*Kras*;*IL6st*^{-/-}), *Kras*^{G12D/+};*Trp53*^{-/-} (*Kras*;*Trp53*^{-/-};*IL6st*^{-/-}), or *Kras*^{G12D/+};*Socs3*^{-/-}-background (*Kras*;*Socs3*^{-/-};*IL6st*^{-/-}). A gp130-overactivity model (*Kras*;*Lgp130*^{ki/ki}) was used to investigate the role of gp130-mediated signaling in pancreatic carcinogenesis from both sides and thus confirm previous results. Based on the *in vivo* findings, *in vitro* experiments to determine therapeutic targetability were performed on *Kras*^{G12D/+};*Trp53*^{-/-}- derived cell lines.

To further elucidate the role of downstream interaction partners in the gp130-signaling axis, *in vivo* models of pancreas-specific deletion of the Shp2-encoding gene *Ptpn11* in *Kras*^{G12D}- (*Kras*;*Ptpn11*^{t/-}) or *Kras*^{G12D/+};*Trp53*^{-/-}-driven (*Kras*;*Trp53*^{-/-};*Ptpn11*^{t/-}) carcinogenesis were used. The clinical relevance of SHP2 was investigated both *in vitro* and *in vivo* in both murine and human PDAC cells and tissues.

5 MATERIALS AND METHODS

5.1 Mouse strains

- *Ptf1a^{+Cre-ex1} (Ptf1a^{tm1(Cre)Hnak})*: The coding sequence of exon 1 (ex1) in the *Ptf1a* locus was replaced with *Cre* recombinase (Nakhai *et al.*, 2007).
- *LSL-Kras^{G12D/+} (Kras^{tm4Tyj})* knock-in mouse: the endogenous *Kras* locus was targeted with a cassette containing a point mutation leading to the exchange of amino acid 12 from glycine to aspartic acid, preceded by a stop-codon flanked by loxP-sites. The mutant transcript can only be expressed after *Cre*-mediated recombination (Jackson *et al.*, 2001).
- *IL6st^{fl/fl} (IL6st^{tm1Wme})*: Exon 16 of *IL6st*, encoding the transmembrane region of gp130, was flanked by two loxP sites. *Cre*-mediated recombination leads to gp130-deletion (Betz *et al.*, 1998).
- *Trp53^{fl/fl} (Trp53^{tm1Bm})*: Insertion of loxP sites flanking exons 2 through 10. *Cre*-mediated recombination leads to the deletion of tumor suppressor p53 (Marino 2000)
- *Ptpn11^{fl/fl} (Ptpn11^{tm1Gsf})*: Exon 3-4 of the *Ptpn11* gene, encoding protein tyrosine phosphatase SHP2, are flanked by loxP sites. *Cre*-mediated recombination leads to deletion of SHP2 (Zhang *et al.*, 2004).
- *Lgp130^{ki/ki}*: transgenic knock-in mouse: introduction of a *Cre*-inducible expression cassette containing a CAG promoter sequence, a lox-STOP-lox sequence and the L-gp130 sequence consisting of a FLAG-sequence, linker sequence and a 39-aa fragment of the human c-jun gene followed by a truncated human wild-type gp130 sequence, containing only the transmembrane and cytoplasmic domain, into the murine *Rosa26* locus. *Cre*-mediated recombination results in the expression of a pre-dimerized constitutively active human gp130 variant (Stuhlmann-Laeisz *et al.*, 2006; Schumacher *et al.*, 2020) – *Lgp130^{kiki}* mice were a kind gift by Prof. Dr. Stefan Rose-John and Prof. Dr. med. Ulrich Keller

Strains were interbred to obtain the following compound mutants:

Kras^{LSL-G12D/+}, *Ptf1a*^{Cre-ex1} (*Kras*); *Kras*^{LSL-G12D/+}, *Ptf1a*^{Cre-ex1}, *Trp53*^{fl/fl} (*Kras*; *Trp53*^{-/-}); *Kras*^{LSL-G12D/+}, *Ptf1a*^{Cre-ex1}, *IL6st*^{fl/fl} (*Kras*; *IL6st*^{-/-}); *Kras*^{LSL-G12D/+}, *Ptf1a*^{Cre-ex1}, *Trp53*^{fl/fl}, *IL6st*^{fl/fl} (*Kras*; *Trp53*^{-/-}; *IL6st*^{-/-}); *Kras*^{LSL-G12D/+}, *Ptf1a*^{Cre-ex1}, *L-gp130*^{ki/+} (*Kras*; *L-gp130*^{ki/+}); *Kras*^{LSL-G12D/+}, *Ptf1a*^{Cre-ex1}, *L-gp130*^{ki/ki} (*Kras*; *L-gp130*^{ki/ki}); *Kras*^{LSL-G12D/+}, *Ptf1a*^{Cre-ex1}, *Ptpn11*^{fl/fl} (*Kras*; *Ptpn11*^{-/-}) and *Kras*^{LSL-G12D/+}, *Ptf1a*^{Cre-ex1}, *Trp53*^{fl/fl}, *Ptpn11*^{fl/fl} (*Kras*; *Trp53*^{-/-}; *Ptpn11*^{-/-}).

All mice were housed under specific pathogen-free conditions with free access to food and water. All mouse related procedures were evaluated and reviewed by the Zentrum für Präklinische Forschung at Klinikum rechts der Isar der Technischen Universität München, which follows the federal German guidelines for ethical animal treatment (Regierung von Oberbayern).

5.2 Genotyping

5.2.1 DNA extraction and polymerase chain reaction (PCR)

Genotyping of mice was performed by DNA extraction from ear clips (initial genotyping) or the tip of the tail. Ear clips were obtained from 3-week-old mice at the time of weaning, tails were collected after sacrifice (post-genotyping) to verify genotype. Ear or tail tissue was lysed in 200 µl DirectPCR Lysis Reagent (Tail) + 10 µl Proteinase K (Roche) for 2-12 hours at 55°C at 300-500 rpm in a ThermoMixer F1.5 (Eppendorf). Samples were then incubated at 85°C four one hour to inactivate the proteinase K. Genotyping PCR was performed with 1-2 µl DNA using the RedTaq and GreenTaq Ready Mix (Sigma). A standard PCR protocol was applied (Table 1). All primers (Table 2) were used at a final concentration of 10 pM.

Table 1: Genotyping PCR standard protocol.

Step	Temperature	Time	Cycle number
Initialization	95°C	5 min	1x
Denaturation	95°C	30 sec	40x
Annealing	58°C	30 sec	
Extension	72°C	60 sec	
Final Elongation	72 °C	10 min	
Final hold	4°C	∞	1x

Table 2: Genotyping primer sequences and product sizes.

Name	Primer (5´-3´)	PCR Products (bp)
<i>Cre</i>	1. ACC AGC CAG CTA TCA ACT CG 2. TTA CAT TGG TCC AGC CAC C 3. CTA GGC CAC AGA ATT GAA AGA TCT 4. GTA GGT GGA AAT TCT AGC ATC ATC C	WT: 350 Cre: 200
<i>Kras</i> <i>G12D</i>	1. CCA TGG CTT GAG TAA GTC TGC 2. CAC CAG CTT CGG CTT CCT ATT 3. AGC TAA TGG CTC TCA AAG GAA TGT A	WT: 300 mut: 200
<i>Kras</i> <i>G12D</i> <i>set 2</i>	1. GTC TTT CCC CAG CAC AGT GC 2. CTC TTG CCT ACG CCA CCA GCT C 3. AGC TAG CCA CCA TGG CTT GAG TAA GTC TGC	WT: 622 mut: 500 recombined: 650
<i>Kras</i> <i>G12D</i> <i>set 3</i>	1. TGT CTT TCC CCA GCA CAG T 2. CTG CAT AGT ACG CTA TAC CCT GT 3. GCA GGT CGA GGG ACC TAA TA	WT: 250 mut: 100 recombined: 300
<i>IL6st</i>	1. GGT GGC TGA TTC ACC TGC ACC TGC A 2. TAC GCT GGG CAG CGT CCT 3. AAC ACA CTC ATG CTG AAA CC	WT: 188 flox: 280 recombined: 450
<i>Trp53</i>	1. CAC AAA AAC AGG TTA AAC CCA 2. AGC ACA TAG GAG GCA GAG AC	WT: 288 flox: 370
<i>Ptpn11</i>	1. ACG TCA TGA TCC GCT GTC AG 2. ATG GGA GGG ACA GTG CAG	WT: 300 flox: 430
<i>Lgp130</i>	1. TGT CGC AAA TTA ACT GTG AAT C 2. GAT ATG AAG TAC TGG GCT CTT 3. AAA GTC GCT CTG AGT TGT TAT	WT: 570 flox: 380
<i>Socs3</i>	1. GCG GGC AGG GGA AGA GAC TGT CTG GGG TTG 2. GGC GCA CGG AGC CAG CGT GGA TCT GCG	WT: 280 flox: 410

5.2.2 Agarose gel electrophoresis

For agarose gel electrophoresis, agarose (Biozym, Hess. Oldendorf) was dissolved by heating in 1xTAE-Buffer (0.4 M Tris, 0.2 M acetic glacial acid, 0.01 M EDTA x NA_2 x $2H_2O$) at a concentration from 1 to 3% (w/v), dependent on PCR-product size. The melted agarose was left to cool to approximately 50°C and ROTI®GelStain (Roth) was added at a final

concentration of 0.5 µg/ml. The agarose solution was poured into an electrophoresis chamber and allowed to solidify. PCR-products along with a DNA-ladder (Peqlab, 1 kb) diluted in loading buffer (Peqlab) were run horizontally at 100 V. Documentation was performed by UV-light (EX/EM 312/516-518 nm, GelDoc™XR system)

5.3 Histology

5.3.1 Tissue sections

Murine tissue samples were fixed in 4% PFA (Merck, Darmstadt, Germany)/PBS for 24-48 h at room temperature (RT) in the dark, dehydrated and embedded in paraffin. A microtome (HM 355 S, MICROM, Walldorf, Germany) was used to cut 2.5 µm sections. Sections were mounted on adhesive-coated slides (SuperFrost® Plus, Menzel, Braunschweig, Germany) and air-dried at RT for 12-18 h. Sections were kept at RT until further analysis.

5.3.2 Hematoxylin and eosin (H&E) staining

For H&E staining, paraffin-embedded tissue sections were deparaffinized in Roti®Histol (Roth) for 2 x 5 minutes followed by rehydration in ethanol of descending concentration (100%, 96%, 70%; 3-5 minutes each) and deionized water (3-5 minutes). Slides were then incubated in hematoxylin solution (Merck Millipore) for 5 minutes, washed with running tap water for 10 minutes and incubated in eosin solution (Merck) for 3.5 minutes. Subsequently, the stained tissue sections were dehydrated in 96% Ethanol and Isopropanol for 25 sec each and Roti®Histol for 2 x 3 minutes. Slides were then covered with Pertex mounting medium (Medite GmbH) and coverslips (Merck). AxioStar Plus (Carl Zeiss, Göttingen, Germany) was used for histological analysis.

5.3.3 Immunohistochemistry

For immunohistochemistry, slides were deparaffinized and rehydrated as described under 4.3.2. After deparaffinization and rehydration, heat induced antigen retrieval was done by boiling the slides for 10-15 minutes in appropriate antigen retrieval buffer (1 mM EDTA (pH 8.0), citrate-based antigen unmasking solution (Vector Laboratories H-3300-250). Slides were then left to cool down for 20 minutes and washed 2 x 5 minutes with water. Endogenous peroxidase was blocked with 3% hydrogen peroxide for 15 min in the dark at RT followed by two 5 minutes washing steps in wash buffer (TBS, TBS-T, PBS, or PBS-T (Table 3) depending on the primary antibody). Unspecific binding was blocked with serum blocking solution (5%-10%goat serum, in wash buffer) for 1 h at RT or overnight at 4 °C. Slides were then incubated with the primary antibody diluted in blocking solution (or wherever indicated in SignalStain

antibody diluent, 8112 Cell Signaling Technology, Danvers, MA) for 12-18 h at 4°C. Primary antibodies used include: SHP2 (3397; 1:200) and pSTAT3 Y705 (9145; 1:100) from Cell Signaling Technologies, and Ki67 (ab15580;1:1,000) from Abcam. The secondary antibody (biotinylated anti-rabbit in goat (BA 1000 Vector)) was applied for 1h at RT following 2 washing steps, avidin-biotin peroxidase complex for biotinylated secondary antibodies was added according to manufacturer directions (Vector Laboratories, CA). Staining was developed with DAB reagent (Vector Laboratories, CA). For pSTAT3 detection the Avidin/Biotin blocking kit (SP2001 Vector) was used to reduce background, according to manufacturer instructions. Hematoxylin was used for counterstaining and slides were subsequently dehydrated and mounted as mentioned above (5.3.2). Image acquisition was achieved on a Zeiss Axiolmager.A1 microscope. Quantitative analyses of tumor areas and immunohistochemistry staining were performed with Axiovision (Zeiss) and ImageScope (Leica).

Table 3: Buffers used for washing.

Name	Components	pH
TBS	20 mM Tris, 137 mM NaCl	7.6
TBST	TBS-buffer, 0.1% (v/v) Tween-20	7.6
PBS	137 mM NaCl, 2.7 mM KCl, 10 mM Na ₂ HPO ₄ , 10 mM KH ₂ PO ₄	7.4
PBST	PBS-buffer, 0.1% (v/v) Tween-20	7.4

5.4. Quantification of Relative Pancreatic Weight, Tumor Incidence

Relative pancreatic weight or relative tumor weight was calculated from the pancreas and body weight obtained during sacrifice (pancreas weight/ body weight). Relative tumor incidence, i.e., the percentage of tumor-bearing mice relative to the total number of sacrificed mice was calculated after histological examination.

5.5. Human PDAC Samples

Human PDAC tissues were obtained from patients who underwent surgical resection at the Koç University Hospital, Istanbul, Turkey (M.E.). All patients provided written informed consent. Immunohistochemistry and Western Blot analysis of the samples were performed as described in the respective sections (5.3.3 and 5.6.2-5.6.4). Analysis was performed by Dr. Dietrich A. Ruess.

5.6 *In vitro* experiments and protein biochemistry

5.6.1 Isolation and culture of primary tumor cells and cell lines

Primary murine tumor cell lines were generated from thinly sliced pieces of explanted pancreatic tumors without enzymatic digestion. Murine cells were cultured in Dulbecco's modified Eagle medium (DMEM) supplemented with 10% FBS, 1% penicillin–streptomycin and 1% MEM non-essential amino acids (all Gibco). The human PDAC cell lines PANC-1 ($KRAS^{p.G12D}$; $p53^{p.R273H}$), YAPC ($KRAS^{p.G12V}$; $p53^{p.H179R}$; $SMAD4^{p.R515fs*22}$), CAPAN-1 ($KRAS^{p.G12V}$; $p53^{p.A159V}$; $SMAD4^{p.S343*}$; $CDKN2A^{p.0}$), CAPAN-2 ($KRAS^{p.G12V}$; $p53^{c.375G>T}$), ASPC-1 ($KRAS^{p.G12D}$; $p53^{p.C135fs*35}$; $SMAD4^{p.R100T}$; $CDKN2A^{p.L78fs*41}$), SU86.86 ($KRAS^{p.G12D}$; $p53^{p.G245S}$; $CDKN2A^{p.0}$), COLO357 ($KRAS^{p.G12D}$), T3M4 ($KRAS^{p.Q61H}$; $p53^{p.Y220C}$) and BXPC3 ($KRAS^{WT}$; $p53^{p.Y220C}$; $CDKN2A^{p.0}$; $SMAD4^{c.1_1659del/1659}$) were purchased from the Deutsche Sammlung von Mikroorganismen und Zellkulturen GmbH (DSMZ). Panc-10.05 ($KRAS^{p.G12D}$; $p53^{p.I255N}$) and MiaPaCa-2 ($KRAS^{p.G12C}$; $p53^{p.R248W}$; $CDKN2A^{p.0}$) cells were purchased from the American Type Culture Collection (ATCC). Mutational status of the cell lines was compiled from the American Type Culture Collection (ATCC), Catalogue of Somatic Mutations in Cancer (COSMIC; Wellcome Trust Sanger Institute) and Cancer Cell Line Encyclopedia (CCLE, Broad Institute) databases. PANC-1 cells were cultured in DMEM, all other human cell lines in RPMI1640 supplemented with 10% FBS, 1% penicillin–streptomycin and 1% MEM non-essential amino acids (all Gibco). All cells were kept at 37 °C in a humidified incubator with 5% CO₂.

5.6.2 Protein Extraction and Quantification

Protein extraction was performed on ice. Snap frozen cell pellets were lysed in ice-cold protein lysis buffer (5.6.2.1) freshly supplemented with a cocktail of protease-inhibitors (1% (v/v)) and phosphatase (1% (v/v)) inhibitors (SERVA, Heidelberg, Germany). Lysates were incubated for 15 on ice and subsequently centrifuged (13,000 rpm, 15 min, 4°C). to remove cell debris. Protein concentration was measured using the Bio Rad Protein Assay Kit (Bio Rad, München, Germany) by mixing 250 µl Bio Rad Protein Assay Kit (diluted 1:5 in dH₂O) with 1 µl protein dilution in a 96-well plate. BSA (1 mg/ml in dH₂O; Sigma) was used as a standard. Extinction was measured at 595 nm and protein concentration was determined by the standard curve. Samples were subsequently adjusted to 1-4 µg/µl (depending on the available amounts of protein) with 5 x Laemmli buffer (300 mM Tris-HCl, pH 6.8, 10% (w/v) SDS, 50% (v/v) Glycerol, 0.05% (w/v) Bromophenol blue, 5% (v/v) 2-Mercaptoethanol), were denatured by heating at 95°C for 5 min. Denaturation was stopped on ice and after a quick spin-down, protein samples

were either loaded onto directly onto the gel (see section 5.6.3) or stored at -80 to -20°C until further use.

Table 4: BSA pipetting scheme for protein standard curve with R = 0.97-0.99

0 µg	1 µg	2 µg	4 µg	6 µg	8 µg
0 µl BSA	1 µl BSA	2 µl BSA	3.85 µl BSA	5.95 µl BSA	8.15 µl BSA

5.6.2.1 Western Blot Lysis buffer recipes

1. IP Buffer

50 mM HEPES, pH 7.9
 150 mM NaCl
 1 mM EDTA, pH 8.0
 0,5% NP-40
 10% Glycerol

2. 5x MLB Buffer

125 mM HEPES, pH 7.5
 750 mM NaCl
 5% Igepal CA-6300
 50 mM MgCl₂
 5 mM EDTA
 10% Glycerol

3. RIPA Buffer

50 mM Tris/HCl pH 7.4
 150 mM NaCl
 1 mM EDTA
 1% NP-40

5.6.3 SDS-PAGE

SDS-polyacrylamide gel electrophoresis for protein separation and subsequent western blot analysis was performed in a Mini-Protean® 3 Cell System (Bio Rad). 20-40 µg protein per sample (depending on the protein of interest) in Laemmli-buffer (described above (5.6.2)) were loaded onto the gel. A 10-250 kDa protein standard (Bio Rad or Proteintech) was used as reference. The gel was with two parts: a short Stacking gel (10% polyacrylamide concentration) used to align and focus the proteins within the sample and a bigger separating gel used to separate the proteins based on size. Polyacrylamide concentration of the separating gel was chosen based on the size of the target protein with a range of 7.5-15%. The samples were run on 70-90 V for 15 minutes and then at 100-120V for another 60-90 minutes until protein separation was sufficient and/or the running-front had left the gel. Table 5 lists the components of the buffers used for SDS-PAGE and Table 6 and 7 show how the gels were made.

Table 5: Buffers used for SDS-PAGE.

Name	Components	pH
Stacking Gel Buffer	0.5 mM Tris-Cl	6.8
Separating Gel Buffer	1.5 mM Tris-Cl	8.8
Running Buffer	25 mM Tris-HCL, 192 mM Glycine, 0.1% (w/v) SDS	-

Table 6: Ingredients for SDS-Stacking Gels (2x gels in 1.5 mm plates)

dH₂O	4.5 ml
Stacking Gel Buffer	2.0 ml
30%/0.8% Acrylamide/Bis solution (Roth, Karlsruhe, Germany)	1.1 ml
10% SDS	75 µl
10% APS (Sigma)	38 µl
TEMED (Fluka, Buchs, Schweiz)	15 µl

Table 7: Ingredients of Separating gels in accordance with varying polyacrylamide concentration (for two gels of 1.5 mm thickness).

Concentrations	7.5%	10%	12%	15%
dH₂O	7.4 ml	6.2 ml	5.1 ml	3.8 ml
Separating Gel Buffer	3.9 ml	3.9 ml	3.9 ml	3.9 ml
30%/0.8% Acrylamide/Bis solution	3.8 ml	5.0 ml	6.0 ml	7.5 ml
10% SDS	150 µl	150 µl	150 µl	150 µl
10% APS	75 µl	75 µl	75 µl	75 µl
TEMED	23 µl	23 µl	23 µl	23 µl

5.6.4 Western Blot

Following SDS-PAGE (mentioned in 4.4.6), proteins were transferred onto a nitrocellulose membrane of 0.45 or 0.2 μm pore size (Merck Millipore) in the Mini Trans-Blot Cell™ System (Bio Rad). Nitrocellulose membranes were incubated in cold transfer buffer (table 8) along with the gel for 1-5 minutes prior to transfer. Western blot was performed in Transfer buffer (pre-cooled to 4°C) on ice at 100 V for 60-90 min (depending on protein size and gel thickness). After transferring proteins, membranes were washed shortly in TBST (Table 7) and then incubated for 1 h at RT on a shaker in blocking solution (Table 8) to block unspecific antibody binding. After this blocking step, the membrane was incubated with primary antibody (generally 1:1000 in blocking solution) (Table 8) overnight at 4°C whilst gently shaking. The primary antibodies used include: Antibodies against ERK1/2 (CST9102 or sc-93/sc-154) and pERK 1/2 (Thr202/Tyr204) (CST9191), SHP2 (CST3397 or sc-280), gp130 (sc-655), STAT3 (CST9139) and pSTAT3 Y705 (CST9131), RSK (CST8408) and pRSK (CST9344 and CST8753) as well as Heat shock protein 90 (HSP90; sc-7947) from Cell Signaling (CST) or Santa Cruz (sc). The antibody against pSHP2 Y542 (ab51174) was purchased from Abcam. Antibodies against alpha-Tubulin (T9026) and the horseradish peroxidase (HRP)-conjugated antibody against β -Actin (A3854) were from Sigma-Aldrich.

After incubation, membranes were washed 3 x 5 min with TBST and then incubated with secondary antibody in blocking solution (Table 8). The secondary antibodies used for subsequent chemiluminescent detection were conjugated to HRP. Depending on the primary antibody we either used an anti-mouse (NA931V) or anti-rabbit (NA934V) (both GE Healthcare; both as 1:10000-1:5000 dilution), for 1 h at RT on a shaker. Before development, membranes were washed again 3 x for 5-15 min with TBST. Development of membranes was performed with the Amersham ECL™ western blot detection reagent (GE Healthcare, Buckinghamshire, UK) and the Amersham Hyperfilm™ ECL (GE Healthcare). Exposure time ranged between 10 seconds and 15 minutes depending on the signal intensity of the protein of interest.

Table 8: Components of solutions used for western blot.

Name	Components
Transfer buffer	25 mM Tris-HCl, 192 mM Glycine, 20% (v/v) Methanol
Blocking solution	5% BSA or 5-% milk in TBST or PBST (depending on antibody)

5.6.5 Plasmids, cloning and transfection.

To generate CRISPR–Cas9 *PTPN11* constructs, the pX458 vector was used to clone in guide RNAs (gRNAs) targeting the *PTPN11* gene. The oligonucleotide sequences for both *PTPN11* gRNAs are listed in table 9.

Table 9: Guide RNA sequences used to generate CRISPR-Cas9 *PTPN11* knockout cells

	forward	reverse
<i>PTPN11</i> gRNA 1	CACCGGAGGAACATGACATCGCGG	AAACCCGCGATGTCATGTTCTCC
<i>PTPN11</i> gRNA 2	CCACGAACATGACATCGCGGAGGTG	AAACCACCTCCGCGATGTCATGTTCC

Forward and reverse oligos for each gRNA were annealed and ligated into the Bbs1-digested pX458 vector. Target cells were then transfected with the pX458-*PTPN11*-gRNA plasmids using polyethylenimine. Positively transfected cells expressing GFP were then FACS sorted as single cells in 96-well plates. Clones were grown out and analyzed for SHP2 status. SHP2-knockout clones were then named after the gRNA and clone name, for example, YAPC #1.1 refers to gRNA 1, clone 1. CRISPR-Cas9 cells were generated by Dr. Guus J. Heynen at the Max Delbrück Center for Molecular Medicine (MDC) in the Helmholtz Society, Berlin. SHP2 knockout cells were used to determine drug sensitivity in a long-term *in vitro* growth assay described in section 5.6.6 with the drugs and inhibitors described in section 5.7.5.

5.6.6 *In vitro* drug screening and colony formation assays

Cells were seeded into 24-well or 96-well plates ($1-4 \times 10^3$ cells per well, depending on the cell line) and allowed to adhere overnight in regular growth media. Cells were cultured in the absence or presence of drugs (see section 5.7.5), as indicated, and refreshed every 2–3 days until the end of the experiment (generally after 10–14 days). At the end of the experiment, culture media was removed, and the wells gently washed with once with cold PBS. Cells were simultaneously fixed and stained in solution containing 6% glutaraldehyde and 0.1% crystal violet for 30 minutes, the crystal violet solution was then suctioned off and the wells were washed 1-2 times with dH₂O. Plates were left to dry overnight and subsequently digitalized on an image scanner. Relative growth was quantified by densitometry using ImageJ software or via lysis of crystal violet in 10% acetic acid (200 μ l/well; 15 minutes on a shaker at RT) and subsequent absorbance measurement in a 96-well plate at 595 nm in Multiscan FC (Thermo) plate reader. For the absorbance measurement, 200 μ l dH₂O were put into all wells and then

50 µl of the crystal violet supernatant was added. For colony formation assays performed in 24-well plates, each well was measured in duplicate and two 24-well plates were combined onto one 96-well plate. All experiments were performed at least twice, and representative results are shown.

5.6.7 Quantitative analysis of drug synergy

Drug synergy was calculated using CompuSyn software (version 1.0), which is based on the median-effect principle and the combination index–isobologram theorem (Chou, 2010). CompuSyn software generates combination index values, where combination index < 0.75 indicates synergism, combination index = 0.75–1.25 indicates additive effects and combination index > 1.25 indicates antagonism (Manchado *et al.*, 2016). Following the instructions of the software, drug combinations at non-constant ratios were used to calculate the combination index in our study.

5.7. In vivo experiments

5.7.1. Anesthesia

An accepted inhalation anesthesia protocol was followed for adult mice. Induction was carried out by vaporization in a chamber at 4-5% Isoflurane and an oxygen flow of 0.5-1.0 l/min. During the surgical process, a 1-2% vaporization of the anesthetic was maintained, with the same oxygen flow. Next, analgesia was administered by subcutaneous injection of buprenorphine at a dose of 0.1 mg / kg. Before starting the surgery, made sure that the mouse completely loses consciousness by stimulating the abdominal skin with a pair of splinter forceps. The animal was placed in a dorso-ventral position on refractory material to avoid hypothermia and the medial lateral region was shaved in the upper left quadrant. The skin of the abdomen was cleaned with disinfectant (Despro Sol Colorless).

5.7.2 Orthotopic Transplantation of $Kras^{G12D/+}Trp53^{R172H/+}$ -derived murine tumor pieces

$Kras;Trp53^{R172H/+}$ tumor pieces were obtained from endogenous C57BL/6J $Kras;Trp53^{R172H/+}$ mouse models and subcutaneously transplanted (see description of subcutaneous transplantation in section 5.7.3) into the flanks of female C57BL/6J host mice for expansion. After 4 weeks, subcutaneous tumors from donor mice were harvested and chopped into ~40 mm³ pieces and orthotopically transplanted into pancreata of 8-week-old female and weight matched 18- 20 g male C57BL/6J mice. A 1-cm longitudinal skin incision was made on the left

upper axillary region of the abdomen of the mouse, the peritoneum was opened, and the pancreas was gently pulled out and exposed the entire pancreatic body together with spleen to the outside by using a pair of blunt-nose forceps. A piece of 40-mm³ tumor-block was implanted by a knot surrounding the pancreas tail at ~2 mm from the end of the tail using a string of 6-0 absorbable suture. The pancreas was put back into the abdominal cavity gently and the surgical opening was closed using a 6-0 absorbable surgical suture. The incision was closed using 1-2 9 mm staples. After 2 weeks, mice were randomly assigned to groups and either sacrificed as baseline or treated with inhibitors or vehicle as described in section 5.7.7.

5.7.3 Human PDAC specimens and patient-derived tissue xenografts

For the patient-derived xenograft therapy trial, samples (all KRAS^{G12D}) were procured and expanded *in vivo* under a Material Transfer Agreement at the Universidad Autónoma de Madrid and with approval of the ethical review board (CEI 60-1057-A068) and the Comunidad de Madrid (Red PROEX 335/14). For subcutaneous transplantation of patient-derived tumor tissue, a 5-10mm mid-lateral skin incision was made. A single section of tumor (~ 50 mm³) embedded in Matrigel was implanted under the skin. The incision was closed using 1-2 9 mm staples. The mouse skin was cleaned with buffered saline and then with 70% ethanol. A maximum of two implants was made per mouse (right and left flanks). Volumes were evaluated every 2–3 days by caliper measurements and the approximate volume (V) of the mass was estimated using the formula $V = D \times d^2/2$, with D being the major tumor axis and d being the minor tumor axis. Established tumors (average volume at inclusion: 150–300 mm³) were randomly assigned to trial arms and treated as specified below. Experiments were terminated once vehicle control tumors reached a critical size at the ethical end point (V = 2,000–4,000 mm³). End-of-treatment tumor material was either fixed in pfa for H&E staining and histological analysis or snap frozen in liquid nitrogen and stored at –80 °C for protein analysis.

Transplantation procedures described in sections 5.7.1 to 5.7.3 and subsequent drug treatment of the transplanted mice was performed by Dr. Laura Ruiz-Cañas at the laboratory of Dr Bruno Sainz Anding at the Instituto de Investigaciones Biomédicas "Alberto Sols" (IIBM) at the Universidad Autónoma de Madrid.

5.7.4 Magnetic resonance imaging (MRI).

MRI imaging of *Kras;Trp53^{-/-}* mice was started at an age of 24-37 days and repeated every week (see *in vivo* therapy treatment schedules). Sedation was achieved via continuous inhalation of 2% isoflurane (Abbott) in 1,6% O₂ using a veterinary anesthesia system (Vetland Medical). Body temperature was maintained and monitored, and eyes were protected by eye ointment. Image acquisition was achieved using a mouse 3T coil inside a preclinical 3T nano scan PET/MR (Mediso) and a T2 weighted fast spin echo sequence (resolution: 0.3×0.3×1

mm³, ~25 slices, echo time 55,52ms; repetition time 3000ms) or a microscopy surface coil inside a 3.0 T clinical device (Philips) and an axial multislice T2-weighted turbo spin echo sequence (resolution: 0.3 × 0.3 × 0.7 mm³, 30 slices, echo time = 90 ms, repetition time > 3 s) respectively. Solid tumor volumes were calculated using OsiriX Lite DICOM viewer (Pixmeo) or Flywheel DICOM viewer by summing truncated pyramid volumes between tumor areas on vicinal slices.

5.7.5 Drugs and inhibitors.

Trametinib, selumetinib, pictilisib, paclitaxel, bazedoxifene and SC144 were purchased from Selleckchem, gemcitabine was provided by the Hospital Pharmacy of Klinikum Rechts der Isar (Technische Universität München), and GS493 and SHP099 were synthesized and kindly provided by M.N., Medicinal Chemistry, Leibniz-Forschungsinstitut für Molekulare Pharmakologie, Berlin, Germany.

For *in vitro* assays: SHP2 inhibitor (RMC-4550) and ERK inhibitor (LY3214996) were purchased from MedKoo Biosciences. For *in vivo* studies: SHP2 inhibitor RMC-4550 was kindly provided by Revolution Medicines, Redwood City, California U.S.A. ERK inhibitor LY3214996 was kindly provided by Eli Lilly and Company, Indianapolis IN 46285 U.S.A.

5.7.6 *In vivo* drug combination dose finding escalation.

Dose finding was established according to modified “3+3” scheme. The SHP2 inhibitor RMC-4550 (Revolution Medicines) was diluted in 50 mM Sodium Citrate Buffer pH = 4 with 1% Hydroxyethylcellulose (Sigma-Aldrich), 0,25% Tween (Sigma-Aldrich) and 0,05 % Antifoam A concentrate (Sigma-Aldrich). The ERK inhibitor LY3214996 (Eli Lilly and Company) powder was dissolved in dH₂O (Braun) with 1% Hydroxyethylcellulose (Sigma-Aldrich), 0,25% Tween (Sigma-Aldrich) and 0,05 % Antifoam A concentrate (Sigma-Aldrich). Non-tumor-bearing mice were put on continuous oral administration of both drugs over 14 days (NSG mice; *Kras*^{G12D}, *p53*^{flox/flox}; *p53*^{flox/flox}; *p53*^{flox/wt} or wild-type mice from *Kras*^{G12D}; *p48-Cre*; *p53*^{flox/flox} litters). Mice were weighed and scored daily for activity, appearance, and body condition. According to a modified “3+3” design (Huang *et al.*, 2007; Le Tourneau, Lee and Siu, 2009), mouse cohorts consisting of 3 animals were given an initial combination dose (d5), followed by increased dose 7 as no side effects were observed in all 3 mice. Up to six mice were assigned to one dose. If combination dose showed side effects in 1/6 of mice, the dose was designated as an admissible dose, opening next dose level for testing. If the dose-limiting toxicity was observed in 2/6 mice, the combination was accepted as a maximum tolerated dose, closing higher doses for testing. If more than two of the six mice experience dose-limiting toxicity, the dose was down staged. The following dose combinations were administered: dose 5 (10 mg/ kg RMC

4550 + 75 mg/ kg LY3214996), dose 7 (30 mg/ kg RMC 4550 + 75 mg/ kg LY3214996), dose 8 (10 mg/ kg RMC 4550 + 100 mg/ kg LY3214996) and dose 9 (30 mg/ kg RMC 4550 + 100 mg/ kg LY3214996). One cohort was administered vehicle to monitor gavage-based side effects.

5.7.7 *In vivo* therapy dosing

5.7.7.1 MEK + SHP2 inhibition

For *in vivo* application in *Kras;Trp53^{-/-}* and NSG mice, trametinib was diluted in 0.5% hydroxypropyl methylcellulose (Sigma-Aldrich) and 0.2% Tween 80 (Sigma-Aldrich) in water. GS493 was dissolved in Kolliphor EL (Sigma-Aldrich) and applied in an emulsion of 10% Kolliphor EL, 10% ethanol and water. Trametinib (1 mg per kg) was administered by oral gavage every other day, whereas GS493 was injected intraperitoneally (30 mg per kg, same schedule) (Lan *et al.*, 2015). *In vivo* dosing and MRI scans were performed together with Dr. Dietrich A. Ruess.

5.7.7.2 ERK + SHP2 inhibition

For *in vivo* application in KCP mice, human cell line xenografts, PDX xenografts and orthotopically transplanted KCPmut mice, dose 8 (10 mg/ kg RMC 4550 + 100 mg/ kg LY3214996) was given by oral gavage as described above. The two compounds were combined following different schedules, in order to identify the optimal treatment regimen (maximum anti-tumor effect with minimum toxicity): continuous administration (daily) of both drugs (Arm A), administration of both drugs 5 days on/ 2 days off (Arm B), or continuous administration of RMC 4550 plus LY3214996 every other day (Arm C), or continuous administration of RMC 4550 plus LY3214996 5 days on/ 2 days off (Arm D). As controls, mice were treated daily with vehicle or with monotherapy. Monotherapy was scheduled either RMC-4550 continuous (Arm E) or LY3214996 (Arm F).

5.8 Statistics

The statistical software Prism 5 (GraphPad Software, Inc.) was used for analysis. Kaplan–Meier survival curves were calculated from all individual survival times of mice from the different genotype cohorts. Curves were compared by log-rank (Mantel–Cox) test to detect significant differences between the groups. If not specified differently, data is displayed as Mean \pm standard deviations (SD). Appropriate statistical tests were performed and are mentioned in the figure legends for each graph. Statistical significance was set at * $p = 0.01$ to 0.05, ** $p = 0.001$ to 0.01, *** $p < 0.001$ and not significant (n.s.) $p > 0.05$.

6. RESULTS

6.1 *IL6st* deletion impedes pancreatic carcinogenesis in mice with *Kras* and *Kras;Trp53^{-/-}* background

The initial step to investigate the role of the gp130 signaling axis in pancreatic carcinogenesis was to create a *Ptf1a-Cre*-driven *Kras;IL6st^{-/-}* mouse line and compare its phenotype to gp130 expressing *Kras* mice at different points in time, i.e., 9, 18, 24 and 36 weeks as well as at a survival endpoint, i.e., when mice had to be sacrificed due to signs of severe morbidity.

Figure 2A shows representative H&E-stained slides of *Kras* and *Kras;IL6st^{-/-}* mice at 9 and 36 weeks of age. Compared to *Kras* mice, the carcinogenic process was delayed in *Kras;IL6st^{-/-}* mice. This was especially notable at the age of 36 weeks, where *Kras;IL6st^{-/-}* mice showed mostly ADM structures, reactive ducts, and low grade PanIN lesions compared to *Kras* mice which showed mostly low and high grade PanIN lesions and in a few cases already showed localized carcinomas. Pancreas-specificity of the *IL6st* gene recombination and thus gp130 protein deletion was confirmed via PCR and Western Blot in the pancreas and liver of 9 and 36-week-old mice (**Figure 2B-C**).

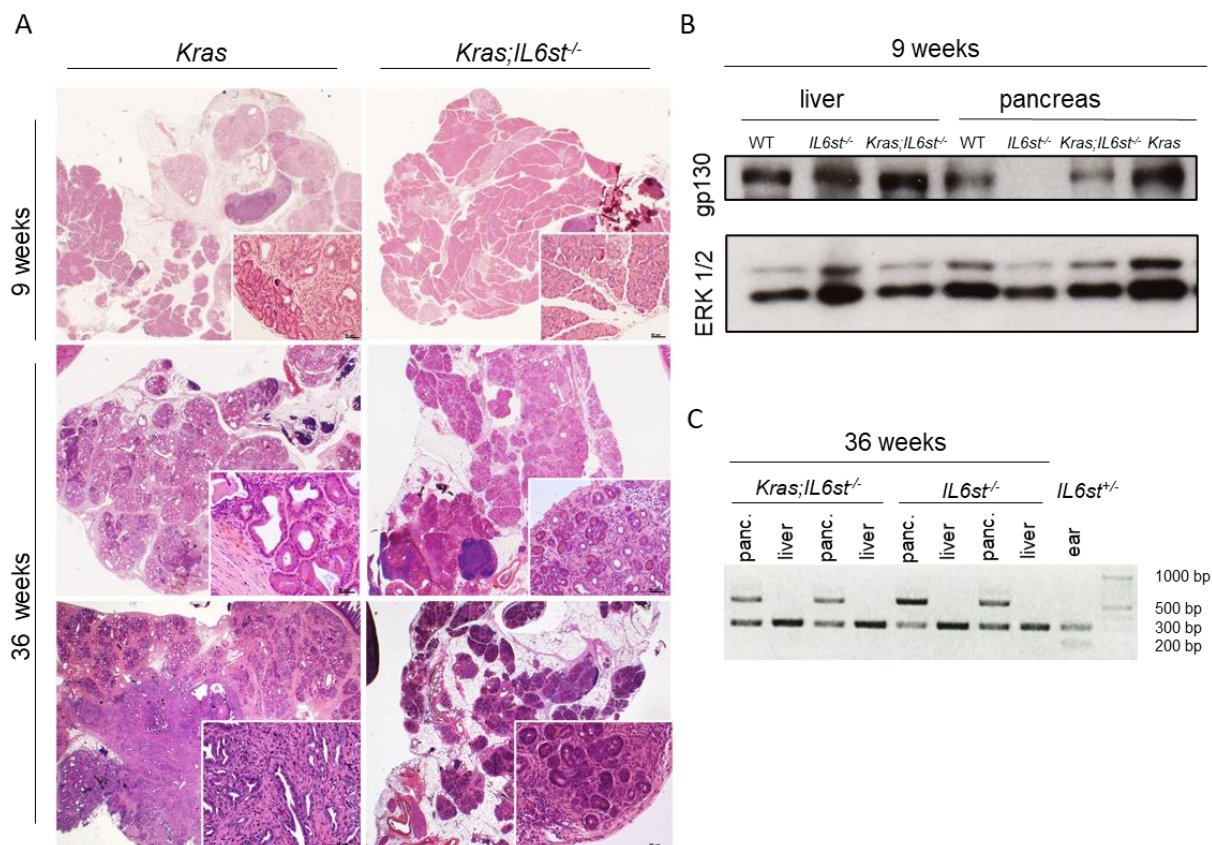


Figure 2: Pancreas-specific deletion of gp130 decelerates pancreatic carcinogenesis in mice with pancreas-specific *Kras*^{G12D}-expression. (A) Representative H&E-stained tissue sections of 9- and 36-week-old *Kras* and *Kras;IL6st^{-/-}* mice at 10x and 200x magnification (insets). 9-week-old mice: *Kras* (n = 4) *Kras;IL6st^{-/-}* (n = 2); 36-week-old mice: *Kras* (n = 4) *Kras;IL6st^{-/-}* (n = 3); (B) Western Blot of pancreas and liver tissues of 9-week-old *IL6st^{flx/flx}*, *IL6st^{-/-}*, *Kras;IL6st^{-/-}* and *Kras* mice. ERK 1/2 was used as loading control. (C) *IL6st*-recombination PCR of pancreas and liver tissue from 36-week-old *Kras;IL6st^{-/-}* and *IL6st^{-/-}* mice. Pancreatic tissues show both the band for the floxed (280 bp) gene as well as for the recombined gene (~500bp), whereas liver tissues only show the floxed band. A lysate from ear tissue of an *IL6st^{+/-}* mouse was used as control.

Preliminary data of 9-week-old mice revealed that gp130-deletion led to reduced pSTAT3 expression and a decrease in proliferating Ki67-positive cells as shown in **Figure 3**. In contrast to *Kras* mice, which showed pSTAT3-positive cells in ADM and PanIN lesions as well as in the surrounding stroma, ADM and PanIN lesions of *Kras;IL6st^{-/-}* mice were almost completely pSTAT3 negative and only stromal and immune cells were pStat3 positive.

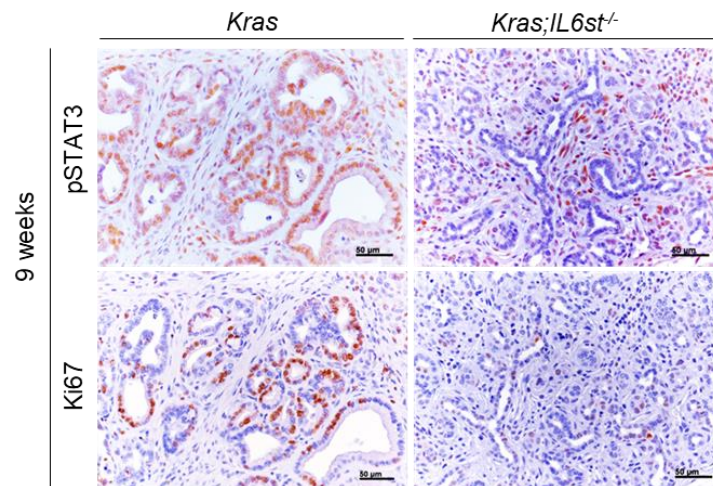


Figure 3: Pancreas-specific gp130 deletion leads to a decrease in STAT3 phosphorylation as well as a decrease in proliferation. Representative IHC-stained tissue sections of 9-week-old *Kras* (n = 2) and *Kras;IL6st^{-/-}* (n = 2) mice at 200x magnification. *Kras;IL6st^{-/-}* pancreata show reduced numbers of pSTAT3- and Ki67-positive cells compared to *Kras* mice of the same age. Scale bars represent 50 µm.

Analysis of moribund *Kras* and *Kras;IL6st^{-/-}* survival mice showed that loss of gp130 by *IL6st*-deletion led to a significant decrease in tumor incidence from 56% in *Kras* to 19% in *Kras;IL6st^{-/-}* mice (**Figure 4A**) but did not prolong survival. In fact, *Kras* mice had a median survival of 444 days compared to a median survival of 338 days in *Kras;IL6st^{-/-}* mice (**Figure 4B**). This is in contrast to observations made in the more aggressive p53-deficient *Kras;Trp53^{-/-}* model of pancreatic carcinogenesis, where pancreas-specific *IL6st*-deletion did not reduce the tumor incidence (data not shown) but led to significantly longer survival, with a median survival of 79 days in *Kras;Trp53^{-/-}IL6st^{-/-}* compared to a median survival of 61 days in *Kras;Trp53^{-/-}* mice (**Figure 4C**).

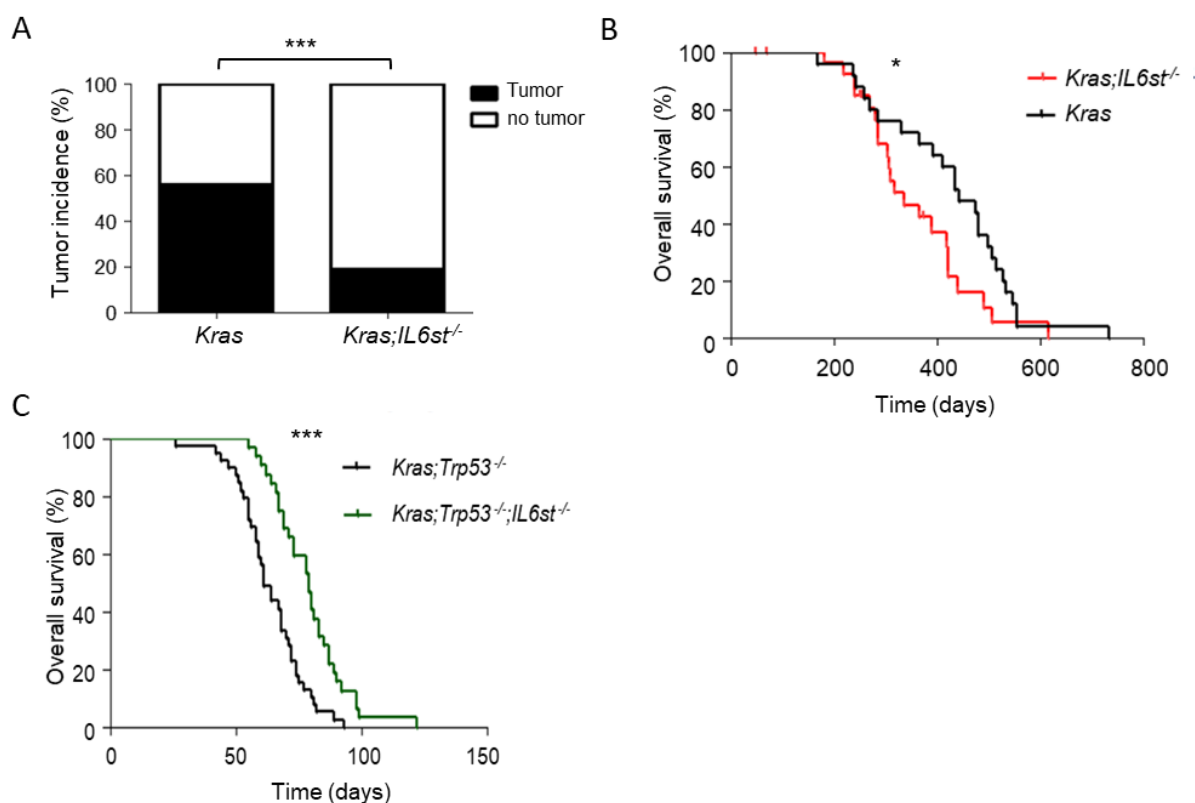


Figure 4: Pancreas-specific gp130 deletion leads to significantly decreased tumor incidence in *Kras;IL6st^{-/-}* and prolonged survival in *Kras;Trp53^{-/-}IL6st^{-/-}* mice. (A) Tumor incidence in moribund *Kras* mice compared to *Kras;IL6st^{-/-}* mice. The number of tumor-bearing mice decreased from 14 in 25 (*Kras*) to 5 in 26 (*Kras;IL6st^{-/-}*) mice. Significance (***) $p < 0.0001$ was determined with Fisher's exact test. **(B)** Kaplan-Meier analysis of overall survival in *Kras* mice ($n = 25$) compared to *Kras;IL6st^{-/-}* mice ($n = 28$). Median survival was reduced from 444 days in *Kras* mice compared to 338 days in *Kras;IL6st^{-/-}* mice. Significance (* $p = 0.042$) was determined with Log-rank (Mantel-Cox) Test. **(C)** Kaplan-Meier analysis of overall survival in *Kras;Trp53^{-/-}* mice ($n = 39$) compared to *Kras;Trp53^{-/-}IL6st^{-/-}* mice ($n = 32$). Median survival was increased from 61 in *Kras;Trp53^{-/-}* mice compared to 79 days in *Kras;Trp53^{-/-}IL6st^{-/-}* mice. Significance (***) $p < 0.0001$ was determined with Log-rank (Mantel-Cox) Test.

6.2 Expression of a constitutively active, transgenic, gp130 receptor accelerates pancreatic carcinogenesis and decreases the life span of mice in a *Kras*^{G12D}-driven model of murine pancreatic cancer

To further our understanding about the role of gp130-mediated signaling in pancreatic cancer, and to possibly confirm the previous results, we decided to use a murine model of gp130 overactivation. In the so-called Lgp130 model developed by the group of Prof. Rose-John in Kiel (Stuhlmann-Laeisz *et al.*, 2006) a chimeric gp130 protein, named Lgp130, consistent of the 39-amino acid Jun leucine zipper sequence of the human transcription factor Jun (O'Shea *et al.*, 1989) and the transmembrane and cytoplasmic domains of the human gp130-receptor. Lgp130 molecules are able to dimerize independent of ligand binding, leading to constitutive, cytokine-independent activation of gp130 signaling. The genetic construct for the expression of Lgp130 was cloned into the ROSA26 locus so that our mice express both the normal murine gp130 receptor as well as the constitutively active Lgp130.

Analysis of 4- and 9-week-old timepoint mice showed a drastically accelerated progression of pancreatic carcinogenesis in *Kras;Lgp130*^{ki/+} mice compared to *Kras* mice of the same age. While 4-week-old *Kras* mice showed mostly intact acini or ADM structures, pancreata of 4-week-old *Kras;Lgp130*^{ki/+} did not have any intact acini left and showed a high amount of PanIN lesions. This phenotype worsened with age and at 9 weeks of age *Kras;Lgp130*^{ki/+} mice had a high number of high-grade lesions, cysts, and carcinoma (**Figure 5A**). Congruent with the literature (Stuhlmann-Laeisz *et al.*, 2006; Schumacher *et al.*, 2020) and the results shown in **Figure 3**, pancreas-specific expression of constitutively active gp130 led to a drastic increase in pSTAT3 expression, and induction of proliferation as shown by an increase in Ki67-positive cells in pancreata of *Kras;Lgp130*^{ki/+} mice compared to pancreata of age-matched *Kras* mice (**Figure 5B**). The drastic acceleration of pancreatic carcinogenesis was also shown to result in significantly decreased survival in both *Lgp130*-heterozygous (*Kras;Lgp130*^{ki/+}) as well as *Lgp130*-homozygous (*Kras;Lgp130*^{ki/ki}) mice compared to *Kras* mice. With median survival of 63.5 and 43.5 days respectively compared to 444 days (**Figure 5C**)

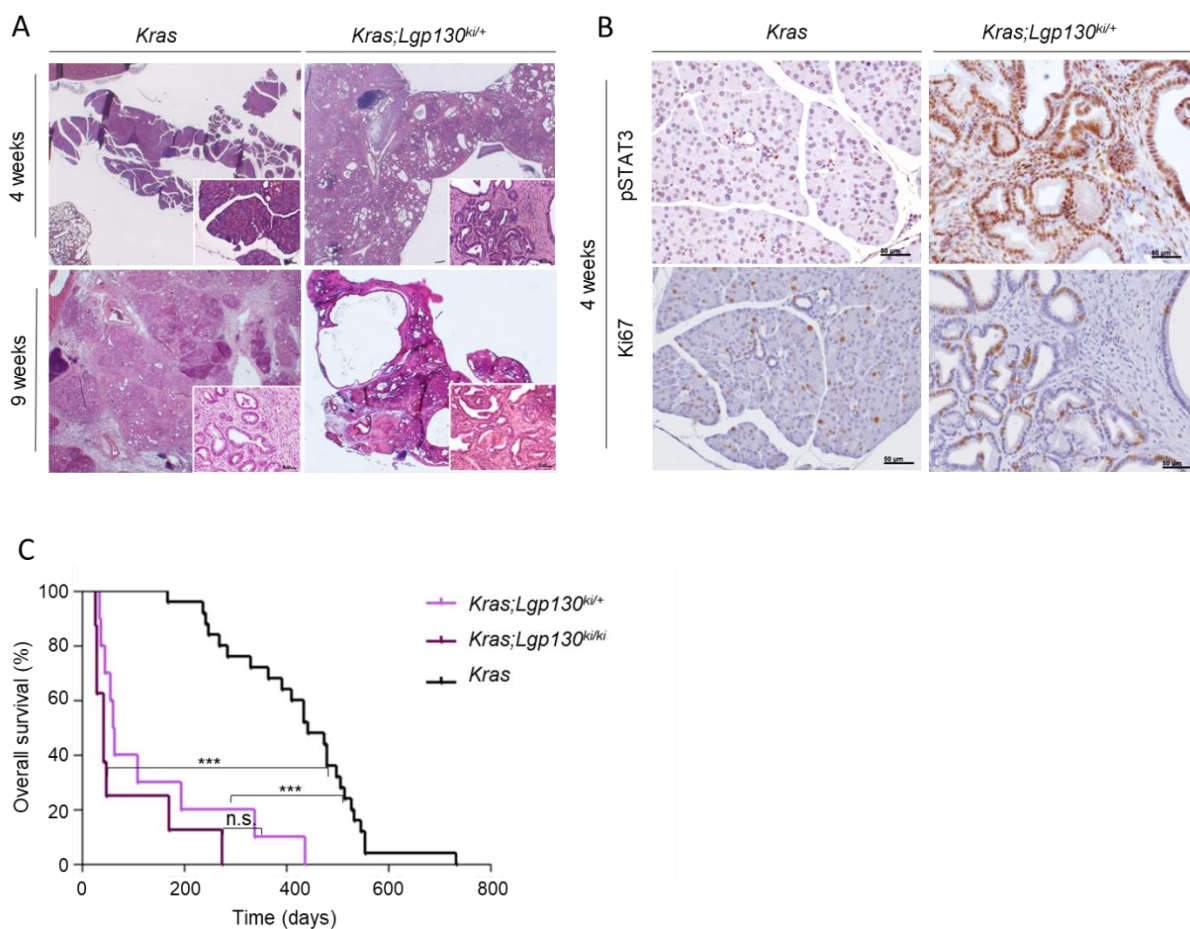


Figure 5: Pancreas-specific expression of constitutively active gp130 accelerates pancreatic carcinogenesis and drastically reduces the life span of *Kras*^{G12D}-expressing mice. (A) Representative H&E-stained tissue sections of 4- and 9-week-old *Kras* and *Kras;Lgp130^{ki/+}* mice at 10x and 200x magnification (insets). 4-week-old mice: *Kras* (n = 2) *Kras;Lgp130^{ki/+}* (n = 2); 9-week-old mice: *Kras* (n = 4) *Kras;Lgp130^{ki/+}* (n = 4). **(B)** representative IHC-stained tissue sections of 4-week-old *Kras* (n = 2) and *Kras;Lgp130^{ki/+}* (n = 2) mice at 200x magnification. *Kras;Lgp130^{ki/+}* pancreata show increased numbers of pSTAT3 and Ki67-positive cells compared to *Kras* mice of the same age. Scale bars represent 50 μ m. **(C)** Kaplan–Meier analysis of overall survival in *Kras;Lgp130^{ki/+}* mice (n = 10) and *Kras;Lgp130^{ki/ki}* (n = 8) compared to *Kras* mice (n = 25). Median survival was decreased from 444 days in *Kras* mice to 63.5 days in *Kras;Lgp130^{ki/+}* mice and 43.5 days in *Kras;Lgp130^{ki/ki}* mice. Significance (***) $p < 0.0001$ and n.s. $p = 0.150$; n.s.: not significant) was determined with Log-rank (Mantel-Cox) Test.

6.3 Pancreas-specific gp130 deletion rescues the phenotype of accelerated carcinogenesis and shortened survival seen in *Kras;Socs3*^{-/-} mice.

As described in one of the previous publications by our group (Lesina *et al.*, 2011), led the homozygous deletion of *Socs3* to significantly accelerated pancreatic carcinogenesis, reduced tumor latency, and a shortened live span compared to *Kras* mice. Here we show that additional pancreas-specific deletion of the *IL6st* (*Kras;Socs3*^{-/-};*IL6st*^{-/-}) was able to rescue this dramatic phenotype. As **Figure 6A** shows, median tumor latency was increased from 63 days in *Kras;Socs3*^{-/-} to 498 days in *Kras;Socs3*^{-/-};*IL6st*^{-/-} mice and the median survival, that had been shortened to 106 days by *Socs3* deletion was increased to 498 days in *Kras;Socs3*^{-/-};*IL6st*^{-/-} mice (**Figure 6B**).

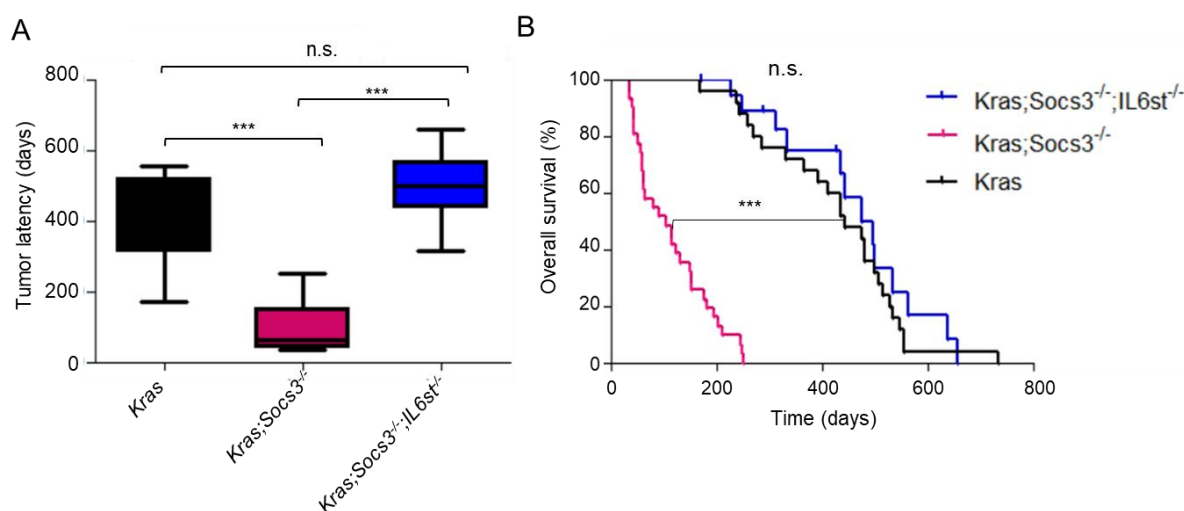


Figure 6: Pancreas-specific gp130 deletion decelerates carcinogenesis and extends survival compared to *Kras;Socs3*^{-/-} mice. (A) Tumor latency in *Kras* (n = 14), *Kras;Socs3*^{-/-} (n = 11) and *Kras;Socs3*^{-/-};*IL6st*^{-/-} mice (n = 11). Median latency 478.5, 63 and 498 days, respectively. Whiskers depict minimum and maximum; Significance (***) $p < 0.0001$ and n.s. $p = 0.16$; n.s.: not significant) was determined with one-way ANOVA and Tukey's Multiple Comparison Test. **(B)** Kaplan–Meier analysis of overall survival in *Kras* (n=25) and *Kras;Socs3*^{-/-} mice (n = 31) compared to *Kras;Socs3*^{-/-};*IL6st*^{-/-} mice (n = 20). Median survival was decreased from 444 days in *Kras* mice to 106 days in *Kras;Socs3*^{-/-} mice and increased to 498 days in *Kras;Socs3*^{-/-};*IL6st*^{-/-} mice. Significance (***) $p < 0.0001$ and n.s. $p = 0.372$; n.s.: not significant) was determined with Log-rank (Mantel-Cox) Test.

6.4 gp130 as therapeutic target in PDAC

6.4.1 *Kras;Trp53*^{-/-} cells are sensitive to gp130 inhibition

Based on the previously described results and the apparent relevance of gp130 and gp130-mediated signaling in pancreatic carcinogenesis, we decided to target the pathway therapeutically with two different gp130 inhibitors. Bazedoxifene is known as a selective estrogen modulator and is commonly used for the prevention of osteoporosis. However, it was recently discovered as a novel small molecular inhibitor of gp130/IL-6 and gp130/IL-11 protein-protein interaction (Li *et al.*, 2014; Wu *et al.*, 2016). SC144 is a newly discovered first-in-class orally active small-molecule gp130 inhibitor which induces gp130 phosphorylation, deglycosylation, and subsequent internalization and degradation (Xu *et al.*, 2013).

As a first step we performed short- (72 h) and long-term (10-14 days) growth inhibition experiments to determine the approximate concentration at which bazedoxifene and SC144 inhibit cell growth by 50% (IC₅₀) (data not shown). Each experiment was performed once in the *Kras;Trp53*^{-/-} cell line K1654 (later termed cell line #1 in **Figure 8** and **9**). The IC₅₀ value calculated from both experiments was 3.325 μ M for bazedoxifene and 0.3825 μ M for SC144. We then analyzed the effects of both inhibitors on gp130 signaling over time by treating K1654 cells with 3.125 μ M bazedoxifene or 0.3125 μ M SC144 for 6, 24, 48 or 72 hours and subsequently performing western blot analysis (**Figure 7**). Neither of the two inhibitors induced a sustained reduction of gp130 protein levels. Both inhibitors were able to markedly reduce STAT3 activity, measured as levels of tyrosine 705 phosphorylated STAT3, over the duration of 72 hours, but had no effect on extracellular-signal regulated kinase (ERK) phosphorylation.

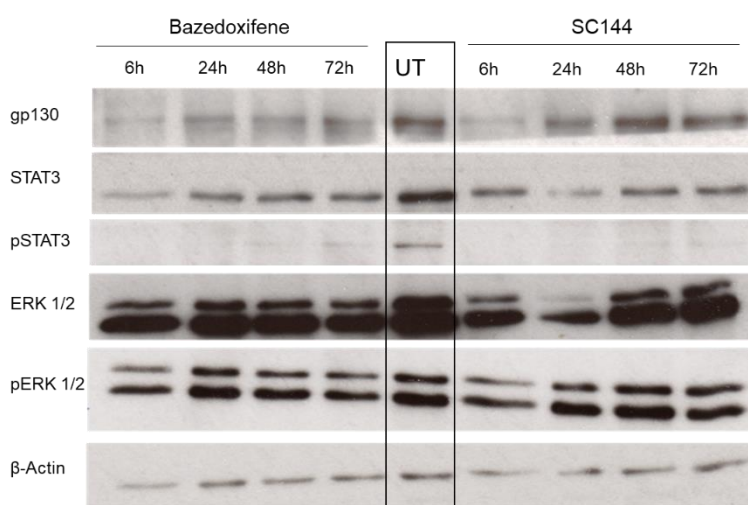


Figure 7: The gp130 inhibitors bazedoxifene and SC144 can robustly inhibit STAT3 phosphorylation but have no impact on ERK 1/2 phosphorylation. The *Kras;Trp53*^{-/-} cell line K1654 was treated with 3.125 μ M bazedoxifene or 0.3125 μ M SC144 for the indicated time. The effect of both inhibitors was compared to an untreated control (UT). Both inhibitors inhibit STAT3 phosphorylation but have no impact on pERK. β -Actin was used as loading control. (n = 1)

6.4.2 gp130 inhibition in combination with classic chemotherapy

We then decided, based on the promising results described above as well as literature reports about the benefit of combined chemotherapy and IL-6 or IL-6R inhibition (Goumas *et al.*, 2015; Long *et al.*, 2017), to analyze the effects of bazedoxifene or SC144 in combination with gemcitabine or paclitaxel, two chemotherapeutic agents commonly used in the treatment of PDAC patients (Schulz and Algül, 2019; Corrie *et al.*, 2020). We performed a colony formation assay and treated 3 different *Kras;Trp53^{-/-}* cell lines over a period of 10 to 14 days. Experiments were repeated independently at least two times each, with similar results. **Figure 8** shows, that although all three cell lines differed in their sensitivity towards both the monotreatments as well as the combinations, none of the tested cell lines was completely unresponsive. The most consistently beneficial combination therapy, with consistently additive and in several cases even synergistic effect, was the combination of bazedoxifene plus paclitaxel.

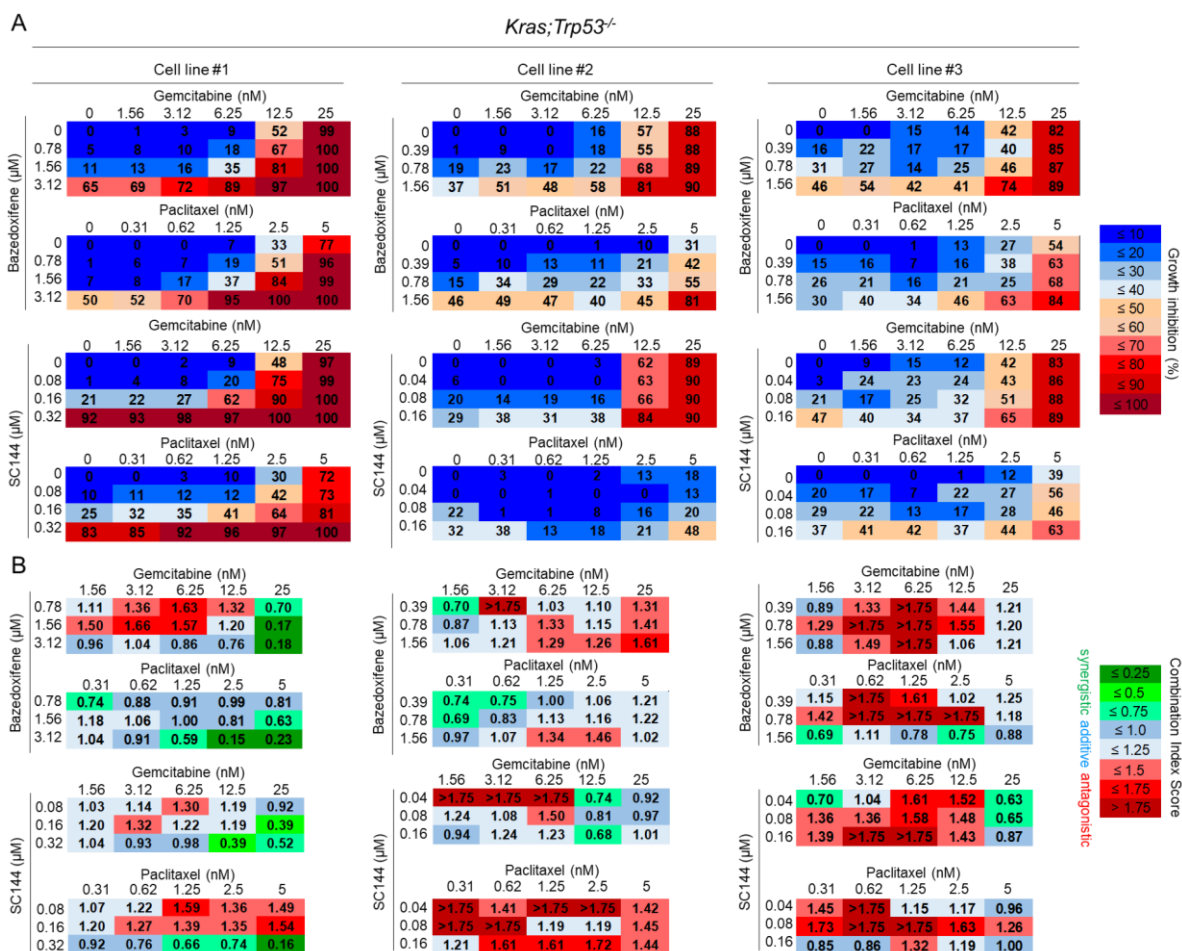


Figure 8: gp130 inhibition in combination to chemotherapy leads to increased growth inhibition. (A) Long-term (10-14d) colony formation assays with murine *Kras;Trp53^{-/-}* PDAC cell lines, classic chemotherapeutic drugs (gemcitabine, paclitaxel) were combined with the gp130 inhibitors bazedoxifene or SC144 at the concentrations indicated. Representative results are shown, box-matrices depict quantification of growth inhibition in relation to untreated control wells. (n ≥ 2) (B) Calculation of the combination index scores with the growth inhibition values determined in (A) via CompuSyn software shows that gp130 inhibition in combination with gemcitabine or paclitaxel has additive and, in some cases, even synergistic effects on PDAC cells. CI = 0.75–1.25 (shades of blue) indicates additive effects and CI > 1.25 (shades of red) indicates antagonism.

6.4.3 gp130 inhibition in combination with MEK targeted therapy

We have shown that both gp130 inhibitors were able to markedly reduce STAT3 phosphorylation in murine *Kras;Trp53^{-/-}* cells but did not reduce the levels of pERK. Increased ERK phosphorylation is a consequence of uninhibited KRAS activity mediated by *KRAS* mutations. In the absence of direct KRAS inhibitors, small molecular inhibitors targeting RAS downstream effector kinases like rapidly accelerated fibrosarcoma (RAF) or MAPK/ERK-Kinase (MEK) were considered to be an effective way to inhibit ERK signaling (Abe *et al.*, 2011; Cox *et al.*, 2014; Hayes *et al.*, 2016). Because intrinsic and acquired resistance to MEK inhibition is a common phenomenon in *KRAS*-mutant cancer (Samatar and Poulikakos, 2014), MEK inhibitors have thus far failed to provide clinical benefit to PDAC patients (Infante *et al.*, 2014). However, combining MEK inhibitors with other targeted therapies might help to overcome these limitations.

Thus, we were interested in the effect of combined gp130/STAT3 and MEK inhibition and decided to treat the three previously used *Kras;Trp53^{-/-}* cells (see section 6.4.2, **Figure 8**) with bazedoxifene or SC144 in combination with the MEK inhibitor trametinib. While cell line #1 was very susceptible to the combination and showed a synergistic effect in 30% (bazedoxifene) to 50% (SC144) of the tested doses, the other two cell lines showed additive effects at best.

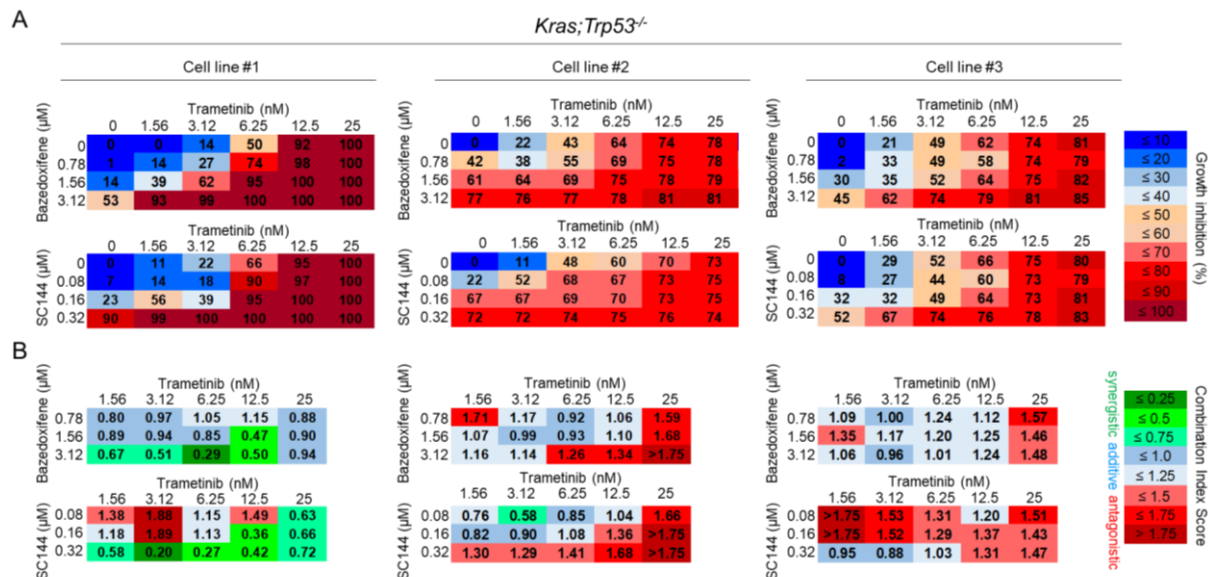


Figure 9: gp130 inhibition in combination with MEK inhibition leads to increased growth inhibition. (A) Long-term (10-14d) colony formation assays with murine *Kras;Trp53^{-/-}* PDAC cell lines, the MEK inhibitor trametinib was combined with the gp130 inhibitors bazedoxifene or SC144 at the concentrations indicated. Representative results are shown, box-matrices depict quantification of growth inhibition in relation to untreated control wells. ($n \geq 2$) (B) Calculation of the combination index scores with the growth inhibition values determined in (A) via CompuSyn software shows that gp130 inhibition in addition to MEK inhibition has additive and, in some cases, even synergistic effects on PDAC cells. $CI < 0.75$ (shades of green) indicates synergism, $CI = 0.75-1.25$ (shades of blue) indicates additive effects and $CI > 1.25$ (shades of red) indicates antagonism.

6.5 Pancreas-specific deletion of the gp130-downstream effector SHP2 abrogates pancreatic tumor formation in *Kras* and *Kras;Trp53^{-/-}* mice

Having thus analyzed the relevance of the gp130 receptor and gp130-mediated signaling in the development of *KRAS*-driven PDAC and its possible benefits in PDAC therapy, we decided to further investigate the role of effector molecules downstream of gp130. STAT3 and its inhibitor SOCS3 had been previously investigated by our group and others (Corcoran *et al.*, 2011; Lesina *et al.*, 2011) so we decided to investigate the role of the phosphotyrosine kinase SHP2. SHP2 was of special interest to us due to its dual role as JAK/STAT pathway inhibitor and RAS/MAPK and PI3K/AKT pathway activator (Schaper and Rose-John, 2015).

SHP2 is encoded by *PTPN11*, so to be able to investigate the role of SHP2 in *KRAS*-driven PDAC, we developed murine *Kras* and *Kras;Trp53^{-/-}* mouse lines with additional pancreas-specific *Ptpn11* deletion. Carcinogenesis in SHP2 proficient compared to SHP2 deficient mice was analyzed at different time points and at the morbidity associated survival endpoint.

Figure 10A shows representative H&E-stained tissue sections of 36-week-old *Kras* and *Kras;Ptpn11^{-/-}* mice. While pancreata of 36-week-old *Kras* mice have almost no intact acini left and consist mostly of PanIN and PDAC lesions, age matched *Kras;Ptpn11^{-/-}* mice do not have PanIN lesions at all. Pancreas-specific *Ptpn11* deletion significantly reduced the tumor incidence (data not shown) and led to significantly prolonged survival in *Kras;Ptpn11^{-/-}* (**Figure 10B**) and *Kras;Trp53^{-/-};Ptpn11^{-/-}* mice (**Figure 10C**)

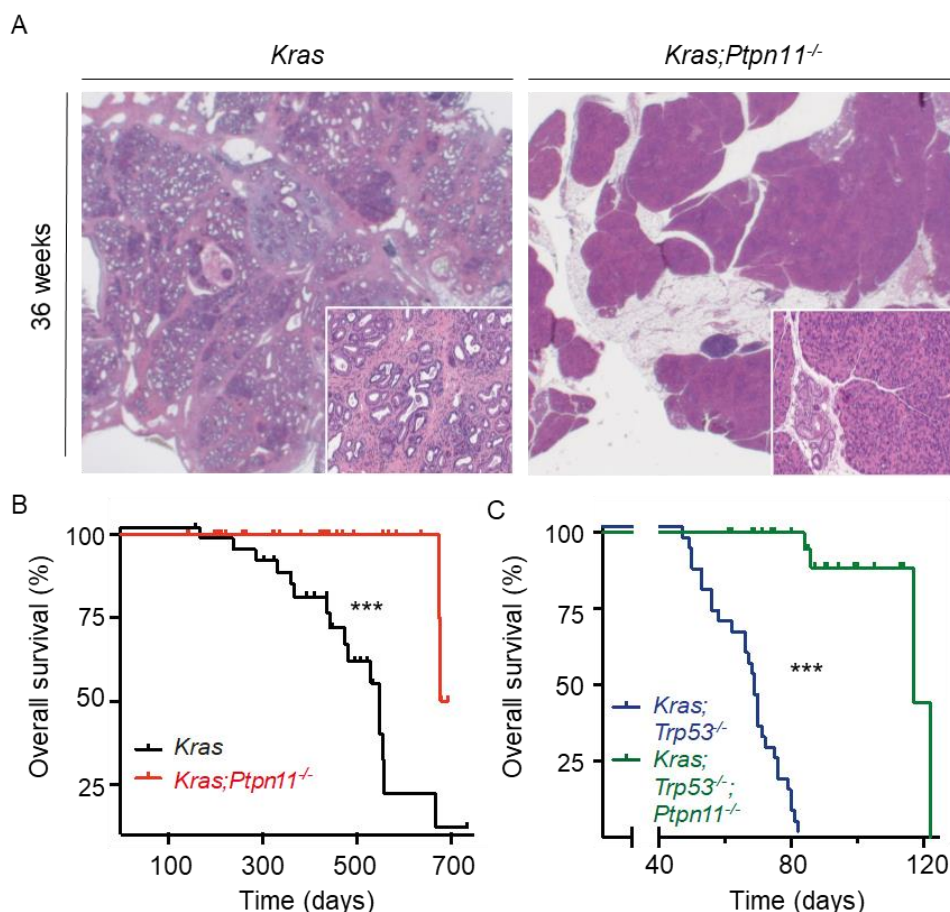


Figure 10: Pancreas-specific deletion of the SHP2-encoding gene *Ptpn11* profoundly inhibits *KRAS*^{G12D}-driven pancreatic carcinogenesis and leads to significantly prolonged survival in both *Kras;Ptpn11^{-/-}* and *Kras;Trp53^{-/-};Ptpn11^{-/-}* mice. (A) Representative H&E-stained sections of pancreata from *Kras* ($n = 5$) and *Kras;Ptpn11^{-/-}* mice ($n = 6$) at 36 weeks of age with similar results. Pictures taken at 10x and 100x magnification (insets). (B) Kaplan–Meier analysis of overall survival of *Kras* mice ($n = 32$, median:548 days) and *Kras;Ptpn11^{-/-}* mice ($n = 30$, median: 685.5 days). Ticks indicate censored mice that were euthanized for decline in clinical condition, but without microscopic evidence of PDAC. Significance (***) $p = 0.0002$) was determined by Log-rank (Mantel–Cox) Test (C) Kaplan–Meier analysis of tumor-free survival of *Kras;Trp53^{-/-}* mice ($n = 29$, median: 69 days) and *Kras;Trp53^{-/-};Ptpn11^{-/-}* mice ($n = 28$, median = 117 days). Ticks indicate censored mice that were euthanized due to decline in clinical condition, without histological evidence of PDAC. Significance (***) $p < 0.0001$) was determined by Log-rank (Mantel–Cox) Test. (Data was published in (Ruess *et al.*, 2018); experiments were performed by D.A. Ruess.)

6.6 SHP2 is expressed and phosphorylated to different extents in human pancreatic cancer tissues and human PDAC cell lines

The drastic inhibition of murine pancreatic carcinogenesis shown in **Figure 10** led us to believe that SHP2 might also play an important role in human PDAC and might thus be of clinical relevance. **Figure 11** shows that SHP2 is differentially expressed (**Figure 11A-B**) and activated (**Figure 11B**), as shown by the levels of SHP2 phosphorylated at tyrosine 542 (Lu, Shen and Cole, 2003), in patient-derived PDAC tissues and human KRAS-mutant and KRAS wild-type PDAC cell lines (**Figure 11C**):

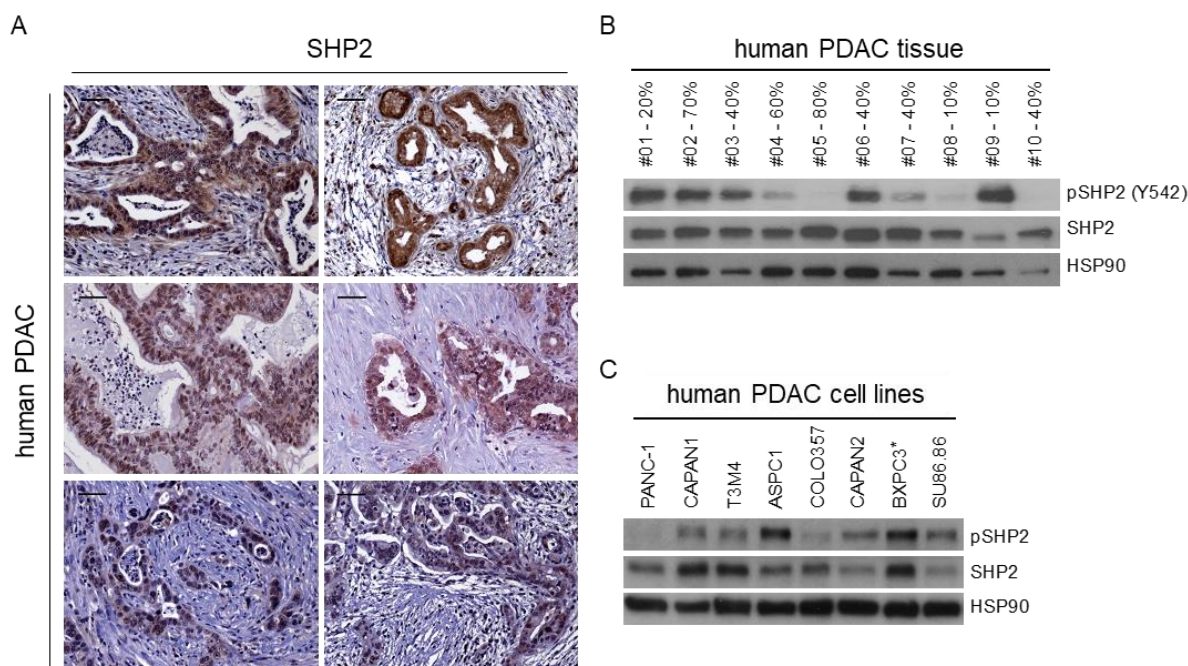


Figure 11: SHP2 is expressed and activated in human PDAC samples. Differential SHP2 expression levels in human PDAC samples were assessed by IHC and western blot. **(A)** Immunohistochemistry staining of epithelial SHP2 in 6 different human PDAC tissues. Scale bars: 100 μ m. **(B)** Western blot of whole tissue lysates. Western blot with lysates were also tested for phosphorylated SHP2 (Y542), which is an indicator for activation/recruitment of the phosphatase. Percentages next to the sample IDs indicate the epithelial fraction of the tumor area, determined by histology. HSP90 served as loading control. One experiment performed. **(C)** Western blot with lysates from eight different human pancreatic cancer cell lines (seven *KRAS* mutant, one *KRAS* wt (*)) for SHP2 and pSHP2 (Y542). HSP90 served as loading control. (n = 1). (Data was published in (Ruess *et al.*, 2018); experiments were performed by D.A. Ruess.)

6.7 *Ptpn11* knockout sensitizes human PDAC cells to MEK inhibition

Having thus shown the importance of SHP2 mediated signaling in murine PDAC carcinogenesis and its expression and activation in human PDAC samples, we decided to try and identify pharmacological vulnerabilities introduced through the loss of SHP2. Our collaborators at the Max Delbrück Center for Molecular Medicine in Berlin used clustered regularly interspaced short palindromic repeats (CRISPR)–CRISPR-associated protein 9

(Cas9)-mediated knockout of *PTPN11* to produce SHP2 deficient clones of two *KRAS*-mutant human PDAC cell lines (YAPC: *KRAS*^{G12V}; PANC-1: *KRAS*^{G12D}). We then used these SHP2 deficient cells to perform a focused drug screen with relevant chemotherapeutic agents (gemcitabine, paclitaxel) or targeted kinase inhibitors against gp130 and RAS pathway associated kinases PI3K (pictilisib) and MEK (trametinib). These experiments showed that *PTPN11*-knockout cells are uniquely susceptible to MEK inhibitors (**Figure 12**).

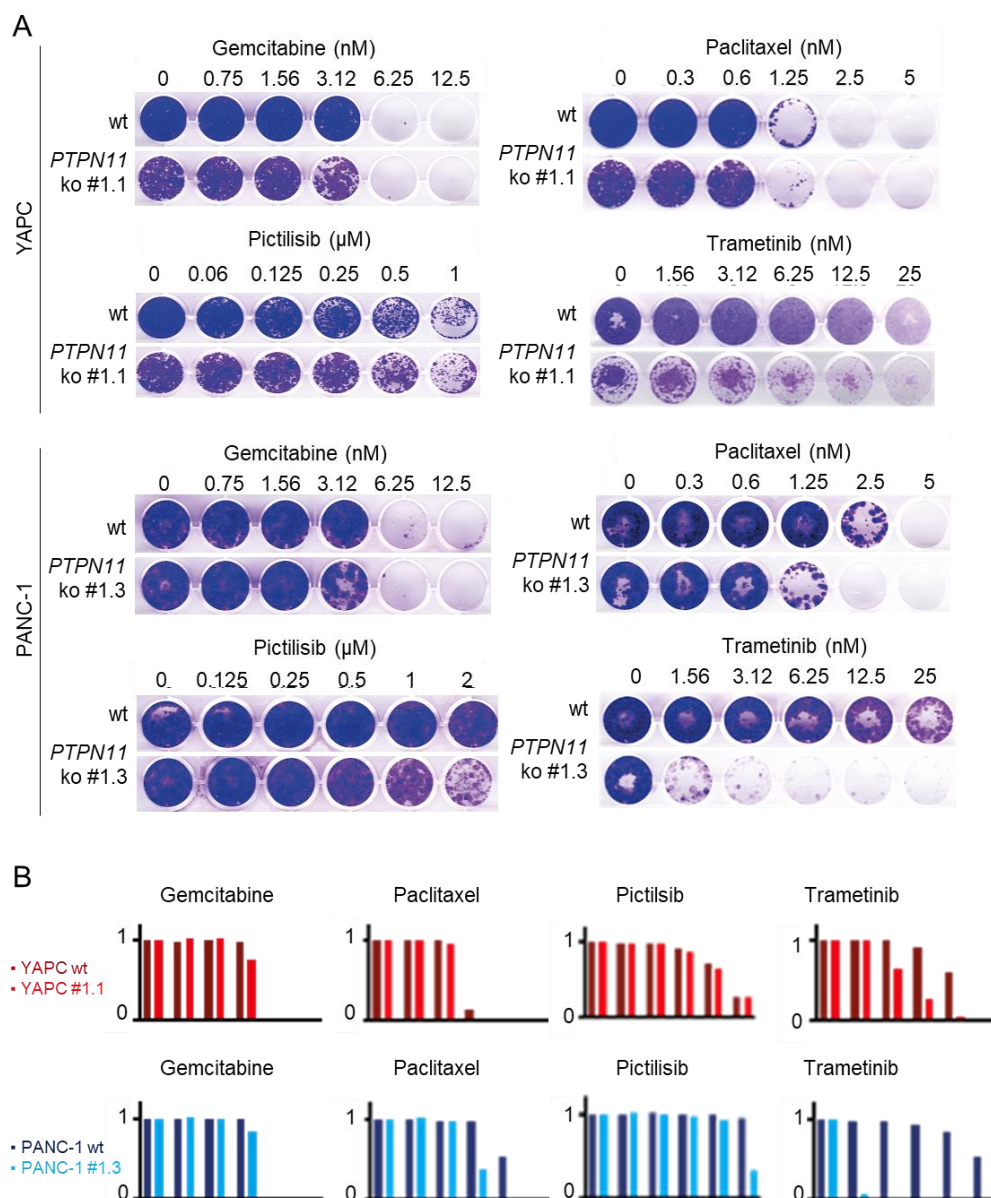


Figure 12: *PTPN11* knockout *KRAS* mutant cancer cell lines are very susceptible to MEK inhibition. (A) Long-term (10-14d) colony formation assays of *PTPN11* knockout (ko) clones YAPC #1.1 and PANC-1 #1.3 in comparison to their wild-type (wt) counterparts using standard chemotherapeutics (gemcitabine, paclitaxel) and selective kinase inhibitors against PI3K (pictilisib) and MEK (trametinib) demonstrating unique susceptibility of the *PTPN11* ko cells to MEK inhibition. (B) Bar graphs representing the quantification of relative crystal violet staining for each cell line and drug concentration shown in (A), compared to the untreated control set as 1. Each bar represents one concentration, colors refer to the respective cell line. YAPC wt (dark red), YAPC #1.1 (light red), PANC-1 wt (dark blue) and PANC-1 #1.3 (light blue). (Data was published in (Ruess *et al.*, 2018); KO cells were generated by G.J. Heynen, experiments were performed by me)

6.8 SHP2 inhibition shows remarkable synergy with MEK inhibition in *KRAS* mutant murine and human PDAC cell lines

While CRISPR-Cas9 mediated gene knockout is a great experimental tool, *in vivo* genome editing is not currently feasible. We thus decided to perform an extensive *in vitro* panel with two newly developed SHP2 inhibitors in combination with chemotherapy (gemcitabine, paclitaxel) or MEK inhibitors (selumetinib, trametinib) in murine and human *KRAS*-mutant PDAC cell lines. GS493 (Grosskopf *et al.*, 2015) acts as a phosphotyrosine mimetic and is thus classified as a substrate-competitive, reversible, catalytic domain inhibitor of SHP2. SHP099 (Garcia Fortanet *et al.*, 2016) is a novel allosteric SHP2 inhibitor that stabilizes the autoinhibited “closed” conformation of the SHP2 molecule. As **Figure 13** shows, was the superior combinatory effect of SHP2 + MEK inhibition compared to SHP2 inhibition + chemotherapy confirmed with both SHP2 inhibitors in all cell lines. Synergistic growth inhibition was seen both in the combination of SHP099 with either selumetinib or trametinib as well as in the combinations of GS493 + either of the two tested MEK inhibitors. Although both SHP2 inhibitors alone appear to be equally effective, or rather ineffective, in terms of *in vitro* growth inhibition, the allosteric SHP2 inhibitor SHP099 appears to have an even greater synergistic effect in combination with MEK inhibitors compared to the competitive SHP2 inhibitor GS493.

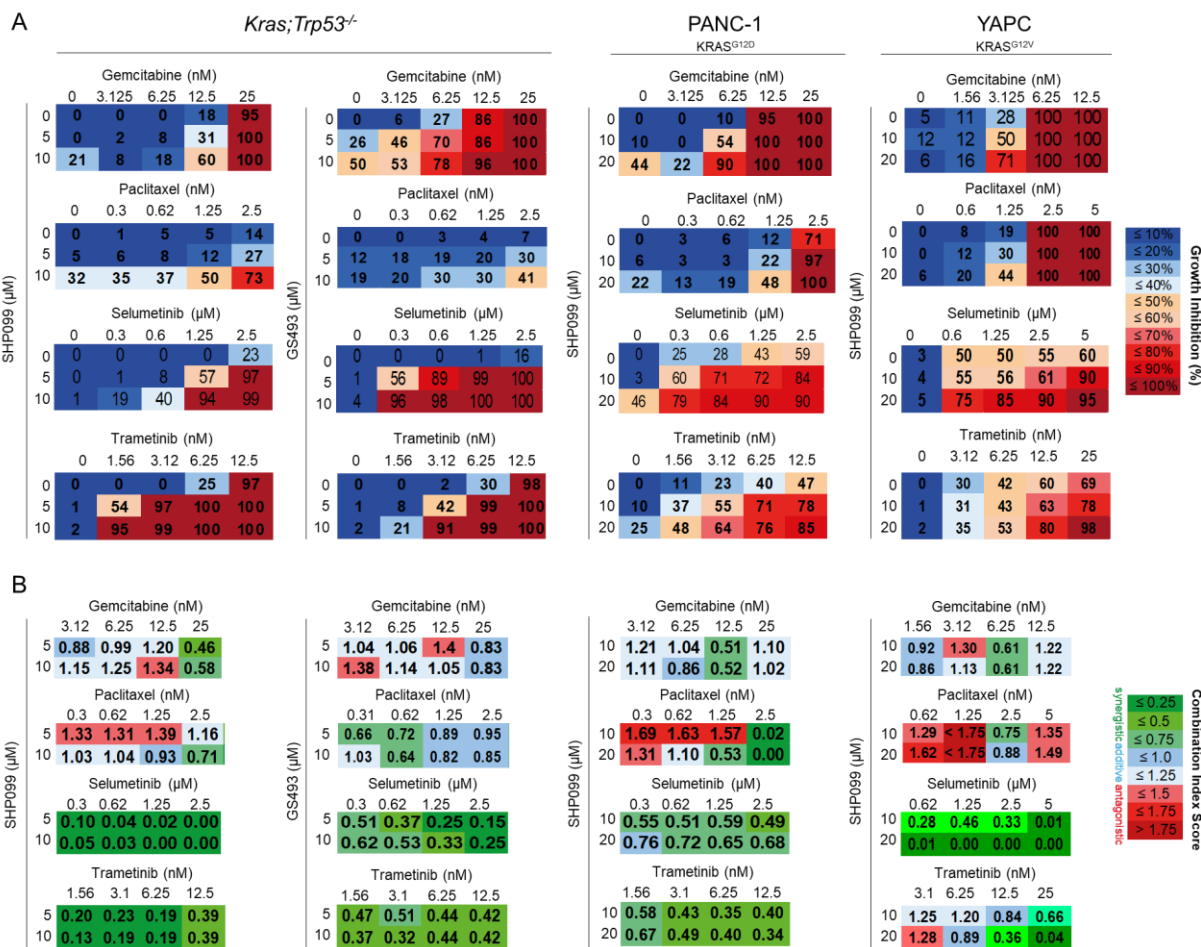


Figure 13: Pharmacological co-treatment panel with various murine and human *KRAS* mutant PDAC cell lines confirms the synergy between MEK and SHP2 inhibitors. (A) Long-term (10-14d) colony formation assays with murine *Kras;Trp53^{-/-}* PDAC and *KRAS* mutant human PDAC cell lines. Chemotherapeutics with relevance to PDAC (gemcitabine/paclitaxel) as well as MEK inhibitors (selumetinib/trametinib) were combined with the SHP2 inhibitors GS493 or SHP099 at the concentrations indicated. Box-matrices depict quantification of growth inhibition in relation to untreated-control wells. ($n \geq 2$). **(B)** Calculation of the combination index scores with the growth inhibition values determined in **(A)** via CompuSyn software demonstrating strong synergism for MEK and SHP2 inhibitor combinations, but not for combinations of gemcitabine or paclitaxel with SHP2 inhibitors. $CI < 0.75$ (shades of green) indicates synergism, $CI = 0.75-1.25$ (shades of blue) indicates additive effects and $CI > 1.25$ (shades of red) indicates antagonism. (Data was published in (Ruess *et al.*, 2018) experiments were performed by me)

6.9 MEK and SHP2 inhibitor combination therapy shows superior *in vivo* efficacy in endogenous *Kras;Trp53^{-/-}* tumors compared to MEK or SHP2 monotherapy

Considering all the previous results, we decided to test the translational relevance of combined SHP2 and MEK inhibition using *in vivo* tumor models. We treated endogenous tumor-bearing *Kras;Trp53^{-/-}* mice with SHP2 inhibitor (GS493) or MEK inhibitor (trametinib) monotherapy or with both inhibitors in combination and measured pancreatic volume changes over time through weekly magnetic resonance imaging (MRI) measurements (**Figure 14A-B**). Similar to the *in vitro* results shown in **Figure 13**, GS493 alone only modestly inhibited tumor progression. Trametinib monotherapy achieved initial pancreatic volume reduction, but eventually, resistant tumors emerged. Only the dual treatment with trametinib + GS493 impeded resistance dynamics and achieved sustained tumor growth inhibition. All treatment arms were able to extend the survival compared to the vehicle cohort (**Figure 14C**). Median survival was increased from 14,5 days in the vehicle cohort to 24 (GS493 monotherapy) and 35 days (trametinib monotherapy and combination therapy respectively). However, a fraction of mice in the trametinib (n = 5) and the trametinib + GS493 (n = 10) cohorts experienced tumor-unrelated morbidity and had to be sacrificed early. Also, for both the T and TG treatment arms, skin rash/eczema at the head/neck and the paws was frequently observed with long-term survivors.

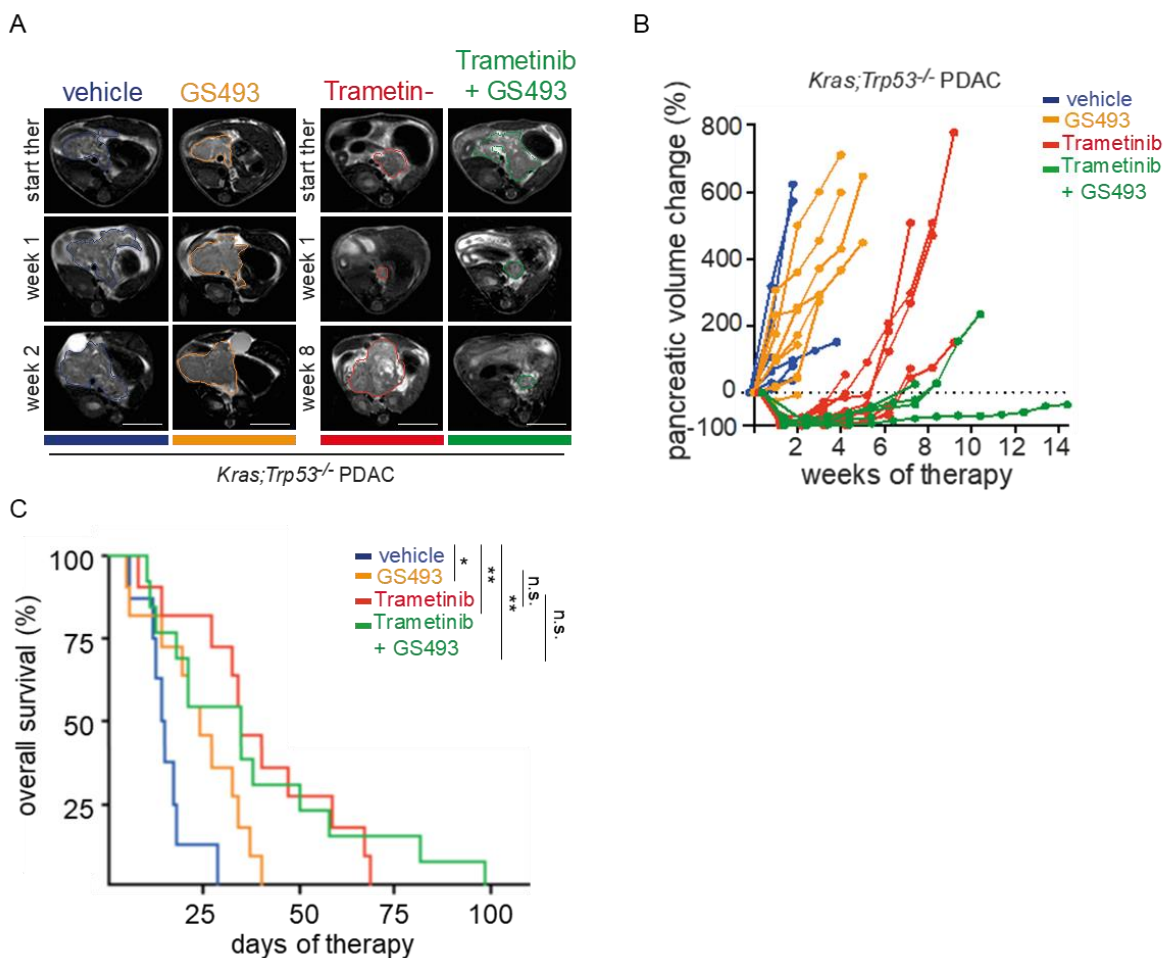


Figure 14: Combined MEK and SHP2 inhibition shows greater efficacy compared to either monotherapy. (A) Representative MRI scan slices depicting PDAC tumor sections of *Kras;Trp53^{-/-}* mice treated with vehicle (V; n = 8), SHP2 inhibitor GS493 (G; n = 11), MEK inhibitor trametinib (T; n = 11) or trametinib + GS493 (TG; n = 13) at the indicated time points (weeks) following the start of therapy (start ther), with similar results among the groups. Scale bars, 1 cm. **(B)** MRI quantification of individual *Kras;Trp53^{-/-}* pancreatic volumes over the course of treatment. (V: n = 8; G: n = 11; T: n = 11; TG: n = 13). The dotted line indicates basal pancreas volume at the start of therapy. **(C)** Kaplan-Meier survival analysis of all mice in the different treatment arms: vehicle (V; n = 8), median: 14.5 days; GS493 (G; n = 11), median: 24 days; trametinib (T; n = 11), median: 35 days; trametinib + GS493 (TG; n = 13), median: 35 days. Significance was determined by log-rank (Mantel-Cox) test. V vs. G: *: $p = 0.0275$; V vs. T: *: $p = 0.0121$; G vs. TG: **: $p = 0.0079$; V vs. TG: ***: $p = 0.0007$; G vs. T: n.s. $p = 0.0877$; T vs. TG: n.s. $p = 0.4283$; n.s.: not significant. Of note: a fraction of animals in the trametinib and the trametinib + GS493 cohort showed signs of severe morbidity resulting in euthanasia before the occurrence of pancreatic volume relapse. (Data was published in (Ruess *et al.*, 2018), experiments were performed by both D.A. Ruess and me)

6.10 Combined ERK and SHP2 inhibition shows synergism in *in vitro* growth inhibition assay and leads to a stronger and more sustained ERK activity inhibition compared to ERKi monotherapy

Having seen these promising *in vitro* and *in vivo* results, we wanted to further investigate the clinical usefulness of a combined two-pronged RAS-pathway inhibition. While the rationale of combined SHP2 and MEK inhibition is sound, the frequently observed side effects and the common occurrence of resistance associated with MEK inhibitors like trametinib (Welsh and Corrie, 2015; Hayes *et al.*, 2016; Yang, Lin and Chu, 2018) made us search for possible alternatives. Since reactivation of ERK is a major mechanism hampering MEK inhibitor efficacy (Ryan *et al.*, 2015; Hayes *et al.*, 2016; Drosten and Barbacid, 2020), direct ERK inhibition might be a worthwhile strategy. The newly developed ERK inhibitor LY3214996 (Bhagwat *et al.*, 2020) was shown to be a selective, potent, and reversible ATP-competitive inhibitor of ERK1/2 activity in *KRAS*- and *BRAF*-mutant cell lines. Through an agreement with Eli Lilly and Company, we were able to obtain enough of the compound to perform several *in vitro* and *in vivo* experiments. A similar agreement was reached with Revolution Medicines, who developed a selective allosteric SHP2 inhibitor with a mode of action similar to that of SHP099 but with even higher potency (Nichols *et al.*, 2018).

Our first goal was to confirm *in vitro* synergy between the ERK inhibitor (ERKi) LY3214996 (LY) and the SHP2 inhibitor (SHP2i) RMC-4550 by colony formation assay using two murine *Kras;Trp53^{-/-}* (**Figure 15A**) and two human *KRAS*-mutant PDAC cell lines (**Figure 15B**). Synergism was measurable in at least 50% of all tested inhibitor combinations in all 4 cell lines. We then analyzed the inhibitors' capacity to inhibit ERK activity *in vitro*. To do that, we treated the same 4 cell lines used in the previous experiment, i.e., two murine *Kras;Trp53^{-/-}* (**Figure 16A**) and two human *KRAS*-mutant PDAC cell lines (**Figure 16B**) with either LY3214996 alone or the LY3214996 + RMC-4550 combination therapy for 6, 72 and 144 hours for western blot analysis. Ribosomal s6 kinase (RSK) is a direct target of ERK (Doehn *et al.*, 2009) therefore we used the levels of pRSK as a read-out for ERK activity. **Figure 16** shows that combined LY3214996 + RMC-4550 treatment inhibited ERK activity more strongly and over a longer period than LY3214996 monotherapy. This was true in both murine (**Figure 16A**) as well as human PDAC cells (**Figure 16B**). These *in vitro* experiments were performed in collaboration with Antonio Mulero Sanchez in the laboratory of Prof. Dr. Rene Bernards at the Netherlands Cancer Institute (NKI) in Amsterdam.

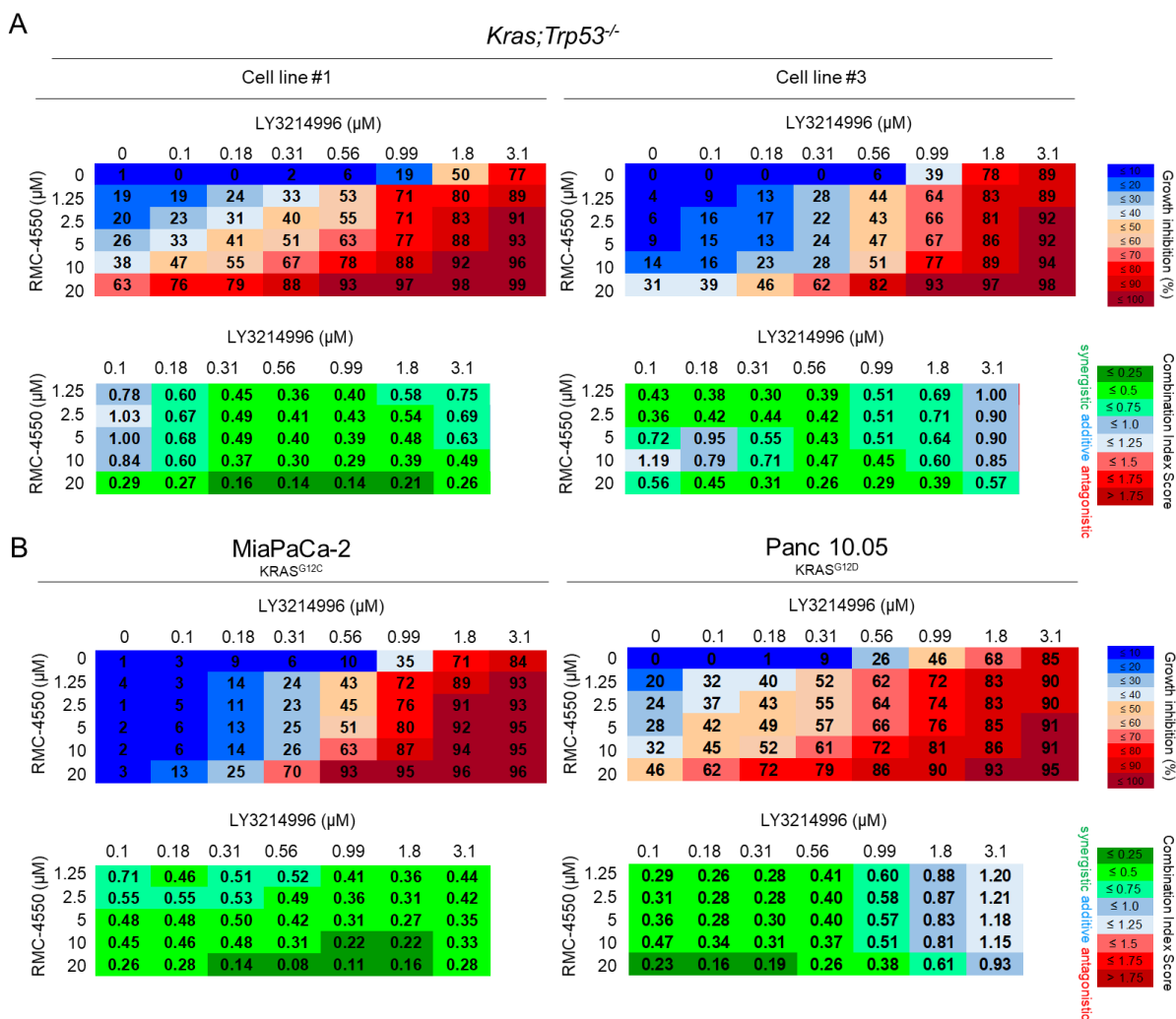


Figure 15: ERK inhibitor LY3214996 and the SHP2 inhibitor RMC-4550 synergistically inhibit growth of murine and human *KRAS*-mutant PDAC cells *in vitro*. (A) Box matrices depicting the quantification of crystal violet stained murine *Kras;Trp53^{-/-}* cells treated with LY3214996 and RMC-4550 in a 6-day colony formation assay (upper panel) and the combination index calculation indicating a strong synergistic effect (lower panel). (depicted are Mean values of 3 independent experiments) (B) Box matrix depicting the quantification of crystal violet stained human *KRAS*-mutant PDAC cells treated with LY3214996 and RMC-4550 in a 6-day colony formation assay (upper panel) and the combination index calculation indicating a strong synergistic effect (lower panel). CI < 0.75 (shades of green) indicates synergism, CI = 0.75–1.25 (shades of blue) indicates additive effects and CI > 1.25 (shades of red) indicates antagonism.

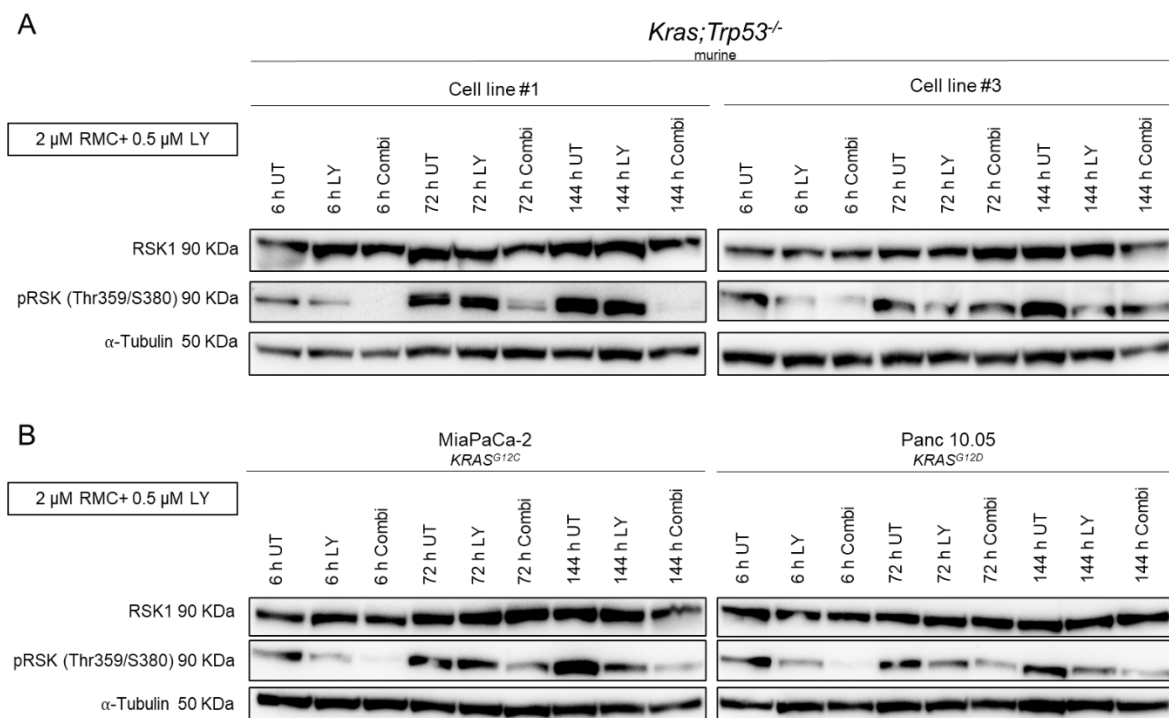


Figure 16: Co-treatment with LY3214996 and RMC-4550 inhibits MAPK pathway activity more strongly and over a longer period than the ERK inhibitor LY3214996 alone. (A) Western Blot from 2 different *Kras;Trp53^{-/-}* cell lines treated with either ERK inhibitor (LY) alone or combined ERK + SHP2 inhibition (Combi) or left untreated (UT) for the indicated times. RSK protein levels were unaffected by the treatment, however pRSK levels, a read-out for ERK activity, were decreased upon ERKi and especially after combined and ERK and SHP2 inhibition. α -Tubulin was used as control for equal protein loading. (n = 2) **(B)** Western Blot from 2 different *Kras;Trp53^{-/-}* cell lines treated with either treated with either ERK inhibitor (LY) alone or combined ERK + SHP2 inhibition (Combi) or left untreated (UT) for the indicated times. RSK protein levels were unaffected by the treatment, however pRSK levels, a read-out for ERK activity, were decreased upon ERKi and especially after combined and ERK and SHP2 inhibition. α -Tubulin was used as control for equal protein loading. Experiments were repeated at least twice with similar results. (n = 2)

6.11 Continuous (daily) treatment with combined LY3214996 + RMC-4550 treatment is well tolerated in wild-type and NSG mice up to a dose of 100 mg/kg LY3214996 + 10 mg/kg RMC-4550

Due to the novelty of both LY3214996 and RMC-4550 and the resulting sparsity of *in vivo* data as well as the non-existent data on combined tolerability, we decided to perform a tolerability study in non-tumor-bearing wild-type ($Kras^{LSLG12D}; Trp53^{flox/flox}$) and NOD scid gamma (NSG) mice to determine the maximum tolerated dose (MTD) of combined LY3214996 and RMC-4550, before progressing to *in vivo* tumor models. The drugs were administered once per day via oral gavage for 14 consecutive days (**Figure 17A**).

Following dosing recommendations by Eli Lilly and Company and Revolution Medicines respectively, we decided on 9 different doses of inhibitor combinations labeled d1 (lowest) through d9 (highest), as illustrated in **Figure 17B**. We applied a modified “3+3” study design (Huang *et al.*, 2007; Le Tourneau, Lee and Siu, 2009) using cohorts of three animals per dose. As depicted in **Figure 17C**, the first cohort is treated at a starting dose, and the subsequent cohorts are treated with ascending or descending doses according to the observed response. Dosing is increased until one or more mice per cohort experiences dose-limiting toxicities (DLT). Should two or more mice experience dose-limiting toxicity, the dose escalation is stopped and the next lower dose, with no more than 1 in 6 mice showing signs of DLT, is determined as MTD. If only one in three mice experiences DLT, the cohort is expanded to 6 mice and the dose-escalation proceeds if none of the additional three mice show signs of DLT, otherwise the previous dose is determined as MTD.

Endpoints used as signs of DLT were weight loss of more than 20%, clinical score (abnormal behavior, signs of physical discomfort) and death. These parameters were evaluated daily, and animals were euthanized when either of these endpoints was met. Medical treatment was provided to prevent unacceptable pain and suffering. Due to ethical and practical considerations, that is to minimize the number of mice in the experiment, dose d5 was chosen as starting dose. **Figure 18** shows the body weight profile of both wild-type (**Figure 18A**) and NSG (**Figure 18B**) mice over the course of 14 days of treatment.

All doses were well tolerated in wild-type mice (**Figure 18A**) but dose d9 (i.e., 100 mg/kg LY + 30 mg/kg RMC) caused dose-limiting weight loss in NSG mice (**Figure 18B**). Although we could have used a higher dose in wild-type mice, we decided to use the same dose in both NSG and wild-type mice and thus used dose d8, i.e., 100 mg/kg LY3214996 + 10 mg/kg RMC-4550 in the following tumor models.

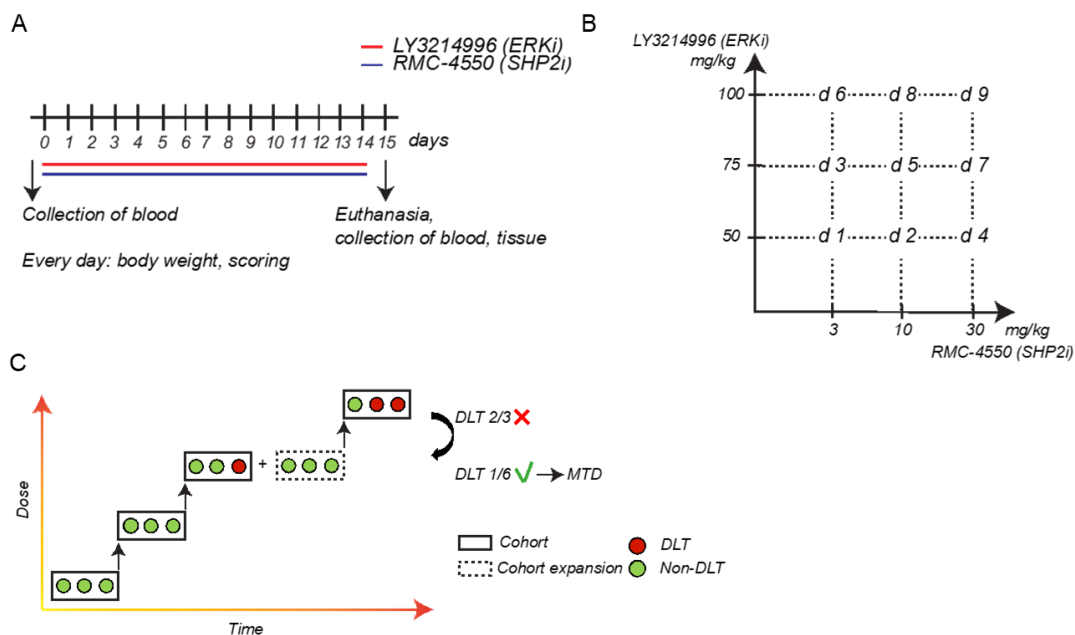


Figure 17: Schematic overview of the modified 3+3 dose-escalation strategy and the doses used to determine MTD in wt and NSG mice over a 14-day treatment period. (A) Treatment schedule. Mice (wt or NSG) were treated daily with a combined dose of ERK + SHP2 inhibitor or vehicle for 14 days via oral gavage. **(B)** Dosage calculation, LY3214996 and RMC-4550 were combined in different concentrations to make up 9 combined doses- For example, 50 mg/kg LY3214996 plus 3 mg/kg RMC-4550 make up dose 1. **(C)** Schematic depiction of the 3+3 dose escalation strategy. 3 mice are used per dose until one or more test subjects show signs of DLT. With 2 or more sick mice, the dose must be reduced, with 1 sick mouse, the cohort is expanded. If none of the additional 3 subjects shows signs of DLT, the next higher dose can be applied.

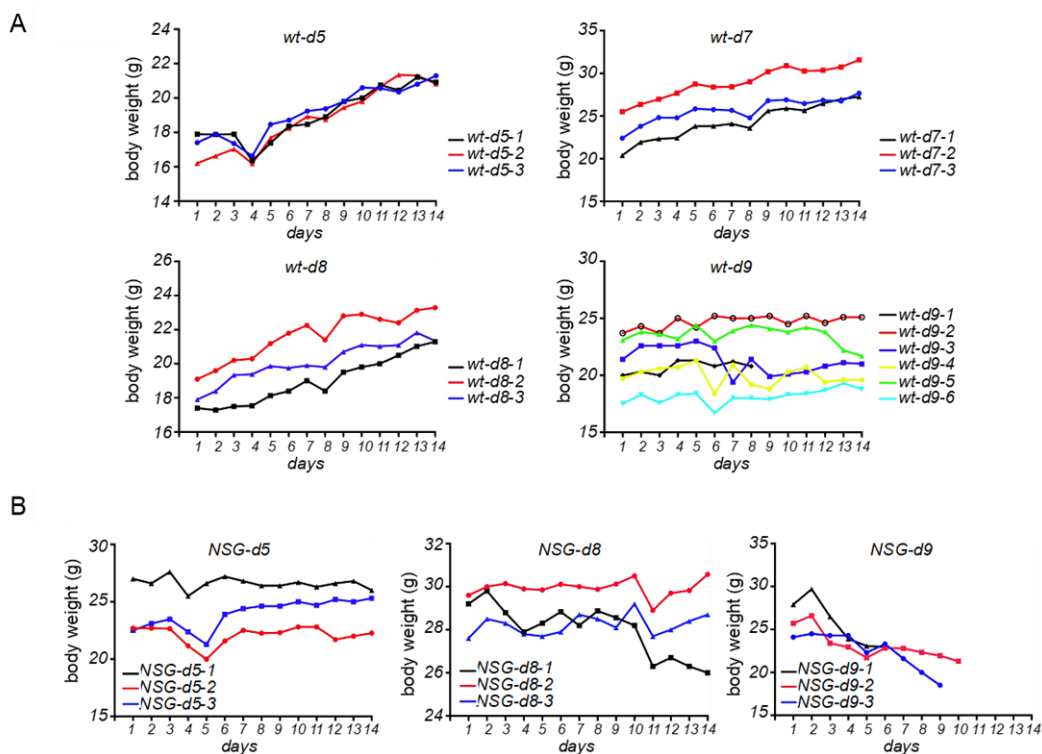


Figure 18: Doses d5 to d8 are well tolerated in both wt and NSG mice. (A) Body weight over time in continuously treated wt mice. Dose 5 (d5) to 8 (d8) were well tolerated without signs of DLT. Dose 9 (d9) was expanded to 6 mice due to signs of DLT in one mouse. **(B)** Doses d5 and d8 were well tolerated (d7 was skipped) in NSG mice however all mice showed signs of DLT in d9. Dose 8 (d8) with 100 mg/kg LY3214996 and 10 mg/kg RMC-4550 was used in subsequent experiments.

6.12 Combined ERK plus SHP2 inhibition shows superior *in vivo* efficacy compared to either inhibitor alone

Having found a well-tolerated dose for the combination therapy of LY3214996 + RMC-4550, we wanted to see whether the superiority of combined SHP2 + ERK inhibition compared to monotherapy seen *in vitro*, could be confirmed *in vivo*. We initially used a model of orthotopically transplanted $Kras^{G12D/+};Trp53^{R172H/+}$ tumors in C57BL/6J mice ($Kras;Trp53^{R172H/+}$). Transplanted tumors were left to grow for 2 weeks, mice were then randomly assigned into either the baseline, vehicle (V), RMC-4550 (B), LY3214996 (C) or combination (A) cohort. Baseline mice were sacrificed to show the presence of well-integrated and growing orthotopic tumors (**Figure 19C** upper panel). All other mice were continuously treated with either vehicle, SHP2 monotherapy, ERK monotherapy or the combination for 14 days via daily oral gavage (**Figure 19A**). As **Figure 19B** shows, significant inhibition of tumor growth, as indicated by the tumor weight at endpoint, was induced by both the combination treatment as well as the respective monotherapies compared to vehicle treated control mice. With the combination therapy (A) being the most effective. The experiments on orthotopic $Kras;Trp53^{R172H/+}$ tumors were conducted in collaboration with Dr. Bruno Sainz Anding and Dr. Laura Ruiz-Cañas at the IIBM in Madrid.

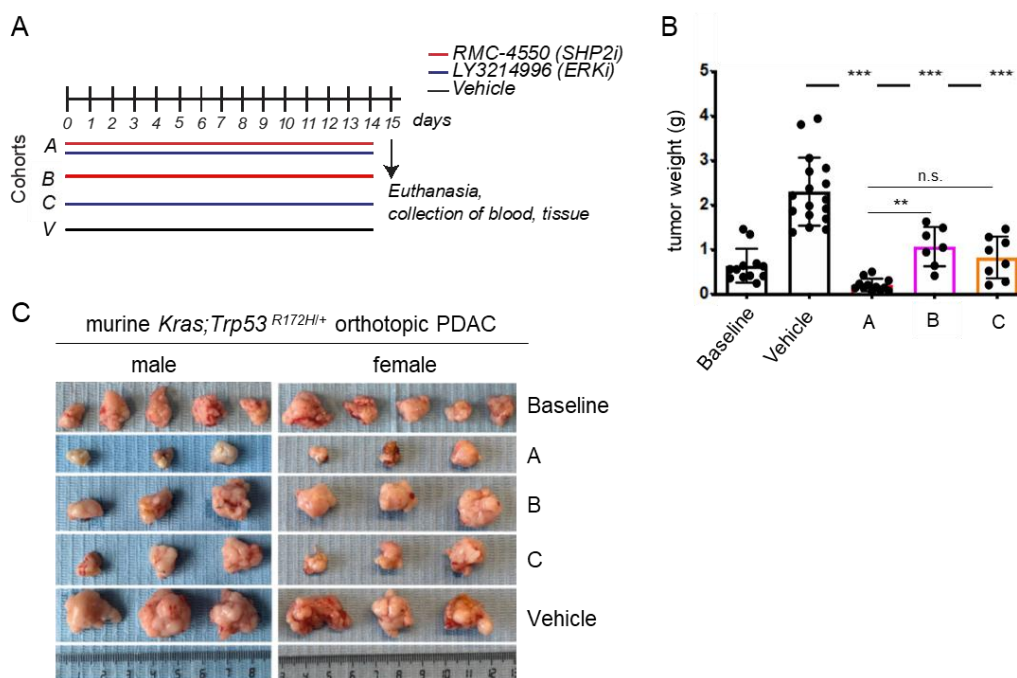


Figure 19: Combined LY3214996 + RMC-4550 treatment induces tumor shrinkage and inhibits tumor growth more effectively than either inhibitor alone. (A) Treatment schedule: Mice were treated daily with either both inhibitors together (A; n = 12), RMC-4550 (B; n = 7), LY3214996 (C; n = 8) or vehicle (V; n = 17) for 14 days. **(B)** Tumor weight of orthotopic tumors at endpoint. Baseline represents a control cohort of randomly picked mice (n = 12) opened 14-days after orthotopic transplantation to confirm the presence of growing tumors. Bar graph represents Mean \pm SD and each dot represents individual tumors. Significance (***) $p < 0.0001$, ** $p = 0.009$ and n.s. $p = 0.089$; n.s.: not significant) was calculated using one-way ANOVA and Tukey's Multiple Comparison Test **(C)** Representative macroscopic images of orthotopic tumors explanted from male and female mice at endpoint.

6.13. All LY3214996 + RMC-4550 treatment schedules show significant tumor growth inhibition in endogenous and orthotopic PDAC models, however continuous treatment is the only schedule able to significantly reduce the number of proliferating cells

Having shown the superior inhibitory capacity of the combination therapy, we then treated animal cohorts with three different schedules of LY3214996 + RMC-4550 combination therapy to determine the optimal treatment regimen, defined as maximum anti-tumor effect with minimum toxicity. These schedules were: The continuous administration (daily) of both drugs in combination (treatment arm A), administration of both drugs 5 days on/ 2 days off (D) or continuous administration of RMC4550 plus LY3214996 5 days on/ 2 days (E). As controls, mice were treated daily with vehicle (V) (**Figure 20A**). Investigation of the optimal treatment regimen was performed in two different murine PDAC models, 1. The previously described orthotopic *Kras;Trp53^{R172H/+}* model and 2. the endogenous *Kras;Trp53^{-/-}* model of spontaneous PDAC formation. None of the tested schedules were associated with dose or schedule-limiting toxicities (data not shown) in either of the two tumor models. All schedules induced significant tumor growth inhibition compared to the control arm (**Figure 20B-C**). While tumor volume reduction in the orthotopic model was only achieved in some mice of cohort A (**Figure 20B**) this effect was seen at least in some of the mice in all treatment arms of the endogenous *Kras;Trp53^{-/-}* model (**Figure 20C**). While the tumor volume changes induced by either of the three combination treatments were statistically not significantly different, the mice in cohort A had the highest amount of intact acini area (**Figure 20D**) and the lowest number of Ki67-positive proliferating cells (**Figure 20E**) leading us to the conclusion, that continuous treatment has superior efficacy compared to the intermittent treatment arms, at least in the endogenous *Kras;Trp53^{-/-}* model.

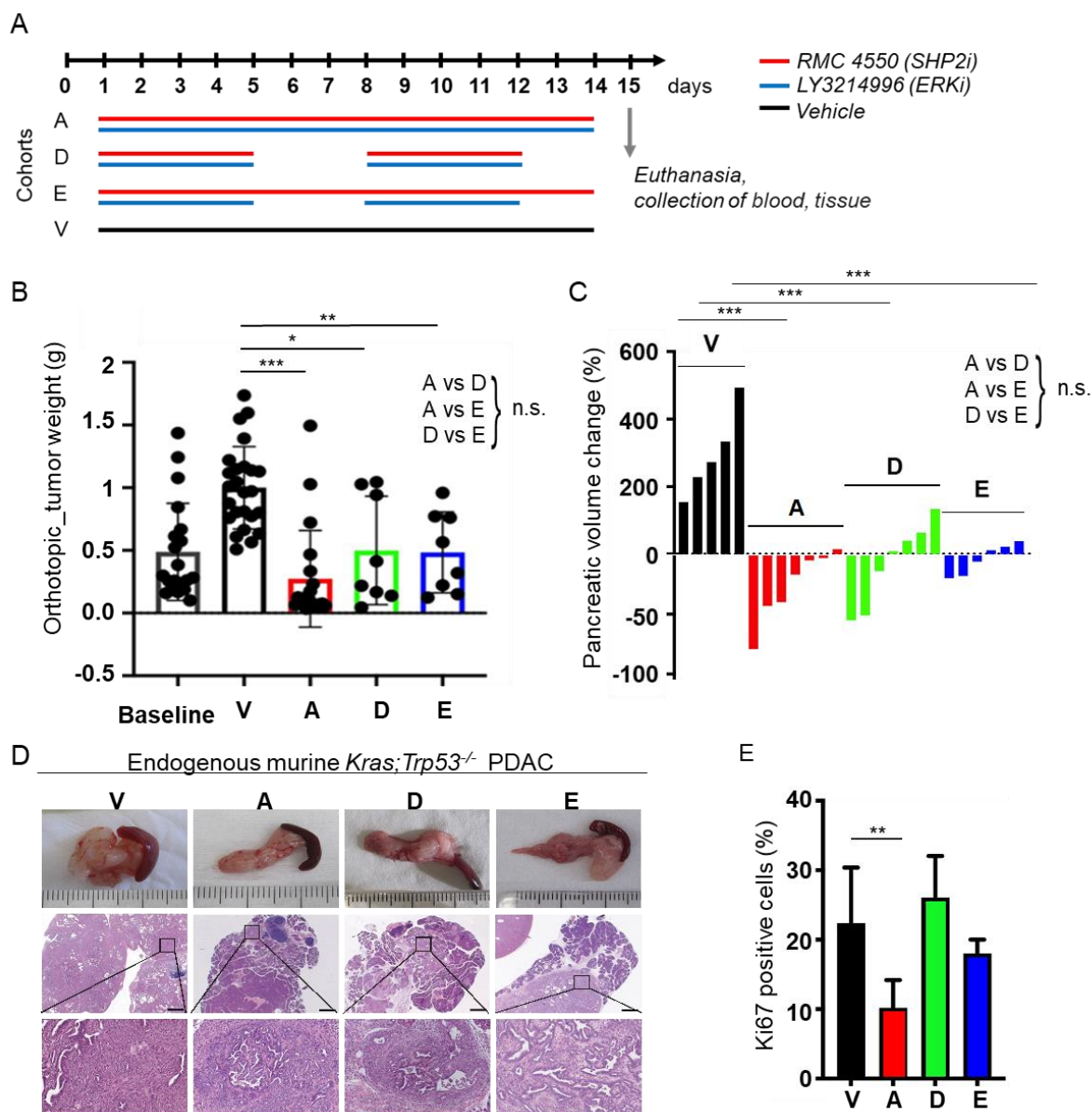


Figure 20: Analysis of 3 different treatment schedules for the ERKi + SHP2i combination therapy shows that continuous daily treatment has superior efficacy compared to intermittent treatment. (A) Treatment schedules used mice were treated with continuous (daily) LY + RMC therapy (A), intermittent 5-days on/2-days off LY + RMC (D) or continuous RMC + intermittent LY (E) or continuous (daily) vehicle treatment (V) via oral gavage for 14 days. **(B)** Tumor weight of orthotopic tumors at endpoint. Baseline represents a control cohort of randomly picked mice ($n = 20$) opened 14-days after orthotopic transplantation to confirm the presence of growing tumors. Bar graph represents Mean \pm SD and each dot represents individual tumors (Vehicle: $n = 25$; A: $n = 20$; D: $n = 8$; E: $n = 8$). Significance ($*** p < 0.0001$, $** p = 0.008$, $* p = 0.011$ and n.s. $p > 0.5$; n.s.: not significant) was determined by one-way ANOVA and Tukey's multiple comparison test. **(C)** Pancreatic volume change (%) in *Kras;Trp53^{-/-}* mice after 14 days of vehicle (V), continuous LY+RMC (A), intermittent LY + RMC (B) or continuous RMC + intermittent LY (D) treatment. The dotted line indicates basal pancreas volume at the start of therapy. Each bar represents the relative volume change from day 0 to day 14 in one mouse. Significance ($*** p < 0.0001$, and n.s. $p > 0.5$; n.s.: not significant) was determined by one-way ANOVA and Tukey's Multiple Comparison Test. **(D)** Representative macro- and microscopic pictures of pancreata in the vehicle and the three combination cohorts. Microscopic pictures were taken at 10x and 200x magnification and scale bar represent 1000 and 50 μm , respectively. **(E)** Quantification of Ki67-positive cells in each cohort. Images were quantified using the ImageScope software from Leica Biosystems. Data represents Mean \pm SD. Significance ($** p = 0.004$) was determined using the unpaired t test.

6.14 LY3214996 + RMC-4550 combination therapy significantly inhibits tumor growth, and induces tumor volume reduction as well as sustained disease control in models of patient-derived *KRAS*-mutant PDAC xenografts

Having shown the significant benefit of combined LY3214996 + RMC-4550 treatment in murine PDAC models, we decided to investigate the impact in a humanized model and determine the optimal treatment regimen in NSG mice bearing subcutaneous patient-derived xenografts (PDX) of three different *KRAS*^{G12D} mutant PDAC tumors. **Figure 21** shows the result for the first two PDX cohorts of mice bearing PDX185 (**Figure 21B-C**) and PDX354 (**Figure 21D-E**). Each of these PDX tumors was transplanted into the flanks of 28 mice, 7 mice per cohort and two tumors per mouse. The mice were then treated for 14 days with either of the three previously described combination treatments or vehicle (**Figure 21A**). All treatment arms significantly inhibited tumor growth and induced tumor volume reduction of both PDX185 and PDX354 tumors, with none being significantly more or less effective than the other combinations (**Figure 21B-E**).

The third PDX specimen (PDX215) was also transplanted into the flanks of 28 mice (7 mice per group; 2 tumors per mouse), however due to signs of severe morbidity in the vehicle cohort, mice were only treated for 7 days. On day 8, all mice of the vehicle cohort as well as 4 mice from all other treatment schedules were euthanized and tumor weight was determined (**Figure 22A**). Similar to PDX185 and PDX354 shown in **Figure 21**, all treatment arms also significantly inhibited tumor growth and induced tumor volume reduction of PDX215, with none being significantly more or less effective than the other combinations (**Figure 22B-C**). The remaining 3 mice in each treatment cohort remained untreated for 12 days after the final dosing on day 7. Tumor volume was measured every 2-3 days and as **Figure 22D** shows, sustained tumor growth control without re-growth to initial (start of therapy) tumor size was observed.

All PDX experiments were conducted in collaboration with Dr. Bruno Sainz Anding and Dr. Laura Ruiz-Cañas at the IIBM in Madrid.

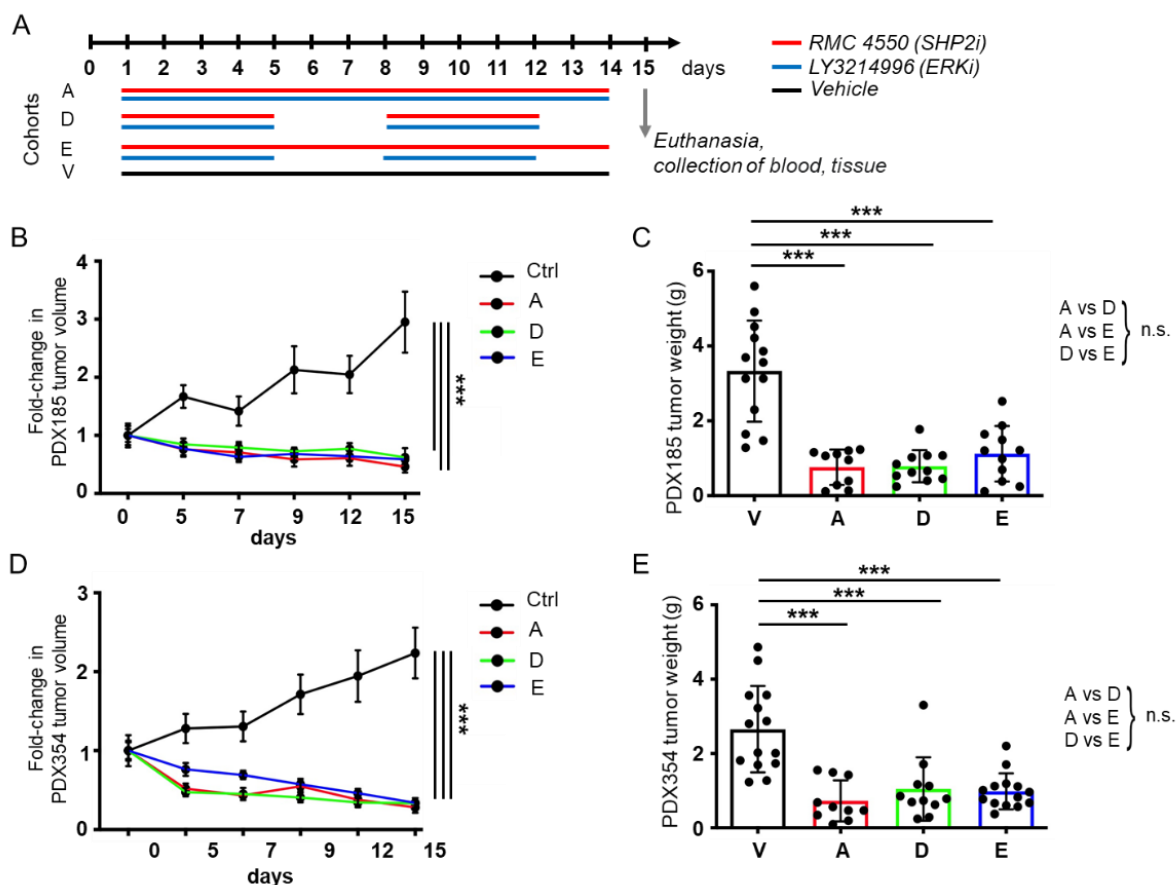


Figure 21: ERKi + SHP2i combination therapy leads to significant tumor growth suppression and tumor volume reduction in two different subcutaneously transplanted patient-derived *KRAS*^{G12D}-mutant PDAC xenografts. (A) Treatment schedule. Mice ($n = 7$ per group) were treated for 14 days with inhibitor or vehicle as shown in the schematic. (B) PDX185: Relative tumor volume change depicted as fold change. Significance ($*** p < 0.0001$ and n.s. $p > 0.1$; n.s.: not significant) was determined using unpaired t test with equal SD (C) Tumor weight (PDX185) at endpoint. Bar graph depicts Mean \pm SD, each dot represents an individual tumor ($n_{\text{Tumor}} = 2$ per mouse). Significance ($*** p < 0.0001$) was determined using one-way ANOVA and Tukey's Multiple Comparison Test. (D) PDX354: Relative tumor volume change depicted as fold change. Significance ($*** p < 0.0001$) was determined using unpaired t test with equal SD (E) Tumor weight (PDX354) at endpoint. Bar graph depicts Mean \pm SD, each dot represents an individual tumor ($n_{\text{Tumor}} = 2$ per mouse). Significance ($*** p < 0.0001$ and n.s. $p > 0.1$; n.s.: not significant) was determined using one-way ANOVA and Tukey's Multiple Comparison Test.

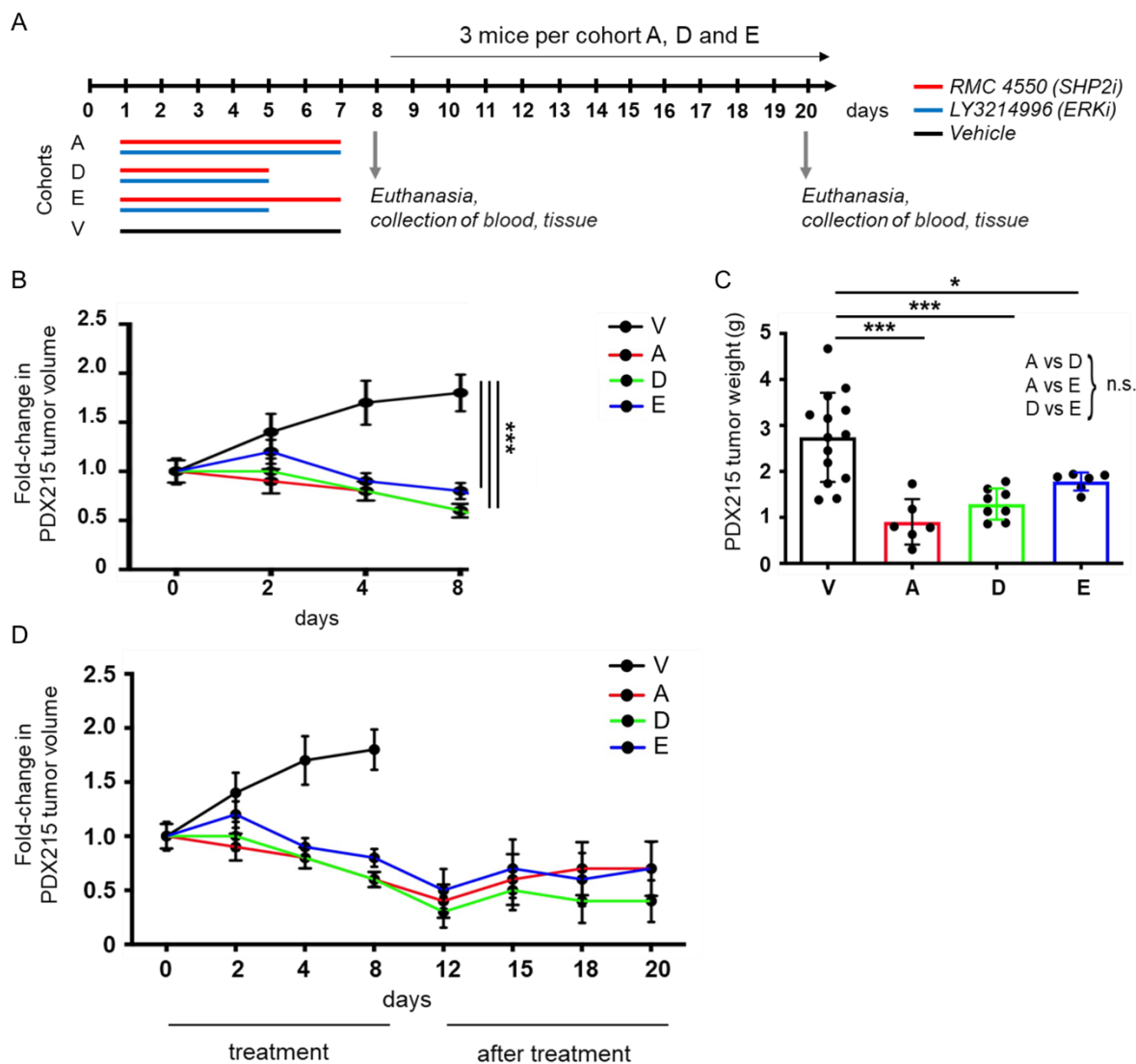


Figure 22: ERKi + SHP2i combination therapy leads to sustained suppression of tumor growth for up to 12 days after end of therapy in one example of subcutaneously transplanted patient-derived *KRAS*^{G12D}-mutant PDAC xenografts. (A) Treatment schedule. Mice ($n = 7$ per group) were treated for 7 days with inhibitor or vehicle as shown in the schematic. On day 8, all mice in the vehicle cohort and 4 mice per treatment cohort were sacrificed due to severe morbidity in the vehicle cohort. The remaining 3 mice in cohort A, B and D were left untreated for another 2 days, tumor volume was measured at the time points indicated in panel (D). (B) Relative tumor volume change depicted as fold change for all mice until day 8. Significance ($*** p < 0.0001$) was determined using unpaired t test with equal SD. (C) Tumor weight at endpoint (day 8), $n = 7$ in the vehicle treated cohort and $n = 4$ in treatment cohorts. Bar graph depicts Mean \pm SD, each dot represents an individual tumor ($n_{\text{Tumor}} = 2$ per mouse). Significance ($*** p < 0.0001$, $* p = 0.029$ and n.s. $p > 0.05$, n.s.: not significant) was determined by one-way ANOVA and Tukey's Multiple Comparison Test. (D) Combined relative tumor volume change (depicted as fold change) for the duration of the treatment and the 12 days afterwards. ($n = 0$ for cohort V and $n = 3$ for cohorts A, B and D).

7. DISCUSSION

Pancreatic ductal adenocarcinoma is one of the deadliest malignancies worldwide (Siegel, Miller and Jemal, 2020). Most patients are diagnosed at stages with inoperable primary tumors or metastatic disease and treatment options are limited (Ruess *et al.*, 2017; Schulz and Algül, 2019). Surgery, which is an option for merely 10–20% of PDAC patients, is the only potentially curative treatment to date (Lambert *et al.*, 2019; Schulz and Algül, 2019). Even after surgery the curation rate is disappointingly low, with a median survival of 15–20 months and a 5-year survival rate of only 8–15% (Lambert *et al.*, 2019). Although chemotherapeutic options have improved over time, many people experience cancer recurrence. Especially those with metastatic disease often only receive palliative care, to alleviate the main physical symptoms and to postpone degradation of quality of life (Lambert *et al.*, 2019). Targeted therapies that have greatly increased survival probabilities in other cancers (Lee, Tan and Oon, 2018) are rare in PDAC. In fact, other than Poly (ADP-ribose)-Polymerase (PARP) inhibitors, which have been approved by the American Food and Drug Administration (FDA) for the treatment of *BRCA*-mutant pancreatic cancer cases (Golan *et al.*, 2019), no targeted therapies have so far proved successful (Ruess *et al.*, 2017). Therefore, the development of new therapies is one of the crucial milestones on the path to improved patient outcome. However, advances in this field can only be made through a better understanding of the signaling pathways, both cell autonomous and microenvironment-mediated, involved in pancreatic carcinogenesis and tumor maintenance.

7.1 gp130-signaling is an important driver in pancreatic carcinogenesis

gp130-mediated signaling is involved in many inflammatory diseases and cancers (Silver and Hunter, 2010), and in 2011 Lesina *et al.*, as well as Corcoran *et al.*, (2011) showed that gp130-mediated STAT3 activation plays an important role in *KRAS*-driven pancreatic carcinogenesis (Corcoran *et al.*, 2011; Lesina *et al.*, 2011). Both IL-6 trans-signaling and LIF-induced gp130 activation were shown to be involved in PDAC development and maintenance, however the effects of pancreas-specific deletion of the gp130 encoding gene *IL6st* had not been investigated prior to this study. We have shown that gp130 deficiency whilst not completely abrogating the formation of ADM and PanIN lesions in *Kras*^{G12D} mice (*Kras;IL6st*^{-/-}) delayed the onset of lesion formation and the progression to late-stage PanIN lesions and full-blown PDAC. Congruent with previous findings (Lesina *et al.*, 2011), levels of pSTAT3 were significantly reduced in the lesions of *Kras;IL6st*^{-/-} compared to *Kras* mice. *IL6st* deletion was shown to significantly reduce tumor incidence but did not increase overall survival of *Kras;IL6st*^{-/-} mice.

In fact, several *Kras;IL6st^{-/-}* mice had to be euthanized early due to tumor unrelated morbidity. Histological analysis of these mice frequently revealed severe pancreatic atrophy with lipid replacement. This suggests that loss of gp130-signaling in *KRAS*-driven pancreatic carcinogenesis does not only inhibit the progression from early to late-stage PanINs but might also induce cell death in gp130-deficient acinar cells.

Transgenic, constitutively active, leucine zipper linked gp130 (Lgp130) is an artificial model with no known realistic counterpart in human PDAC. However, it provides a useful tool to analyze pancreas-specific gp130-mediated signaling and the role of downstream effectors in pancreatic homeostasis and pancreatic carcinogenesis. Since the leucine zipper part of Lgp130 induces ligand-independent gp130 homodimerization, it is an especially suitable model for the simulation of constitutive IL-6 and IL-11-mediated gp130 activation (Rose-John, 2018). The Lgp130 model, together with the *Kras;Socs3^{-/-};IL6st^{-/-}* model, corroborates the fact that although mutant *KRAS* is an important mediator of pancreatic carcinogenesis (Iacobuzio-Donahue *et al.*, 2012) extracellular factors like cytokines or growth factors still play an important role for both initial lesion formation as well as PDAC progression. Congruently, *Kras;Trp53^{-/-}*-driven pancreatic carcinogenesis, which does not rely on gp130-signaling for consistent STAT3 activation (Wörmann *et al.*, 2016), was decelerated and survival prolonged upon *IL6st*-deletion.

7.2 The gp130-receptor is a potential therapeutic target in PDAC

The relevance of gp130-mediated signaling in *KRAS*-driven PDAC shown in this study was corroborated through several different studies about the role of different gp130-utilizing cytokines in PDAC. Especially IL-6 and LIF have been implicated by several independent studies (Corcoran *et al.*, 2011; Lesina *et al.*, 2011; Holmer *et al.*, 2014; Bressy *et al.*, 2018; Lee *et al.*, 2019; Shi *et al.*, 2019) both in the processes of carcinogenesis and metastasis as well as the maintenance of fully formed PDAC tumors. Furthermore, both OSM and IL-35 induced gp130 activation have been shown to play a part in acquired radio-resistance and metastasis in PDAC (Huang *et al.*, 2017; Nguyen *et al.*, 2020). Our findings, as well as the data presented in the above-mentioned studies, suggest that gp130 and the gp130-mediated signaling pathways might be promising therapeutic targets in the treatment of PDAC. In fact, Goumas *et al.*, (2015) have shown that inhibition of IL-6 signaling with the anti-IL-6R antibody tocilizumab that inhibits both classic IL-6 as well as IL-6 trans-signaling, or the fusion protein sgp130Fc which specifically blocks IL-6 trans-signaling, led to significantly reduced tumor size, decreased local recurrence and reduced the number of distant metastases in conservative or adjuvant therapy in a model of orthotopically transplanted human Colo357 cells in SCID/bg mice (Goumas *et al.*, 2015). Furthermore, Long *et al.*, (2017) showed that IL-6R-blocking

antibodies targeted inflammatory monocytes which are known as mediators of chemoresistance, inhibited STAT3 phosphorylation and decreased proliferation of *Kras*^{G12D/+};*Trp53*^{R172H/+} tumor cells *in vivo*. Combined IL-6 receptor blockade and gemcitabine therapy induced tumor cell apoptosis, tumor volume regression, and resulted in improved overall survival (Long *et al.*, 2017).

Along with protein-based therapies like anti-IL-6 and anti-IL-6R antibodies or soluble gp130 fusion proteins (sgp130Fc), small molecular inhibitors of gp130 have been discovered. Small molecules are often associated with better oral availability and overall pharmacokinetics, low toxicity, and low antigenicity (Thilakasiri *et al.*, 2019b). The two most prominent small molecular gp130 inhibitors in the literature are bazedoxifene (Wu *et al.*, 2016; Fu and Lin, 2018; Burkhardt *et al.*, 2019; Chen *et al.*, 2019) and SC144 (Oshima *et al.*, 2009; Plasencia *et al.*, 2009; Xu *et al.*, 2013; Grande *et al.*, 2016; Chen *et al.*, 2019; Li *et al.*, 2019; Lu *et al.*, 2020).

Bazedoxifene, an FDA approved selective estrogen modulator used in the management of menopausal hot flashes and prevention of menopausal osteoporosis (Komm, Mirkin and Jenkins, 2014; Wu *et al.*, 2016), was discovered to be an effective inhibitor of IL-6/gp130 or IL-11/gp130 protein-protein interactions (PPIs) using *in silico* drug repurposing methods like multiple ligand simultaneous docking (MLSD) (Wu *et al.*, 2016). Wu *et al.*, (2016) also showed that bazedoxifene inhibited IL-6 - and IL-11-mediated STAT3 phosphorylation and STAT3 DNA binding, induced apoptosis, and suppressed tumor growth in human pancreatic cancer cell lines (HPAC, PANC-1, HPAF-II, BxPC-3, and Capan-1) *in vitro* as well as *in vivo* (Capan-1, HPAF-II) (Wu *et al.*, 2016).

SC144/gp130 interaction was initially shown in ovarian cancer (Xu *et al.*, 2013), where SC144 showed *in vitro* cytotoxicity and suppressed tumor growth in human cell line xenografts. Xu *et al.*, (2013) proposed the following mode of action: SC144 binding induces conformational changes and activity loss in the cell surface-bound gp130 receptor. The decrease in gp130 activity then leads to inactivation of downstream signaling pathways involving STAT3 and AKT and results in inhibited cell-cycle progression and angiogenesis, and the promotion of apoptosis. Higher concentrations of SC144 were also shown to induce gp130 deglycosylation and gp130 internalization followed by degradation (Xu *et al.*, 2013).

While SC144 might be a promising drug candidate because of its ability to inhibit all IL-6 family cytokine-induced gp130-activation, and to directly bind gp130, bazedoxifene has the advantage of being FDA approved and already on the market. This would presumably simplify the realization of a clinical study in PDAC patients since the availability of clinical safety and tolerability data would drastically reduce the risk for patients as well as the costs and the time required.

In fact, a small case study of 7 patients with advanced pancreatic and gastric adenocarcinomas who received bazedoxifene as monotherapy or in combination with chemotherapy, reported promising preliminary results, based on which a large-scale, prospective clinical study will be initiated (Burkhardt *et al.*, 2019). Reportedly, treatment with bazedoxifene mono- or combination therapy demonstrated stable disease and tumor marker reduction in 5 patients, metabolic regression on PET-CT in 3 patients and overall improved quality of life. Especially encouraging was the report of complete remission in a patient with locally advanced unresectable PDAC who had previously received chemotherapy and palliative radiotherapy (Burkhardt *et al.*, 2019; Thilakasiri *et al.*, 2019b; Thilakasiri *et al.*, 2019a)

While our *Kras;Trp53^{-/-}* cells showed a somewhat heterogenous response when treated with combination treatments of either gp130 inhibitor + chemotherapy or gp130 inhibitor + trametinib, the collective data suggests that further investigation into the therapeutic targeting of gp130 in PDAC will be worthwhile. In fact, *Kras;Trp53^{-/-}* cells with their gp130-independent STAT3 activation (Wörmann *et al.*, 2016) might be an example of more resistant cell types and thus even a partial response as shown in this study is promising. Further investigation in murine *Kras*, *Kras;Trp53^{+/-}* and *Kras;Trp53^{R172H/+}* cells as well as human PDAC cells and tissues in *in vitro* and *in vivo* models is needed to further elucidate the therapeutic potential of gp130-combination therapies. For clinical purpose it might also be warranted to stratify the patients according to the cancer specific levels of gp130 expression (Corcoran *et al.*, 2011).

7.3 The tyrosine phosphatase SHP2 is critically important for *KRAS*-driven pancreatic carcinogenesis

The non-receptor tyrosine phosphatase SHP2 encoded by *PTPN11* is a downstream effector of several growth factor, integrin, and cytokine receptors (Neel, Gu and Pao, 2003; Dance *et al.*, 2008). Downstream of gp130, SHP2 is reported to have both inhibitory (JAK/STAT) as well as activating (RAS/MAPK and PI3K/AKT) roles (Schaper and Rose-John, 2015). Considering the important role of gp130 and STAT3 activation in pancreatic carcinogenesis, we expected *Ptpn11* deletion in murine models of pancreatic carcinogenesis to result in exacerbated tumor phenotypes similar to those reported for *Kras;Socs3^{-/-}* mice (Lesina *et al.*, 2011). However, to our surprise, pancreas-specific *Ptpn11* deletion in *Kras*-driven murine cancer models (*Kras;Ptpn11^{-/-}* or *Kras;Trp53^{-/-};Ptpn11^{-/-}*) had the opposite effect and resulted in virtually complete abrogation of pancreatic carcinogenesis (Ruess *et al.*, 2018). We therefore conclude, that in the context of *KRAS*-driven carcinogenesis the role of SHP2 as RAS/MAPK activator exceeds that of SHP2 as JAK/STAT inhibitor.

As mentioned before, *KRAS* mutations are considered as an early and critical step in pancreatic tumorigenesis (Iacobuzio-Donahue *et al.*, 2012), and mutant RAS-GTPases are commonly considered to be constitutively active (Matallanas *et al.*, 2011). However, our findings, corroborated by Mainardi *et al.*, (2018), undermine that concept and in fact, Hunter *et al.*, (2015) showed, that mutant *KRAS* proteins maintain at least some of their intrinsic GTPase activity along with the ability to be stimulated by GAP binding, as well as a retained capacity for and dependency on GEF-mediated GTP loading (Hunter *et al.*, 2015). Thus, to be able to better understand the role of SHP2 in mutant *KRAS* signaling, it is necessary to take a closer look at wild-type *KRAS* signaling.

Wild-type *KRAS*, like the other RAS isoforms HRAS and NRAS, is a guanine nucleotide binding protein acting as a molecular switch in key signaling pathways. It becomes activated through the exchange of GDP to GTP which, under physiological circumstances, is controlled through ligands binding to extracellular receptors. Receptor activation then induces nucleotide exchange with the help of guanine nucleotide exchange factors (GEF), such as Son of sevenless 1 (SOS1) (Dance *et al.*, 2008; Hunter *et al.*, 2015). SOS1-*KRAS* binding induces conformational changes which allow GDP to dissociate and GTP to bind. Active RAS most importantly binds to RAF or PI3K and induces MEK/ERK or PI3K/AKT signaling (Dance *et al.*, 2008). RAS deactivation, or the conversion from GTP to GDP bound state is a result of RAS intrinsic GTPase activity and can be accelerated through the binding of GTPase-activating proteins (GAP) (Hunter *et al.*, 2015).

Although the exact mechanism through which SHP2 regulates RAS activation remains unclear, growing evidence suggests that loss of SHP2 activity results in disrupted SOS-dependent GTP loading (Bunda *et al.*, 2015; Nichols *et al.*, 2018; Mattox *et al.*, 2019). The fact that mutant *KRAS* proteins are not constitutively bound to GTP, but instead maintain some of their GTPase activity means that there is still a conversion from GTP to GDP-bound RAS which results in mutant RAS proteins being dependent on GEF-mediated re-activation and thus SHP2 activity. In addition, others have reported Src kinase-dependent tyrosine-phosphorylation and SHP2-dependent dephosphorylation sites on RAS proteins. Src-mediated tyrosine phosphorylation was shown to mediate GEF and GAP insensitivity, reduced effector binding and a stalled GTPase cycle. In this context, SHP2-mediated *KRAS* dephosphorylation is required to maintain effector binding and SHP2 inhibition results in disrupted RAS/RAF-mediated signal transduction (Bunda *et al.*, 2015; Kano *et al.*, 2019).

7.4 Synergism between SHP2 and RAS-effector Kinases MEK and ERK provides rationale for a “two-pronged” therapy approach for KRAS-mutant cancer

Not only do *KRAS* mutations drive pancreatic tumorigenesis, even full-blown PDAC tumors mostly remain RAS-dependent (Collins *et al.*, 2012; Ying *et al.*, 2012), making *KRAS* an interesting therapeutic target for pancreatic cancer. Then again, for more than three decades of research, direct targeting of RAS has proven to be a very challenging, if not impossible, task. Due to the lack of deep, hydrophobic pockets on the surface of *KRAS* which are necessary for tight binding of small molecules, RAS oncoproteins were long considered to be 'undruggable' targets. But only recently, two novel *KRAS*^{G12C} inhibitors, MRTX849 (Mirati Therapeutics) and AMG 510 (Amgen) have entered clinical development. Both compounds work by forming a covalent bond specifically with the mutant cysteine (Cys 12) in GDP-bound, inactive, *KRAS*^{G12C}. The covalent occupancy of Cys 12 locks the protein in its inactive conformation and thus blocks the oncogenic signal transmission. (Ostrem and Shokat, 2016; Bar-Sagi, Knelson and Sequist, 2020; Hallin *et al.*, 2020; Nollmann and Ruess, 2020). While the point mutation encoding *KRAS*^{G12C} is present in approximately 13% of lung and 3% of colorectal cancer, it represents only 1% of *KRAS* mutations in pancreatic cancer (Witkiewicz *et al.*, 2015; 'AACR Project GENIE: Powering Precision Medicine through an International Consortium', 2017). The majority of PDAC patients carry other *KRAS* point mutations, encoding for the mutant *KRAS* proteins *KRAS*^{G12D} (41%), *KRAS*^{G12V} (34%) and *KRAS*^{G12R} (16%) (Witkiewicz *et al.*, 2015), and will therefore not benefit from these recent developments.

In the absence of direct inhibitors, most of the current attempts are aimed at blocking downstream RAS effectors in the MAPK or PI3K/AKT pathway (Drosten and Barbacid, 2020; Nollmann and Ruess, 2020).

We have shown that the loss of SHP2 function, via CRISPR-Cas9 mediated knockout or pharmacological inhibition, leaves *KRAS*-mutant PDAC cells uniquely sensitive to MEK and ERK inhibition. The synergy between these inhibitors up- and downstream of RAS significantly exceeds the effects of any other drug combination we tested. MEK and ERK inhibitors have not yet been approved for clinical use in PDAC, which is partly due to the associated adverse events and partly due to rapidly occurring resistance and tumor recurrence (Sun *et al.*, 2014; Tolcher *et al.*, 2015; Welsh and Corrie, 2015). However, we were able to show that additional SHP2 inhibition significantly delayed the onset of resistance and tumor regrowth in MEK treated mice compared to MEK inhibitor monotherapy. We, as well as Mainardi *et al.*, (2018), have seen that increased ERK phosphorylation after prolonged MEK inhibition correlates with increases in SHP2 activity (Mainardi *et al.*, 2018; Ruess *et al.*, 2018), a fact that is congruent

with literature describing *PTPN11*/SHP2 as a central node in MEK inhibitor resistance in RAS/MAPK pathway hyperactivated contexts (Prahallad *et al.*, 2015; Fedele *et al.*, 2018).

While these results were already very promising and provide a clear rationale for the clinical application of combined up- and downstream inhibition in the absence of direct RAS inhibitors, we decided to further evaluate this “two-pronged” approach using SHP2 + ERK inhibition. ERK inhibitors have only recently entered clinical development (Pathania and Rawal, 2020) and hold promise for a more tolerable toxicity profile. Additionally, even though the onset of tumor regrowth was delayed in mice treated with combined SHP2 and MEK inhibition compared to MEK inhibitor monotherapy, intrinsic or acquired resistance through the reactivation of ERK signaling, and subsequent tumor recurrence is still a concern. Direct inhibition of ERK provides an opportunity to overcome these limitations and lead to improved clinical efficacy (Hayes *et al.*, 2016; Bhagwat *et al.*, 2020).

We have shown that the allosteric SHP2 inhibitor RMC-4550 and the ERK inhibitor LY3214996 synergistically inhibit PDAC growth *in vitro* and *in vivo* without signs of toxicity. Furthermore, we have seen promising signs of sustained tumor growth control for 12-days after the last *in vivo* treatment. Leading us to the conclusion that combined ERK + SHP2 inhibition is in fact a promising treatment concept that should be investigated in a clinical setting.

These results, however, are not able, nor are they meant, to declare one combination treatment as superior to the other. Both MEK and SHP2 as well as ERK and SHP2 inhibitor combinations have proven remarkably effective in PDAC *in vivo* models and both combinations have the potential to bring much needed treatment options for *KRAS*-driven PDAC and other *KRAS*-driven cancer types to the clinic.

8. CONCLUSION AND OUTLOOK

The present study shows the important role of gp130-mediated signaling in PDAC and provides rationales for novel treatment options in mutant *KRAS*-driven tumors.

While the direct targeting of gp130 or gp130/IL-6 interaction with small molecule inhibitors like SC144 or bazedoxifene was not exhaustively investigated in this study, the generated results are promising and lay the ground-stone for further research in our group, using different murine and human PDAC cells as well as *in vivo* models. Special focus will be placed on the combination with MEK or ERK inhibitors.

The Lgp130 model can and will be used to further investigate the roles of downstream effectors STAT3 and SHP2 in the context of activated or in-fact overactive gp130 signaling both in pancreatic carcinogenesis and in normal pancreatic development and pancreatic homeostasis.

Our discovery of almost complete abrogation of pancreatic carcinogenesis through the deletion of the SHP2 encoding gene *PTPN11* showed that in the context of *KRAS* mutation SHP2 acts rather as a MAPK-pathway activator than a JAK/STAT pathway inhibitor, thus disputing the concept of constitutively active mutant-*KRAS*. This discovery opened the gates for a completely novel two-pronged approach of RAS-pathway inhibition. The combination of SHP2 inhibitors with either MEK or ERK inhibitors could provide a targeted therapy for the approximately 90% of PDAC patients with *KRAS* mutations other than *KRAS*^{G12C}, for whom so far, no targeted therapies are available. In-fact, the data we generated is so promising that we are planning to start a clinical trial in patients with *KRAS*-mutant PDAC, lung and colon cancer in cooperation with the Netherlands Cancer Institute (NKI) and the support of Revolution Medicines as well as Eli Lilly and Company in the near future.

We will also continue to analyze the samples we have generated in our LY3214996 + RMC-4550 treated mice to further elucidate the mechanisms through which tumor growth suppression and tumor volume reduction are achieved and try to determine which, if any, resistance mechanisms might be induced upon continuous long-term treatment. With regards to the clinical application, we will also try to identify reliable and preferably minimally invasive obtainable bio markers of therapy response in patients.

9. REFERENCES

'AACR Project GENIE: Powering Precision Medicine through an International Consortium' (2017) *Cancer Discovery*, 7(8), pp. 818 LP – 831. doi: 10.1158/2159-8290.CD-17-0151.

Abe, H. *et al.* (2011) 'Discovery of a Highly Potent and Selective MEK Inhibitor: GSK1120212 (JTP-74057 DMSO Solvate)', *ACS medicinal chemistry letters*. American Chemical Society, 2(4), pp. 320–324. doi: 10.1021/ml200004g.

Algül, H. *et al.* (2007) 'Mechanisms of disease: chronic inflammation and cancer in the pancreas--a potential role for pancreatic stellate cells?', *Nature clinical practice. Gastroenterology & hepatology*. Department of Internal Medicine, Technical University of Munich, Munich, Germany., 4(8), pp. 454–462. doi: 10.1038/ncpgasthep0881.

Amrutkar, M. and Gladhaug, I. P. (2017) 'Pancreatic cancer chemoresistance to gemcitabine', *Cancers*, 9(11), pp. 1–23. doi: 10.3390/cancers9110157.

Andersson, L. C. *et al.* (1978) 'Activated human T lymphocytes display new surface glycoproteins', *Proceedings of the National Academy of Sciences of the United States of America*, 75(7), pp. 3455–3458. doi: 10.1073/pnas.75.7.3455.

Bar-Sagi, D., Knelson, E. H. and Sequist, L. V (2020) 'A bright future for KRAS inhibitors', *Nature Cancer*, 1(1), pp. 25–27. doi: 10.1038/s43018-019-0016-8.

Betz, U. A. *et al.* (1998) 'Postnatally induced inactivation of gp130 in mice results in neurological, cardiac, hematopoietic, immunological, hepatic, and pulmonary defects', *The Journal of experimental medicine*. The Rockefeller University Press, 188(10), pp. 1955–1965. doi: 10.1084/jem.188.10.1955.

Bhagwat, S. V. *et al.* (2020) 'ERK inhibitor LY3214996 targets ERK pathway–driven cancers: A therapeutic approach toward precision medicine', *Molecular Cancer Therapeutics*. doi: 10.1158/1535-7163.MCT-19-0183.

Bressy, C. *et al.* (2018) 'LIF Drives Neural Remodeling in Pancreatic Cancer and Offers a New Candidate Biomarker.', *Cancer research*. United States, 78(4), pp. 909–921. doi: 10.1158/0008-5472.CAN-15-2790.

Bunda, S. *et al.* (2015) 'Inhibition of SHP2-mediated dephosphorylation of Ras suppresses oncogenesis', *Nature Communications*, 6(1), p. 8859. doi: 10.1038/ncomms9859.

Burkhardt, C. *et al.* (2019) 'Bazedoxifene as a novel strategy for treatment of pancreatic and gastric adenocarcinoma.', *Oncotarget*, 10(34), pp. 3198–3202.

Carioli, G. *et al.* (2020) 'European cancer mortality predictions for the year 2020 with a focus on prostate cancer', *Annals of Oncology*. Elsevier, 31(5), pp. 650–658. doi: 10.1016/j.annonc.2020.02.009.

- Chen, X. *et al.* (2019) 'Blocking IL-6/GP130 Signaling Inhibits Cell Viability/Proliferation, Glycolysis, and Colony Forming Activity in Human Pancreatic Cancer Cells.', *Current cancer drug targets*, 19(5), pp. 417–427. doi: 10.2174/1568009618666180430123939.
- Chou, T.-C. (2010) 'Drug Combination Studies and Their Synergy Quantification Using the Chou-Talalay Method', *Cancer Research*, 70(2), pp. 440 LP – 446. doi: 10.1158/0008-5472.CAN-09-1947.
- Collins, M. A. *et al.* (2012) 'Oncogenic Kras is required for both the initiation and maintenance of pancreatic cancer in mice', *The Journal of Clinical Investigation*. The American Society for Clinical Investigation, 122(2), pp. 639–653. doi: 10.1172/JCI59227.
- Corcoran, R. B. *et al.* (2011) 'STAT3 plays a critical role in KRAS-induced pancreatic tumorigenesis', *Cancer Research*. doi: 10.1158/0008-5472.CAN-11-0908.
- Corrie, P. G. *et al.* (2020) 'Scheduling nab-paclitaxel combined with gemcitabine as first-line treatment for metastatic pancreatic adenocarcinoma', *British Journal of Cancer*, 122(12), pp. 1760–1768. doi: 10.1038/s41416-020-0846-2.
- Cox, A. D. *et al.* (2014) 'Drugging the undruggable RAS: Mission Possible?', *Nature Reviews Drug Discovery*. doi: 10.1038/nrd4389.
- Dance, M. *et al.* (2008) 'The molecular functions of Shp2 in the Ras/Mitogen-activated protein kinase (ERK1/2) pathway', *Cellular Signalling*, 20(3), pp. 453–459. doi: <https://doi.org/10.1016/j.cellsig.2007.10.002>.
- Doehn, U. *et al.* (2009) 'RSK is a principal effector of the RAS-ERK pathway for eliciting a coordinate promotile/invasive gene program and phenotype in epithelial cells', *Molecular cell*, 35(4), pp. 511–522. doi: 10.1016/j.molcel.2009.08.002.
- Dolenšek, J., Rupnik, M. S. and Stožer, A. (2015) 'Structural similarities and differences between the human and the mouse pancreas.', *Islets*, 7(1), p. e1024405. doi: 10.1080/19382014.2015.1024405.
- Drosten, M. and Barbacid, M. (2020) 'Targeting the MAPK Pathway in KRAS-Driven Tumors', *Cancer Cell*. Elsevier, 37(4), pp. 543–550. doi: 10.1016/j.ccell.2020.03.013.
- Ebrahimi, B. *et al.* (2004) 'Cytokines in pancreatic carcinoma: correlation with phenotypic characteristics and prognosis.', *Cancer*. United States, 101(12), pp. 2727–2736. doi: 10.1002/cncr.20672.
- Eulendorf, R. *et al.* (2012) 'Interleukin-6 signalling: more than Jaks and STATs.', *European journal of cell biology*. Germany, 91(6–7), pp. 486–495. doi: 10.1016/j.ejcb.2011.09.010.
- Fedele, C. *et al.* (2018) 'SHP2 Inhibition Prevents Adaptive Resistance to MEK Inhibitors in Multiple Cancer Models', *Cancer Discovery*, 8(10), pp. 1237 LP – 1249. doi: 10.1158/2159-8290.CD-18-0444.

- Fu, S. and Lin, J. (2018) 'Blocking Interleukin-6 and Interleukin-8 Signaling Inhibits Cell Viability, Colony-forming Activity, and Cell Migration in Human Triple-negative Breast Cancer and Pancreatic Cancer Cells.', *Anticancer research*. Greece, 38(11), pp. 6271–6279. doi: 10.21873/anticancer.12983.
- Garcia Fortanet, J. *et al.* (2016) 'Allosteric Inhibition of SHP2: Identification of a Potent, Selective, and Orally Efficacious Phosphatase Inhibitor.', *Journal of medicinal chemistry*. United States, 59(17), pp. 7773–7782. doi: 10.1021/acs.jmedchem.6b00680.
- Golan, T. *et al.* (2019) 'Maintenance Olaparib for Germline *BRCA* -Mutated Metastatic Pancreatic Cancer', *New England Journal of Medicine*, 381(4), pp. 317–327. doi: 10.1056/NEJMoa1903387.
- Goumas, F. A. *et al.* (2015) 'Inhibition of IL-6 signaling significantly reduces primary tumor growth and recurrences in orthotopic xenograft models of pancreatic cancer.', *International journal of cancer*. United States, 137(5), pp. 1035–1046. doi: 10.1002/ijc.29445.
- Grande, F. *et al.* (2016) 'Identification and Preclinical Evaluation of SC144, a Novel Pyrroloquinoxaline Derivative with Broad-Spectrum Anticancer Activity.', *Mini reviews in medicinal chemistry*. Netherlands, 16(8), pp. 644–650. doi: 10.2174/138955751608160307175649.
- Grasso, C., Jansen, G. and Giovannetti, E. (2017) 'Drug resistance in pancreatic cancer: Impact of altered energy metabolism', *Critical Reviews in Oncology/Hematology*. Elsevier Ireland Ltd, 114, pp. 139–152. doi: 10.1016/j.critrevonc.2017.03.026.
- Grosskopf, S. *et al.* (2015) 'Selective inhibitors of the protein tyrosine phosphatase SHP2 block cellular motility and growth of cancer cells in vitro and in vivo.', *ChemMedChem*. Germany, 10(5), pp. 815–826. doi: 10.1002/cmdc.201500015.
- Guo, X.-Y. *et al.* (2019) 'Exosomes and pancreatic diseases: status, challenges, and hopes', *International journal of biological sciences*. Ivyspring International Publisher, 15(9), pp. 1846–1860. doi: 10.7150/ijbs.35823.
- Hallin, J. *et al.* (2020) 'The KRASG12C inhibitor MRTX849 provides insight toward therapeutic susceptibility of KRAS-mutant cancers in mouse models and patients', *Cancer Discovery*. doi: 10.1158/2159-8290.CD-19-1167.
- Hayes, T. K. *et al.* (2016) 'Long-Term ERK Inhibition in KRAS-Mutant Pancreatic Cancer Is Associated with MYC Degradation and Senescence-like Growth Suppression', *Cancer cell*. 2015/12/24, 29(1), pp. 75–89. doi: 10.1016/j.ccell.2015.11.011.
- Heo, T.-H., Wahler, J. and Suh, N. (2016) 'Potential therapeutic implications of IL-6/IL-6R/gp130-targeting agents in breast cancer', *Oncotarget*. Department of Chemical Biology, Ernest Mario School of Pharmacy, Rutgers, The State University of New Jersey, Piscataway, NJ, USA., 7(13), pp. 15460–15473. doi: 10.18632/oncotarget.7102.

Hingorani, S. R. *et al.* (2003) 'Preinvasive and invasive ductal pancreatic cancer and its early detection in the mouse', *Cancer Cell*. Elsevier, 4(6), pp. 437–450. doi: 10.1016/S1535-6108(03)00309-X.

Hingorani, S. R. *et al.* (2005) '*Trp53^{R172H}* and *Kras^{G12D}* cooperate to promote chromosomal instability and widely metastatic pancreatic ductal adenocarcinoma in mice', *Cancer Cell*. Elsevier, 7(5), pp. 469–483. doi: 10.1016/j.ccr.2005.04.023.

Holmer, R. *et al.* (2014) 'Interleukin-6: a villain in the drama of pancreatic cancer development and progression', *Hepatobiliary & Pancreatic Diseases International*, 13(4), pp. 371–380. doi: [https://doi.org/10.1016/S1499-3872\(14\)60259-9](https://doi.org/10.1016/S1499-3872(14)60259-9).

Huang, C. *et al.* (2017) 'Tumour-derived Interleukin 35 promotes pancreatic ductal adenocarcinoma cell extravasation and metastasis by inducing ICAM1 expression', *Nature communications*. Nature Publishing Group, 8, p. 14035. doi: 10.1038/ncomms14035.

Huang, X. *et al.* (2007) 'A parallel phase I/II clinical trial design for combination therapies.', *Biometrics*. United States, 63(2), pp. 429–436. doi: 10.1111/j.1541-0420.2006.00685.x.

Hunter, J. C. *et al.* (2015) 'Biochemical and Structural Analysis of Common Cancer-Associated KRAS Mutations', *Molecular Cancer Research*, 13(9), pp. 1325 LP – 1335. doi: 10.1158/1541-7786.MCR-15-0203.

Iacobuzio-Donahue, C. A. *et al.* (2012) 'Genetic Basis of Pancreas Cancer Development and Progression: Insights from Whole-Exome and Whole-Genome Sequencing', *Clinical Cancer Research*, 18(16), pp. 4257 LP – 4265. doi: 10.1158/1078-0432.CCR-12-0315.

Infante, J. R. *et al.* (2014) 'A randomised, double-blind, placebo-controlled trial of trametinib, an oral MEK inhibitor, in combination with gemcitabine for patients with untreated metastatic adenocarcinoma of the pancreas.', *European journal of cancer (Oxford, England : 1990)*. England, 50(12), pp. 2072–2081. doi: 10.1016/j.ejca.2014.04.024.

Jackson, E. L. *et al.* (2001) 'Analysis of lung tumor initiation and progression using conditional expression of oncogenic K-ras.', *Genes & development*, 15(24), pp. 3243–3248. doi: 10.1101/gad.943001.

Kano, Y. *et al.* (2019) 'Tyrosyl phosphorylation of KRAS stalls GTPase cycle via alteration of switch I and II conformation.', *Nature communications*, 10(1), p. 224. doi: 10.1038/s41467-018-08115-8.

Komm, B. S., Mirkin, S. and Jenkins, S. N. (2014) 'Development of conjugated estrogens/bazedoxifene, the first tissue selective estrogen complex (TSEC) for management of menopausal hot flashes and postmenopausal bone loss.', *Steroids*. United States, 90, pp. 71–81. doi: 10.1016/j.steroids.2014.06.004.

Lambert, A. *et al.* (2019) 'An update on treatment options for pancreatic adenocarcinoma.', *Therapeutic advances in medical oncology*, 11, p. 1758835919875568. doi: 10.1177/1758835919875568.

- Lan, L. *et al.* (2015) 'Shp2 signaling suppresses senescence in PyMT-induced mammary gland cancer in mice.', *The EMBO journal*, 34(11), pp. 1493–1508. doi: 10.15252/embj.201489004.
- Lee, J. W. *et al.* (2016) 'Genetically Engineered Mouse Models of Pancreatic Cancer: The KPC Model (LSL-Kras(G12D/+);LSL-Trp53(R172H/+);Pdx-1-Cre), Its Variants, and Their Application in Immuno-oncology Drug Discovery', *Current protocols in pharmacology*, 73, pp. 14.39.1-14.39.20. doi: 10.1002/cpph.2.
- Lee, J. W. *et al.* (2019) 'Hepatocytes direct the formation of a pro-metastatic niche in the liver', *Nature*, 567(7747), pp. 249–252. doi: 10.1038/s41586-019-1004-y.
- Lee, Y. T., Tan, Y. J. and Oon, C. E. (2018) 'Molecular targeted therapy: Treating cancer with specificity.', *European journal of pharmacology*. Netherlands, 834, pp. 188–196. doi: 10.1016/j.ejphar.2018.07.034.
- Lesina, M. *et al.* (2011) 'Stat3/Socs3 Activation by IL-6 Transsignaling Promotes Progression of Pancreatic Intraepithelial Neoplasia and Development of Pancreatic Cancer', *Cancer Cell*. doi: 10.1016/j.ccr.2011.03.009
- Li, H. *et al.* (2014) 'Drug design targeting protein-protein interactions (PPIs) using multiple ligand simultaneous docking (MLSD) and drug repositioning: discovery of raloxifene and bazedoxifene as novel inhibitors of IL-6/GP130 interface.', *Journal of medicinal chemistry*. United States, 57(3), pp. 632–641. doi: 10.1021/jm401144z.
- Li, X. *et al.* (2019) 'Synergistic inhibition of GP130 and ERK signaling blocks chemoresistant bladder cancer cell growth.', *Cellular signalling*. England, 63, p. 109381. doi: 10.1016/j.cellsig.2019.109381.
- Long, K. B. *et al.* (2017) 'IL6 Receptor Blockade Enhances Chemotherapy Efficacy in Pancreatic Ductal Adenocarcinoma.', *Molecular cancer therapeutics*, 16(9), pp. 1898–1908. doi: 10.1158/1535-7163.MCT-16-0899.
- Lu, T. *et al.* (2020) 'Up-regulation of hypoxia-inducible factor antisense as a novel approach to treat ovarian cancer.', *Theranostics*, 10(15), pp. 6959–6976. doi: 10.7150/thno.41792.
- Lu, W., Shen, K. and Cole, P. A. (2003) 'Chemical Dissection of the Effects of Tyrosine Phosphorylation of SHP-2', *Biochemistry*. American Chemical Society, 42(18), pp. 5461–5468. doi: 10.1021/bi0340144.
- Mainardi, S. *et al.* (2018) 'SHP2 is required for growth of KRAS-mutant non-small-cell lung cancer in vivo letter', *Nature Medicine*, 24(7), pp. 961–967. doi: 10.1038/s41591-018-0023-9.
- Manchado, E. *et al.* (2016) 'A combinatorial strategy for treating KRAS-mutant lung cancer.', *Nature*, 534(7609), pp. 647–651. doi: 10.1038/nature18600.
- Marino, S. *et al.* (2000) 'Induction of medulloblastomas in p53-null mutant mice by somatic inactivation of Rb in the external granular layer cells of the cerebellum.', *Genes & development*, 14(8), pp. 994–1004.

- Matallanas, D. *et al.* (2011) 'Mutant K-Ras activation of the proapoptotic MST2 pathway is antagonized by wild-type K-Ras.', *Molecular cell*. United States, 44(6), pp. 893–906. doi: 10.1016/j.molcel.2011.10.016.
- Mattox, T. E. *et al.* (2019) 'Exploiting RAS Nucleotide Cycling as a Strategy for Drugging RAS-Driven Cancers', *International journal of molecular sciences*. MDPI, 21(1), p. 141. doi: 10.3390/ijms21010141.
- Mizrahi, J. D. *et al.* (2020) 'Pancreatic cancer', *The Lancet*, 395(10242), pp. 2008–2020. doi: [https://doi.org/10.1016/S0140-6736\(20\)30974-0](https://doi.org/10.1016/S0140-6736(20)30974-0).
- Morrison, A. H., Byrne, K. T. and Vonderheide, R. H. (2018) 'Immunotherapy and Prevention of Pancreatic Cancer', *Trends in Cancer*, 4(6), pp. 418–428. doi: 10.1016/j.trecan.2018.04.001.
- Nakhai, H. *et al.* (2007) 'Ptf1a is essential for the differentiation of GABAergic and glycinergic amacrine cells and horizontal cells in the mouse retina.', *Development (Cambridge, England)*. England, 134(6), pp. 1151–1160. doi: 10.1242/dev.02781.
- Neel, B. G., Gu, H. and Pao, L. (2003) 'The 'Shp'ing news: SH2 domain-containing tyrosine phosphatases in cell signaling', *Trends in Biochemical Sciences*. doi: 10.1016/S0968-0004(03)00091-4.
- Neesse, A. *et al.* (2015) 'Stromal biology and therapy in pancreatic cancer: a changing paradigm.', *Gut*. England, 64(9), pp. 1476–1484. doi: 10.1136/gutjnl-2015-309304.
- Nguyen, A. M. *et al.* (2020) 'Upregulation of CD73 Confers Acquired Radioresistance and is Required for Maintaining Irradiation-selected Pancreatic Cancer Cells in a Mesenchymal State', *Molecular & Cellular Proteomics*, 19(2), pp. 375 LP – 389. doi: 10.1074/mcp.RA119.001779.
- Nichols, R. J. *et al.* (2018) 'RAS nucleotide cycling underlies the SHP2 phosphatase dependence of mutant BRAF-, NF1- and RAS-driven cancers.', *Nature cell biology*, 20(9), pp. 1064–1073. doi: 10.1038/s41556-018-0169-1.
- Nollmann, F. I. and Ruess, D. A. (2020) 'Targeting Mutant KRAS in Pancreatic Cancer: Futile or Promising?', *Biomedicines*, 8(8). doi: 10.3390/biomedicines8080281.
- O'Shea, E. K. *et al.* (1989) 'Preferential heterodimer formation by isolated leucine zippers from fos and jun.', *Science (New York, N.Y.)*. United States, 245(4918), pp. 646–648. doi: 10.1126/science.2503872.
- Ohtani, T. *et al.* (2000) 'gp130-mediated signalling as a therapeutic target', *Emerging Therapeutic Targets*. Taylor & Francis, 4(4), pp. 459–479. doi: 10.1517/14728222.4.4.459.
- Orth, M. *et al.* (2019) 'Pancreatic ductal adenocarcinoma: biological hallmarks, current status, and future perspectives of combined modality treatment approaches', *Radiation Oncology*. Radiation Oncology, 14(1), p. 141. doi: 10.1186/s13014-019-1345-6.

- Oshima, T. *et al.* (2009) 'Combination effects of SC144 and cytotoxic anticancer agents.', *Anti-cancer drugs*. England, 20(5), pp. 312–320. doi: 10.1097/CAD.0b013e328323a7ca.
- Ostrem, J. M. L. and Shokat, K. M. (2016) 'Direct small-molecule inhibitors of KRAS: from structural insights to mechanism-based design.', *Nature reviews. Drug discovery*. England, 15(11), pp. 771–785. doi: 10.1038/nrd.2016.139.
- Pandol, S. J. (2015) 'Normal Pancreatic Function', *Pancreapedia: Exocrine Pancreas Knowledge Base*. doi: 10.3998/panc.2015.17
- Pathania, S. and Rawal, R. K. (2020) 'An update on chemical classes targeting ERK1/2 for the management of cancer.', *Future medicinal chemistry*. England, 12(7), pp. 593–611. doi: 10.4155/fmc-2019-0339.
- Plasencia, C. *et al.* (2009) 'Discovery of a novel quinoxalinhydrazide with a broad-spectrum anticancer activity.', *Cancer biology & therapy*. United States, 8(5), pp. 458–465. doi: 10.4161/cbt.8.5.7741.
- Prahallad, A. *et al.* (2015) 'PTPN11 Is a Central Node in Intrinsic and Acquired Resistance to Targeted Cancer Drugs.', *Cell reports*. United States, 12(12), pp. 1978–1985. doi: 10.1016/j.celrep.2015.08.037.
- Rawla, P., Sunkara, T. and Gaduputi, V. (2019) 'Epidemiology of Pancreatic Cancer: Global Trends, Etiology and Risk Factors.', *World journal of oncology*, 10(1), pp. 10–27. doi: 10.14740/wjon1166.
- Rose-John, S. (2018) 'Interleukin-6 Family Cytokines.', *Cold Spring Harbor perspectives in biology*, 10(2). doi: 10.1101/cshperspect.a028415.
- Rose-John, S., Scheller, J. and Schaper, F. (2015) "Family reunion" – A structured view on the composition of the receptor complexes of interleukin-6-type and interleukin-12-type cytokines', *Cytokine & Growth Factor Reviews*, 26(5), pp. 471–474. doi: <https://doi.org/10.1016/j.cytogfr.2015.07.011>.
- Ruess, D. A. *et al.* (2017) 'Pharmacotherapeutic Management of Pancreatic Ductal Adenocarcinoma: Current and Emerging Concepts', *Drugs and Aging*, 34(5), pp. 331–357. doi: 10.1007/s40266-017-0453-y.
- Ruess, D. A. *et al.* (2018) 'Mutant KRAS-driven cancers depend on PTPN11/SHP2 phosphatase', *Nature Medicine*, 24(7), pp. 954–960. doi: 10.1038/s41591-018-0024-8.
- Ryan, M. B. *et al.* (2015) 'Targeting RAS-mutant Cancers: Is ERK the Key?', *Trends in Cancer*, 1(3), pp. 183–198. doi: <https://doi.org/10.1016/j.trecan.2015.10.001>.
- Samatar, A. A. and Poulikakos, P. I. (2014) 'Targeting RAS-ERK signalling in cancer: promises and challenges.', *Nature reviews. Drug discovery*. England, 13(12), pp. 928–942. doi: 10.1038/nrd4281.

- Schaper, F. and Rose-John, S. (2015) 'Interleukin-6: Biology, signaling and strategies of blockade', *Cytokine & Growth Factor Reviews*, 26(5), pp. 475–487. doi: <https://doi.org/10.1016/j.cytogfr.2015.07.004>.
- Schulz, D. and Algül, H. (2019) 'Chemotherapy of pancreatic cancer in patients with poor performance.', *Chinese clinical oncology*. China, p. S22. doi: 10.21037/cco.2019.08.01.
- Schumacher, N. *et al.* (2020) 'Cell-autonomous hepatocyte-specific GP130 signalling is sufficient to trigger a robust innate immune response in mice', *Journal of Hepatology*. Elsevier. doi: 10.1016/j.jhep.2020.09.021.
- Sheahan, A. V. *et al.* (2018) 'Targeted therapies in the management of locally advanced and metastatic pancreatic cancer: a systematic review', *Oncotarget*, 9(30), pp. 21613–21627. doi: 10.18632/oncotarget.25085.
- Shi, Y. *et al.* (2019) 'Targeting LIF-mediated paracrine interaction for pancreatic cancer therapy and monitoring', *Nature*, 569(7754), pp. 131–135. doi: 10.1038/s41586-019-1130-6.
- Siegel, R. L., Miller, K. D. and Jemal, A. (2020) 'Cancer statistics, 2020', *CA: A Cancer Journal for Clinicians*. American Cancer Society, 70(1), pp. 7–30. doi: <https://doi.org/10.3322/caac.21590>.
- Silver, J. S. and Hunter, C. A. (2010) 'gp130 at the nexus of inflammation, autoimmunity, and cancer.', *Journal of leukocyte biology*, 88(6), pp. 1145–1156. doi: 10.1189/jlb.0410217.
- Smigiel, J. M., Parameswaran, N. and Jackson, M. W. (2017) 'Potent EMT and CSC Phenotypes Are Induced By Oncostatin-M in Pancreatic Cancer', *Molecular cancer research : MCR*. 2017/01/04, 15(4), pp. 478–488. doi: 10.1158/1541-7786.MCR-16-0337.
- Stuhlmann-Laeisz, C. *et al.* (2006) 'Forced dimerization of gp130 leads to constitutive STAT3 activation, cytokine-independent growth, and blockade of differentiation of embryonic stem cells.', *Molecular biology of the cell*, 17(7), pp. 2986–2995. doi: 10.1091/mbc.e05-12-1129.
- Sun, C. *et al.* (2014) 'Intrinsic resistance to MEK inhibition in KRAS mutant lung and colon cancer through transcriptional induction of ERBB3.', *Cell reports*. United States, 7(1), pp. 86–93. doi: 10.1016/j.celrep.2014.02.045.
- Thilakasiri, P. *et al.* (2019a) 'Repurposing the selective estrogen receptor modulator bazedoxifene to suppress gastrointestinal cancer growth.', *EMBO molecular medicine*, 11(4). doi: 10.15252/emmm.201809539.
- Thilakasiri, P. S. *et al.* (2019b) 'Repurposing of drugs as STAT3 inhibitors for cancer therapy.', *Seminars in cancer biology*. England. doi: 10.1016/j.semcan.2019.09.022.
- Tolcher, A. W. *et al.* (2015) 'A phase IB trial of the oral MEK inhibitor trametinib (GSK1120212) in combination with everolimus in patients with advanced solid tumors.', *Annals of oncology : official journal of the European Society for Medical Oncology*. England, 26(1), pp. 58–64. doi: 10.1093/annonc/mdu482.

- Le Tourneau, C., Lee, J. J. and Siu, L. L. (2009) 'Dose escalation methods in phase I cancer clinical trials', *Journal of the National Cancer Institute*. 2009/05/12. Oxford University Press, 101(10), pp. 708–720. doi: 10.1093/jnci/djp079.
- Wang, M.-T. *et al.* (2019) 'Blockade of leukemia inhibitory factor as a therapeutic approach to KRAS driven pancreatic cancer', *Nature Communications*, 10(1), p. 3055. doi: 10.1038/s41467-019-11044-9.
- Welsh, S. J. and Corrie, P. G. (2015) 'Management of BRAF and MEK inhibitor toxicities in patients with metastatic melanoma.', *Therapeutic advances in medical oncology*, 7(2), pp. 122–136. doi: 10.1177/1758834014566428.
- Witkiewicz, A. K. *et al.* (2015) 'Whole-exome sequencing of pancreatic cancer defines genetic diversity and therapeutic targets', *Nature Communications*. doi: 10.1038/ncomms7744.
- Wörmann, S. M. *et al.* (2016) 'Loss of P53 Function Activates JAK2–STAT3 Signaling to Promote Pancreatic Tumor Growth, Stroma Modification, and Gemcitabine Resistance in Mice and Is Associated With Patient Survival', *Gastroenterology*. doi: 10.1053/j.gastro.2016.03.010.
- Wu, X. *et al.* (2016) 'Bazedoxifene as a Novel GP130 Inhibitor for Pancreatic Cancer Therapy.', *Molecular cancer therapeutics*, 15(11), pp. 2609–2619. doi: 10.1158/1535-7163.MCT-15-0921.
- Xu, S. *et al.* (2013) 'Discovery of a novel orally active small-molecule gp130 inhibitor for the treatment of ovarian cancer.', *Molecular cancer therapeutics*. United States, 12(6), pp. 937–949. doi: 10.1158/1535-7163.MCT-12-1082.
- Yang, J. C.-H., Lin, C.-C. (Josh) and Chu, C.-Y. (2018) '49 - Management of Toxicities of Targeted Therapies', in Pass, H. I., Ball, D., and Scagliotti, G. V. B. T.-I. T. O. (Second E. (eds). Philadelphia: Elsevier, pp. 490-500.e3. doi: <https://doi.org/10.1016/B978-0-323-52357-8.00049-4>.
- Ying, H. *et al.* (2012) 'Oncogenic Kras Maintains Pancreatic Tumors through Regulation of Anabolic Glucose Metabolism', *Cell*. Elsevier, 149(3), pp. 656–670. doi: 10.1016/j.cell.2012.01.058.
- Zeng, S. *et al.* (2019) 'Chemoresistance in Pancreatic Cancer', *International journal of molecular sciences*. MDPI, 20(18), p. 4504. doi: 10.3390/ijms20184504.
- Zhang, E. E. *et al.* (2004) 'Neuronal Shp2 tyrosine phosphatase controls energy balance and metabolism', *Proceedings of the National Academy of Sciences of the United States of America*, 101(45), pp. 16064 LP – 16069. doi: 10.1073/pnas.0405041101.
- Zhou, Q. and Melton, D. A. (2018) 'Pancreas regeneration', *Nature*. 2018/05/16, 557(7705), pp. 351–358. doi: 10.1038/s41586-018-0088-0.

Parts of this thesis have been published in:

Ruess DA, Heynen GJ, **Ciecielski KJ**, Ai J, Berninger A, Kabacaoglu D, Görgülü K, Dantes Z, Wörmann SM, Diakopoulos KN, Karpathaki AF, Kowalska M, Kaya-Aksoy E, Song L, van der Laan EAZ, López-Alberca MP, Nazaré M, Reichert M, Saur D, Erkan MM, Hopt UT, Sainz B Jr, Birchmeier W, Schmid RM, Lesina M, Algül H. Mutant KRAS-driven cancers depend on PTPN11/SHP2 phosphatase. *Nat Med.* 2018 Jul;24(7):954-960.

Additional publications include:

- Kabacaoglu D, **Ciecielski KJ**, Ruess DA and Algül H. Immune Checkpoint Inhibition for Pancreatic Ductal Adenocarcinoma: Current Limitations and Future Options. *Front. Immunol.* 2018 9:1878. <https://doi.org/10.3389/fimmu.2018.01878>
- Görgülü K, Diakopoulos KN, Ai J, Schoeps B, Kabacaoglu D, Karpathaki AF, **Ciecielski KJ**, Kaya-Aksoy E, Ruess DA, Berninger A, Kowalska M, Stevanovic M, Wörmann SM, Wartmann T, Zhao Y, Halang W, Voronina S, Tepikin A, Schlitter AM, Steiger K, Artati A, Adamski J, Aichler M, Walch A, Jastroch M, Hartleben G, Mantzoros CS, Weichert W, Schmid RM, Herzig S, Krüger A, Sainz B Jr, Lesina M, Algül H. Levels of the Autophagy-Related 5 Protein Affect Progression and Metastasis of Pancreatic Tumors in Mice. *Gastroenterology.* 2019 Jan;156(1):203-217.e20.
- Görgülü, K, Diakopoulos, KN, Kaya-Aksoy, E, **Ciecielski, KJ**, Ai, J, Lesina, M, and Algül, H. The Role of Autophagy in Pancreatic Cancer: From Bench to the Dark Bedside. *Cells* 2020 9(4):1063. doi: 10.3390/cells9041063.
- **Ciecielski KJ**, Berninger A, Algül H. Precision Therapy of Pancreatic Cancer: From Bench to Bedside. *Visc Med.* 2020 Oct;36(5):373-380. doi: 10.1159/000509232. Epub 2020 Oct 6. PMID: 33178734; PMCID: PMC7590788.

10. ABBREVIATIONS

ADM	Acinar to ductal metaplasia
ANOVA	Analysis of variance
ATCC	American Type Culture Collection
BRCA	BReast Cancer (gene)
BrdU	Bromodeoxyuridine
CCLE	Cancer Cell Line Encyclopedia
CLC	Cardiotrophin-like cytokine
CNTF	Ciliary neurotrophic factor
COPD	Chronic obstructive pulmonary disease
COSMIC	Catalogue of Somatic Mutations in Cancer
CT-1	Cardiotrophin 1
dH ₂ O	Deionized water
DLT	Dose limiting toxicity
ERK	Extracellular-signal Regulated Kinases
ERKi	ERK inhibitor
FBS	Fetal bovine serum
FDA	Food and drug administration (US)
GEMM	Genetically engineered mouse model
gp130	Glycoprotein 130
H&E	Hematoxylin and eosin
HRP	Horseradish peroxidase
IC ₅₀	Half maximal inhibitory concentration
IHC	Immune histochemistry
IL	Interleukin
IL-6R	Interleukin 6 receptor
KIR	Kinase inhibitory region
KRAS	Kirsten rat sarcoma
LIF	Leukemia inhibitory factor
LY	Eli Lilly and Company compound LY3214996
MAPK	Mitogen-activated protein kinase
MEK	MAPK/ERK Kinase
MLSD	Multiple ligand simultaneous docking
MRI	Magnetic resonance imaging
MS	Multiple sclerosis
MTD	Maximum tolerated dose
NEAA	Non-essential amino acid
NP	Neuropoietin
OSM	Oncostatin M
PAGE	Polyacrylamide gel electrophoresis
PanIN	Pancreatic intraepithelial neoplasia
PARP	Poly(ADP-ribose)-Polymerase
PBS	Phosphate buffered saline
PC	Pancreatic cancer

Abbreviations

PCR	Polymerase chain reaction
PDAC	Pancreatic ductal adenocarcinoma
PET-CT	Positron emission tomography–computed tomography
PFA	Paraformaldehyde
PI3K	Phosphatidylinositol 3-kinases
PPIs	Protein protein interactions
RA	Rheumatoid arthritis
RAF	Rapidly accelerated fibrosarcoma
RAF	Rapidly accelerated fibrosarcoma
RAS	Rat sarcoma
RMC	Revolution Medicines compound 4550
RSK	Ribosomal s6 kinase
SDS	Sodium Dodecyl Sulfate
sgp130	Soluble gp130
SHP2	Src homology region 2 domain-containing phosphatase-2
SHP2i	SHP2 inhibitor
SOCS3	Suppressor of cytokine signaling 3
STAT3	Signal transducer and activator of transcription 3
TBS	TRIS buffered saline
TBST	TRIS buffered saline + 0.1% Tween 20
UT	Untreated control
WT	Wild-type

11. ACKNOWLEDGEMENTS

First, I would like to express my sincere gratitude to my thesis advisor Prof. Dr. med. Hana Algül for the opportunity to work in his group and his support and guidance during the past 4 years. I am very thankful for the trust that he placed in me by involving me in the planning and execution of several different projects and the writing of manuscripts. I would also like to convey my heartfelt gratitude towards PD. Dr. Marina Lesina for her constant guidance and encouragement. I am furthermore very grateful to Prof. Dr. Philipp Jost and Prof. Dr. Maximilian Reichert for the input and guidance they provided as members of my thesis advisory committee.

I am grateful to Prof. Dr. Stefan Rose-John and Prof. Dr. med. Ulrich Keller for kindly gifting us the *Lgp130^{kiki}* mice needed to start breeding our own *Kras;Lgp130^{kiki}* mice, and to Dr. Guus J. Heynen at the Max Delbrück Center for Molecular Medicine (MDC) in the Helmholtz Society, Berlin for the SHP2 knockout cells. I would also like to express my sincere gratitude to our collaborators Prof. Dr. Rene Bernards, Dr. Sara Mainardi and Antonio Mulero Sanchez at the Netherlands Cancer Institute in Amsterdam as well as Dr. Bruno Sainz Anding and Dr. Laura Ruiz-Cañas at the Instituto de Investigaciones Biomédicas "Alberto Sols" (IIBM) at the Universidad Autónoma de Madrid for the wonderful collaboration on our project regarding the combined inhibition of ERK and SHP2 in *KRAS*-driven PDAC.

Furthermore, I would like to thank Dr. med. Dietrich A. Ruess, for all that he taught me whilst we worked. I greatly benefitted from his vast knowledge and his ability to convey this knowledge to others. He is a great source of inspiration and a great contributor to the success of the SHP2 research. Special thanks also to my friend and colleague Alexandra Berninger, without whom none of the work regarding the combined inhibition of ERK and SHP2 would have been possible. I feel very grateful for my colleague and friend Dr. Ezgi Kaya-Aksoy who was both a source of great fun as well as stability throughout the years and who was a great support in the past months of writing whenever I felt unsure or overwhelmed. Thank you to my friend and colleague Dr. Kivanç Görgülü who always has an open ear and can always be counted on to provide help with both work- and non-work-related problems. I feel extremely grateful to have been surrounded by colleagues who became friends, and thus I would like to thank Derya, Nan, Nina, Fränze, Larissa, and Yuhui for their friendship and for making my work life so enjoyable.

Acknowledgements

Now I would like to express special thanks to my friends and family. To my dearest friend Anne, for the years of friendship and support. I am so glad we got to spend a big part of our PhD journey together in Munich. Thank you to Theresa, my dear friend and favorite “colleague next door”, I am so glad to have met you. To my friends Jasmin, Helen, Kiki and to all my ‘Hünxer Homies’: Schützi, Sina, Christian, Kody, Suse, Haucki, Jessi, Sarah, Dominic, Lukas, and Carina, I am very glad to have you in my life.

I am extremely grateful to my family, especially my parents Sigrid and Thomas Ciecieski, for all their love and constant support. I love you very much and I am very lucky to have you. To my brothers Leon and Christoph and my sister-in-law Tina whom I all love dearly even though I might not talk about it much. To my nieces Mathilda and Frieda who have brought so much joy to my life and whom I love with all my heart. To my grandparents Wilma and Walter Blümel who let me live in their home for the first 8 months of my life in Munich and thus allowed me to fully focus on my new job without the added stress of having to find an apartment. I am so glad my PhD position brought me to Munich and closer to you.

You guys - Mama, Papa, Leon, Christoph, Tina, Mathilda, Frieda, Oma & Opa - are the best family I could ever wish for and I am so deeply grateful for each and every one of you.

Thank you, Roland, for your love and support. Thank you for understanding me so well, for making me feel comfortable, happy, and secure, and for giving me the necessary nudge to finish writing this thesis. Without you 2020 and especially the past months would have been quite unbearable. I cannot wait to see what our future holds. I love you.